STUDY OF THE TRANSVERSE OPTICAL PUMPING

BY

NORIAKI TSUKADA

March 1974

KYOTO UNIVERSITY

Kyoto, Japan

STUDY OF THE TRANSVERSE OPTICAL PUMPING

By

NORIAKI TSUKADA

March 1974

Kyoto University

Kyoto, Japan

ACKNOWLEDGEMENTS

The author would like to express his great appreciation to Professor Toru Ogawa for his continuous guidance, many discussions and suggestions throughout the present work, and his careful reading of the manuscript. The author is deeply indebted to Dr. Tsutomu Yabuzaki for his discussions and suggestions. It would have been impossible to show this thesis without his help and stimulating discussions.

The author also wish to express his deep appreciation to Professors Ken-ichi Maeda, Susumu Kato, Iwane Kimura and Hiroshi Oya for their useful and critical discussions on many problems and for enlightening him on the attitude of research.

Some parts of the work were performed by the help of Messrs. Takuo Koyama and Yasushi Murakami, who were graduate students of Professor Ogawa's group.

Thanks are also due to discussions with other staffs of Ionosphere Research Laboratory and Professor Kimura's group.

The author wishes to acknowledge Dr. Shigeru Ando of Mitsubishi Electric Corporation for preparing the absorption cells and lamps.

Numerical calculations in this work were performed at the Data Processing Center of Kyoto University.

ABSTRACT

Radiofrequency spectroscopy is a field of atomic physics which has been growing fast during last years: electronic and nuclear magnetic resonance, double resonance, multiple quantum transitions, Autler-Townes effect, new kind of parametric magnetic resonances, etc. have been widely studied and used for various physical applications.

The "method of optical detection of magnetic resonance", that is "optical pumping", proposed by Kastler in 1950 is a very ingenious and prolific technique in radiofrequency spectroscopy. This thesis gives a theoretical and experimental study on the effects of the transverse optical pumping in the optical pumping experiments by use of the phenomenological Bloch equation.

With optical pumping it is possible to achieve selective population of atomic sublevels for an arbitrary angle between the pumping light beam and an external static magnetic field. Adding the arbitrary directions of the applied rf field and the pumping light beam, we encounter a variety of phenomena. Longitudinal optical pumping, with respect to the static magnetic field, combined with a linearly oscillating transverse field gives the multiple quantum resonances heralding the real absorption of an odd number of photons. On the other hand, the resonances involving an even number of photons are observed with transverse optical pumping. These resonances termed the Haroche resonances and they stem from virtual transitions at points of level crossing in the coupled atom-field system. Consequently they are not broadened to lowest order in the radiofrequency (rf) field amplitudes, and they can be used to obtain more accurate measurements of the power shifts than the multiple quantu resonances.

For longitudinal pumping, several papers have recently been devoted to the calculation of higher order terms appearing in the expression of the Bloch

Siegert shift. This renewal of interest has been stimulated by an article of Chang and Stehle who derive the shift from quantum electrodynamics calculation. This expression obtained by Chang and Stehle is in complete disagreement with the results of several other theoretical approaches: Shireley's theory using Floquet states, Pegg and Series' treatment based on appropriate changes of reference frames, Stenholm's calculations leading to continued fractions.

We carry out an exact treatment of the case of the transverse optical pumping. The Bloch equations are solved analytically in terms of continued fractions, and the solutions are used both to compute exact results for the generalized Bloch-Siegert shifts of the transverse resonances, the Haroche resonances, and to obtain analytic results for some limiting cases. When the doublet becomes degenerate, i.e., for the Hanle effect, our results display the Cohen-Tannoudji effect, where the rf field dresses the g-factor of the atom by a Bessel function. Then we measure with great precision the positions of the Haroche resonances with optically pumped cesium atoms. The Haroche resonances make us possible to obtain more accurate measurements of the power shifts, because they have narrow linewidth compared with the multiple quantum resonances. The experimental results of the power shifts of the Haroche resonances agree well with the continued fraction solutions. Hence we can conclude that the Bloch-Siegert shift for large values of the rf field is expressed by the semiclassical results of Shireley, Pegg and Series, and Stenholm rather than by the electrodynamics result of Chang and Stehle.

Furthermore, it is shown that the medium irradiated by a strong linearly oscillating rf field becomes anisotropic and the atomic g-factor is drastically modified by the oscillating rf field when the Hanle effect or parametric resonance takes place.

For a rotating rf field, whose rotating plane is perpendicular to a static magnetic field, the Bloch equation is exactly solved analytically. The resonance at twice the rotating rf frequency and the Hanle curve, which shifts towards the high field region and is broadened as the intensity of the rotating rf field is increased, are predicted. The theoretical results predicted are verified experimentally.

The consequences of misalignment of a rotating or an oscillating rf field are also investigated. The main effects of misalignment of the rf field are appearance of the different two types of the resonances, i.e., the longitudinal resonance and the transverse resonance, at integral multiples of the rf freqency. It is shown that there is no essential difference between the parametric resonance and the Haroche resonance and that both resonances are exhibited by an inclusive formula.

At the end of this thesis, we report the observation of the new type resonances when the static magnetic field with an arbitrary intensity is oriented in an arbitrary direction with respect to the strong oscillating rf field. These resonances appear at the points which satisfy the condition that the magnetic field component, parallel to the oscillating rf field axis, becomes the integral multiples of the rf frequency. The behavior of these resonances is similar to that of the Haroche resonance. The new type resonances observed experimentally can be derived from a theoretical analysis based on the numerical integration of the Bloch equations.

CONTENTS

ACKNOWLEDGEMENT

ABSTRACT

CHAPTER 1. GENERAL FEATURES 1

1.1. Introduction 1

1.2. The Principle of the Optical Pumping 5

1.3. Review of Various Resonance Effects in RF Spectroscopy 8

1.3.1. The Longitudinal Resonance 10

(a) Ordinary Resonance 10

(b) Multiple Quantum Resonance 11

1.3.2. The Transverse Resonance 12

(a) The Hanle Effect 12

(b) Parametric Resonance 13

(c) Haroche Resonance 13

(d) Off-diagonal Resonance 14

1.4. Outline of the Present Work 15

CHAPTER 2. BLOCH EQUATION AND THE MONITORING OPERATOR 18

2.1. Introduction 18

2.2. The Bloch Equation and the Equation of Motion for the Density Operator 18

2.2.1. Density Matrix and the Bloch Equation 18

2.2.2. Orientations as a Bulk Magnetization 20

2.3. Monitoring Operator and the Exciting Operator 23

2.4. Behavior of the Magnetic Moment in a Static Field 28

2.4.1. The Hanle Effect 28

2.4.2. Anticrossing Experiment 30

2.5. Conclusion 36

CHAPTER 3. EFFECTS OF THE TRANSVERSE PUMPING IN THE PRESENCE OF THE ROTATING RF FIELDS 37

3.1. Introduction 37

3.2. Effects of the Transverse Pumping in the Presence of a Rotating RF Field 40

3.2.1. Theory 42

3.2.2. Experiments and Discussion 50

3.3. Effects of the Transverse Pumping in the Presence of Two Rotating RF Fields 60

3.3.1. Theory 60

(a) Transformations of the Magnetic Fields 60

(b) The Bloch Equation and the Orientation Parameter M_0' in the Frame $S^{(4)}$ 63

(c) Absorption of the Pumping Light Beam 66

3.3.2. Special Cases and Discussion 71

3.4. Misalignment Effects of the Rotating RF Field 74

3.4.1. Theory 74

3.4.2. The Case of the Longitudinal Pumping 78

3.4.3. The Case of the Transverse Pumping 79

3.5. Conclusion 81

CHAPTER 4. EFFECTS OF THE TRANSVERSE PUMPING IN THE PRESENCE OF AN OSCILLATING RF FIELD 83

4.1. Introduction 83

4.2. Modification of the Atomic g-factor by the Oscillating RF Field 86

4.2.1. Theory 87

(a) Phenomenological Description of Spin System 87

(b) Quantum Mechanical Treatment 91

4.2.2. Experiments and Discussion 93

4.2.3. Frequency Shift due to the Nonresonant RF Field 103

4.3. Mixture of the Longitudinal Resonance and the Transverse Resonance 106

4.3.1. Theory 107

4.3.2. Discussion 113

4.4. Conclusion 115

CHAPTER 5. SATURATION EFFECTS IN RF SPECTROSCOPY 117

5.1. Introduction 117

5.2. Saturation Effects of the Transverse Resonance 119

5.2.1. The Bloch Equation and Continued Fraction 119

5.2.2. Computed Results 123

5.2.3. Experiments 126

5.2.4. Discussion 131

5.2.5. Modulation in Absorption for the Longitudinal Pumping 137

5.3. Saturation Effects in Magnetic Resonances for General Magnetic Fields Configuration 144

5.3.1. Experimental Results 146

5.3.2. Theoretical Discussions 155

(a) Equation of Motion 155

(b) Numerical Results 155

5.3.3. Comparisons between the Experimental Results and the Numerical Results 166

5.3.4. Competition of the Longitudinal Resonance and the Transverse Resonance 169

5.4. Conclusion 172

CHAPTER 6. SUMMARY AND CONCLUSION 175

APPENDIX A	Density Matrix Treatment for the Rotating RF Field	180
APPENDIX B	Parametric Resonance	182
APPENDIX C	Transient Phenomena in the Presence of the Oscillating RF Field	185
REFERENCES		188

CHAPTER 1

GENERAL FEATURES

1.1. Introduction

The optical spectra of atoms gave the impulse which lead to Bohr's theory of the atom and subsequently to the quantum mechanical description of matter. The technical advances during last two decades have lead to much more powerful methods for atomic investigations. These include optical pumping, double resonance and level crossing methods.

Optical pumping is a method for producing important changes in the population distribution of atoms and ions among their energy states by optical irradiation. The method of optical pumping was proposed by Kastler (1950) as a method to change the relative populations of Zeeman levels and of the hyperfine levels of the ground state of atoms. These population changes can be monitored by the change of intensity of the light transmitted by the sample cell in which optical pumping is produced or by the change of intensity or of polarization of the scattered resonance light. Population changes produced by thermal relaxation or by radio frequency resonance can be detected in this manner.

The method of optical pumping and optical detection can be used, either together or separately to investigate excited states of atoms. The pioneering work in this direction is the study of radio frequency resonance in the excited state 6^3P_1 of the mercury atom, made by Brossel and Bitter (1952). In this case polarized optical resonance radiation 2537 A is used to obtain a selective excitation of Zeeman sublevels of the excited state, and magnetic resonance is detected by the change of the polarization of the reemitted resonance radiation.

This method of studying excited states was called the "double resonance"

method by its authors. Two resonances, an optical resonance and a magnetic resonance are associated in it. More generally, two monochromatic radiations of different frequencies in the electromagnetic spectrum are simultaneously applied to an atomic system. Since 1950, both excited states and ground states of atoms have been studied extensively by optical pumping and by optical detection methods. An excellent reviews on the results obtained on excited states and on ground states or on metastable atomic states have been published by Kastler (1957), Carver (1963), Cohen-Tannoudji and Kastler (1966), Series (1970) and Happer (1972).

The presence of a strong light will affect the atomic levels and shift the resonances by measurable amounts (Barrat and Cohen-Tannoudji 1961a,b, Cohen-Tannoudji 1962a,b, Kastler 1963). The effects of virtual and real multiple photon transitions between the levels have been considered by Cohen-Tannoudji and his coworkers (Cohen-Tannoudji 1962a,b, Polonsky and Cohen-Tannoudji 1965a,b,c, Cohen-Tannoudji and Haroche 1965, 1966, 1969a,b). The phenomena connected with crossing and anticrossing of energy levels lead to interference phenomena (Colegrove, Franken, Lewis and Sands 1959, Franken 1961, Rose and Carovillano 1961, Eck, Foldy and Wider 1963).

For a long time, quantum electrodynamics was applied to problems involving only a few quanta of radiation and hence they could be treated within perturbation theory. The covariant formulation provides an efficient tool for the treatment of high energy scattering of radiation from matter. During the last two decades another aspect of the problem has emerged. For the low energies where atoms and molecules have their spectra, experimental methods have developed into directions where the nonlinear properties of the interaction become important. The concept of quantum mechanical coherence in strong radio frequency and microwave fields has been used widely to investigate atomic spectra (Cohen-Tannoudji and Kastler 1966, Cohen-Tannoudji

1962a,b, Novikov et al. 1970).

The problem of optical coherence can fruitfully be discussed both along classical and quantum mechanical lines (Mandel and Wolf 1965), and using the states advocated by Glauber (1963) one can establish useful correspondences (Mandel and Wolf 1966). The significant difference between semiclassical and quantized field theories lies in the treatment of spontaneous emission. The interaction matrix elements which determine the evolution of the atomic state vector under stimulated emission and absorption are identical in the two theories;for those situations in which spontaneous emission plays no significant role. Recently, Pegg(1973c) showed that a recent quantum-electrodynamic derivation by Chang and Stehle (1971) of double-quantum resonance-frequency shifts is equivalent to a previous known semiclassical approximation, and that neither of these methods was adequate to account for the results of Kush's experiments (1956). A more exact semiclassical computation was given which was reasonable agreement with Kush's results in the region where these results are meaningful. He concluded that the assertion of Chang and Stehle that quantum electrodynamics is necessary for such situation is unfounded.

In the radio frequency spectroscopy of atoms the number of photons is easily made large, which together with the low frequencies involved makes saturation phenomena important in many experiments. Combining several fields one can achieve multiple photon process or double resonance phenomena, which have been used to give information about atomic parameters.

The plan of this thesis is to discuss about the interaction between atoms and magnetic fields by using the phenomenological Bloch equation. The interaction of atoms with radio frequency fields of small intensity can be treated readily by semiclassical and quantum mechanical theories for the case of the longitudinal pumping (with respect to the static field). In particular, the interaction of spin-1/2 atom in a static magnetic field $\mathbf{H}_0$ with a weak linearly oscillating rf (radio frequency) field $\mathbf{H}_1 \cos \omega t$

perpendicular to H_0 is well known. When the oscillating field strength is increased a shift in the resonance frequency, the Bloch-Siegert shift, occurs. The position of the resonance is shifted from $\omega_0 = \omega$ to $\omega_0 = \omega [1 - 1/16(\omega_1/\omega)^2]$, where $\omega = \gamma H_0$, $\omega_1 = \gamma H_1$ and γ is the gyromagnetic ratio (Ramsey 1955). At higher oscillating field strength multiple quantum transitions become evident (Margerie and Brossel 1955, Winter 1955, 1959), and eventually the next term in the series for the resonance frequency, the term in H_1^4, becomes important. The value of this next term has not been well established and, in fact, Pegg (1973b) has pointed out that different approaches have led to different results (Shirley 1965, Chang and Stehle 1971). Chang and Stehle claim that semiclassical or classical theory does not give the correct result for the Bloch-Siegert shift when terms of order higher than H_1^2 are important, and that quantum electrodynamics is needed for such calculations. Furthermore, they claim that semiclassical theory cannot properly take care of the multiple quantum transitions. However, Pegg (1972b) and Tsukada, Yabuzaki and Ogawa (1973) have shown independently how the "multiple quantum resonance" in magnetic resonance can be described entirely by a semiclassical model or classical model. These resonances occur as normal magnetic resonances induced by rotating harmonics of the applied field in the oscillating frame or frequency modulated frame. In the laboratory frame the applied field has only two rotating components and no such multiplicity of harmonics, but at field strengths where the Bloch-Siegert shift becomes important, this frame is not the most appropriate to use.

The basic problem is to obtain a time-dependent Schrödinger equation in at least approximately integrable form. When the components of the Hamiltonian do not commute, this can be achieved by converting into a predominantly static form. Cohen-Tannoudji and Haroche (1969a,b) have

done this by including the field Hamiltonian in the total quantum system. Conservation of the energy then ensures a static total Hamiltonian. Shirley's (1965) approach is a replacement of the atomic Hamiltonian matrix by an infinite static Floquet matrix. While this is a semiclassical theory, nowhere involving explicit field quantization, Shirley shows that this Floquet states can be interpreted physically as quantum field state. Indeed, his Floquet frequency diagram is identical with that derived by Cohen-Tannoudji and Haroche (1969a,b), and his results can be applied directly to their approach (Allegrini and Arimond 1971).

The more conventional approach is to view the atomic Hamiltonian or magnetic fields from a reference frame in which it appears predominantly static. Transformations to two particular reference frame have been used for this purpose: the well-known rotating frame used for dealing with weak oscillating fields (Salwen 1955), and the oscillating frame used for high frequency oscillating fields (Pegg and Series 1970,1973).

While Pegg's results agree well with those of Shirley (1965) and Stenholm (1972a,b), they are in gross disagreement with those obtained by Chang and Stehle (1971) from quantum electrodynamics. Theoretical and experimental results given in this article appear to support the semiclassical theory by Pegg (1973a,b) and Stenholm (1972a,b).

1.2. The Principle of the Optical Pumping

By "optical pumping" we mean the use of light to produce a population of a set of energy levels of a system which is different from the normal Boltzmann distribution at the temperature of the experiment. The energy levels in question might be magnetic energy levels of an atom in which case the optical pumping would refer to either the orientation or alignment of the atoms by the light beam.

Optical pumping produces unequal populations of different magnetic sublevels of the ground state of atoms. Let us take an example: the case of an alkali atom in its ground state which is a $^2S_{1/2}$ state with electron spin-1/2 divided by a magnetic field into two Zeeman sublevels: $m = -1/2$ and $m = +1/2$. For simplicity let us disregard nuclear spin. Such a model has a particularly simple form and provides an adequate approximation to the behavior of real alkali atoms. By absorption of optical resonance radiation (the D_1 and D_2 lines), the atoms is raised to the $^2P_{1/2}$ and $^2P_{3/2}$ states which are the excited states nearest to the ground state.

Figure 1.1 shows the Zeeman structure of the levels involved and of the spectral transitions between them: (a) is an energy scheme: the energy of the state is given by the vertical position of the horizontal line representing the state. Spectral transitions are indicated by vertical arrows. (b) is a polarization scheme: magnetic sublevels of a same state are represented by equidistant points on a horizontal line. The arrows indicate the Zeeman transitions. In this scheme vertical arrows correspond to $\Delta m = 0$ or π transitions, arrows with a positive slope to $\Delta m = +1$ or σ^+ transitions, arrows with negative slope to $\Delta m = -1$ or σ^- transitions. The encircled number indicates the relative transition probabilities in an arbitrary scale.

We recall the selection rules for Zeeman lines of a dipole transition: only $\Delta m = 0$ and $\Delta m = \pm 1$ transitions are allowed. The polarization rules for electric dipole transitions are the following: $\Delta m = 0$ corresponds to π polarization: the light is linearly polarized with its electric vector parallel to the magnetic field, $\Delta m = +1$ corresponds to σ^+ polarization: the light is circularly polarized in a plane perpendicular to the field. The sence of rotation is the sence of the electric current in a coil generating the magnetic field. $\Delta m = -1$ corresponds to σ^- polarization: the light is circularly polarized in a plane perpendicularly to the field.

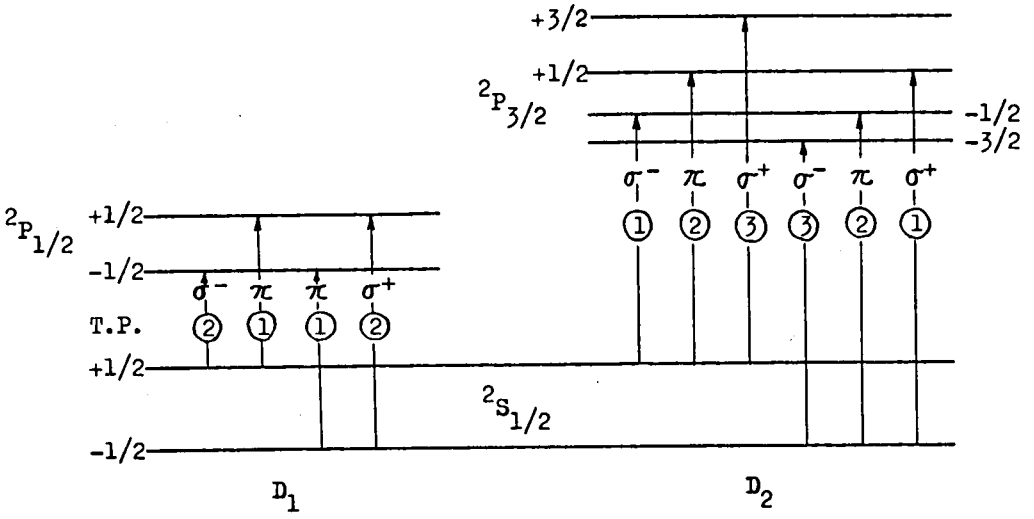

(a)

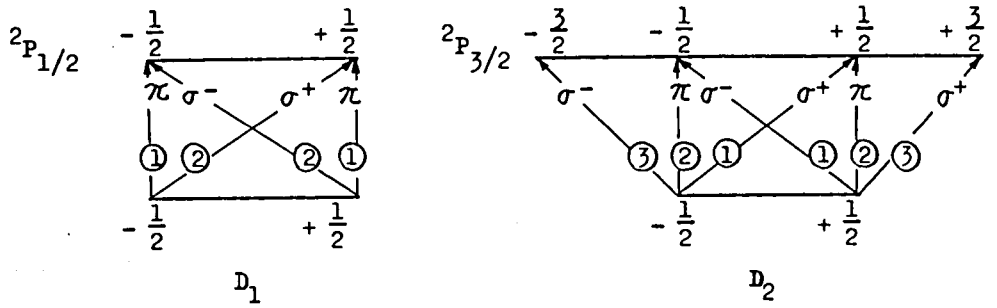

(b)

Fig. 1.1. (a). Zeeman structure of the D_1 and D_2 resonance lines of alkali atoms. Energy scheme.

(b) Zeeman structure of the D_1 and D_2 lines. Polarization scheme.

PD: Photo-Detector, PL: Polarized Light

The sense of rotation is opposite to σ^+. For magnetic dipole transitions the selection rules are the same. In the polarization rule the word electric vector has to be replaced by magnetic vector of the electromagnetic radiation field.

An observer looking in the field direction and receiving light propagated in the direction opposite to the field sees σ^+ light rotating clockwise and calls it "right-handed polarized". An observer looking in the opposite direction and receiving light propagated in the field direction sees σ^+ light rotating anti-clockwise and calls it "left-handed".

The atoms are illuminated with circularly polarized resonance radiation, say σ^+. Suppose that the incident light contains only D_1 line. In this case, only one of the upward transitions shown in Fig.1.1 will take place. Atoms from the $m = -1/2$ level of the ground state will be raised to the $m = +1/2$ level of the upper state. Falling back by spontaneous emission to the ground state, part of them will return to the initial Zeeman level, part of them will transit, by emission of the π component, to the $m = +1/2$ level of the ground state. According to the transition probabilities of three atoms having each absorbed one photon, two will return to the initial level and one will go to the+1/2 level.

After a small number of absorption processes a high degree of population change can be obtained in this manner.

1.3. Review of Various Resonance Effects in RF Spectroscopy

We review in briefly the various resonance effects in rf spectroscopy. The various resonance effects are due to both the longitudinal pumping (with respect to the static magnetic field) and the transverse pumping. Difference of the characters between the resonance effects caused by the longitudinal pumping and those caused by the transverse pumping is remarkable.

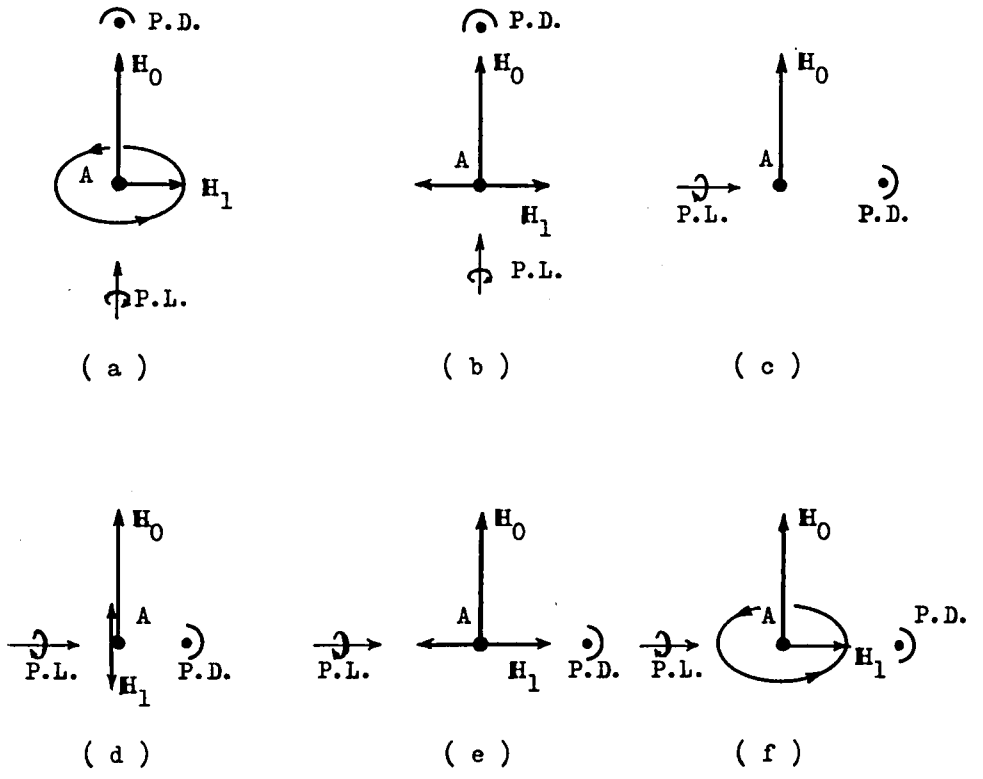

Fig. 1.2. Schematic diagrams of various magnetic resonances.

(a) Ordinary magnetic resonance.

(b) Multiple quantum resonance.

(c) Hanle effect (level crossing experiment).

(d) Parametric resonance.

(e) Haroche resonance.

(f) Off-diagonal resonance.

The resonances caused by the longitudinal pumping and the resonances caused by the transverse pumping appear as a decrease or an increase of the pumping light transmitted through the vapor cell. Therefore, we conventionally separate the various resonances into two types: the longitudinal resonances and the transverse resonances. The longitudinal resonances caused by the longitudinal pumping are strongly broadened by the rf field, but the transverse resonances caused by the transverse pumping are hardly broadened by the rf field and the width of the transverse resonances are decided mainly by the decay constant without affection of the intensity of the rf field. The longitudinal and the transverse resonances correspond to the anticrossing and the crossing of the energy levels, respectively (Cohen-Tannoudji and Haroche 1969a,b, Haroche 1971a,b). The ordinary resonance and the multiple quantum resonances belong to the longitudinal resonance, and the parametric resonance, the Haroche resonance and the off-diagonal or coherence resonance belong to the transverse resonance.

1.3.1. Longitudinal Resonances

(a) Ordinary Resonance

The well-known paramagnetic ordinary resonance is described classically as the induced conical precession of the magnetic moment vector about the direction of a static magnetic field $\mathbf{H}_0$ under the action of a rotating magnetic field $\mathbf{H}_1$ or a weak oscillating field $\mathbf{H}_1 \cos \omega t$ perpendicular to the static field $\mathbf{H}_0$. This situation is shown in Fig.1.2(a).

This type of resonance was first investigated in the field of nuclear magnetic resonance. The theory of various molecular beam magnetic resonance methods and of the resonance absorption and nuclear induction experiments is usually chiefly concerned with the calculation of the effect of weak oscillating or rotating magnetic field on nuclear magnetic moments in the presence of a strong magnetic field. Some of the simplest problems

of this sort were first solved by Rabi (1937), Schwinger (1937), and Bloch (1946) by a straightforward quantum mechanical of transition probabilities or by related methods.

The use of a rotating coordinate system to solve magnetic resonance problem has been reported by Rabi, Ramsey and Schwinger (1954). They have shown that on a coordinate system rotating with the applied rotating magnetic field the effective field is reduced by the Larmor field appropriate to the rotational frequency. On such a coordinate system problems can more readily be solved since this is no time variation of the field. The solution in a stationary frame of reference is then obtained by a transformation from the rotating to the stationary frame. This procedure has been widely applied both to the molecular beam magnetic resonance method and to resonance absorption and nuclear induction experiments.

When the oscillating field is increased a shift in the resonance frequency, the Bloch-Siegert shift, occurs. The position of resonance is shifted from $\omega_0 = \omega$ to $\omega_0 = \omega\,[\,1 - (1/16)\cdot(\,\omega_1/\omega\,)^2]$. At higher oscillating field strength multiple quantum transitions become evident. However, if a rotating rf field is used instead of an oscillating field, we observe no shift in resonance frequency.

(b) Multiple Quantum Transition

An oscillating rf field is applied perpendicularly to H_0 (see Fig.1.2(b)). The frequency ω being fixed, we observe, as we vary ω_0, several resonant variation of the transmitted light. Transitions between two levels are induced by the rf field. We observe an odd spectrum of resonances: they occur for $\omega_0 = (2n + 1)\omega$, where n is an integer. They are broadened and shifted as we increase the amplitude H_1.

The first observation of multiple quantum transitions on optically pumped atoms has been performed on alkali atoms (Margerie and Brossel 1955).

Theoretical investigation has been made by Winter (1955,1959). Strong exciting fields are required to observe multiple quantum transitions, since all photons must impinge on the atom before its virtual intermediate states decay back to the original state. Further investigations of multiple quantum transitions have been treated semiclassically by Shirley (1965), quantum electrodynamically by Chang and Stehle (1971) and by using the Green function by Gush et al.(1972). Recently, theoretical investigations of higher order terms in the Bloch-Siegert shift was reported by Pegg (1973a,b) and Stenholm (1972a,b). Higher order terms in the Bloch-Siegert shift obtained by Stenholm (1972b), Pegg (1973b), Cohen-Tannoudji et al (1973a,b) and Hannaford et al.(1973) support those derived by Shirley (1965) by means of Floquet theory, and are in gross disagreement with those derived by Chang and Stehle (1971) from quantum electrodynamics, particularly at extremely high field intensities.

1.3.2. Transverse Resonances

(a) The Hanle Effect

The pumping light beam is perpendicular to the field $\mathbf{H}_0$ in the absence of rf field as shown in Fig. 1.2(c). If there is no magnetic field, i.e., $H_0 = 0$, the pumping light beam orients the magnetization of vapor $\mathbf{M}$ in its own direction. In mathematical terms, the density matrix which describes the atoms in the ground state has non-zero off-diagonal elements. If $H_0 = 0$, the magnetic dipole of the vapor which has been just pumped by the light beam is pointing along the light beam direction. Immediately afterwards it begins to precess around $\mathbf{H}_0$ at the Larmor frequency of the ground state. After a mean time τ, the atom undergoes a disorientating collision or absorbs another photon and its orientation is destroyed or changes completely. The resulting magnetization at time $t = 0$ is the vectorial sum of all the

dipoles, created at time -t (t goes from 0 to $+\infty$). They have an amplitude proportional to $\exp(-t/\tau)$ and make an angle $\omega_0 t$ from their initial direction. Hence the transverse pumping creates a magnetization in the vapor only for small fields. These predictions have been confirmed experimentally on the odd isotopes of Cd (Lehmann and Cohen-Tannoudji 1964). This phenomenon is very similar to the Hanle effect of excited state, or zero field level crossing (Hanle 1924, Mitchell and Zemansky 1934) which appears in the excited state.

(b) Parametric Resonance

The pumping light beam direction is perpendicular to $\mathbf{H}_0$, but $\mathbf{H}_1 \cos \omega t$ is now parallel to $\mathbf{H}_0$ as shown in Fig. 1.2(d). As the rf field contains only π photons, it is impossible to have transition from one Zeeman sublevel to the other.

In the absence of the rf field, there is no creation of the transverse magnetization except for $\omega_0 \tau \ll 1$. Neverthless, as we vary H_0, ω being fixed, and observe the absorption of the pumping light, we get a full spectrum of resonances. They occur for $\omega_0 = n\omega$. As the intensity of the rf field is increased, we observe no shift and no broadening of the resonance curves. These resonances may be detected at the various harmonics $p\omega$ of the signal. Their intensity as a function of H_1 has been theoretically predicted and experimentally measured (Favré and Geneux 1964, Aleksandrov, Constantinov, Perel'and Khodovoi 1964, Polonsky and Cohen-Tannoudji 1965).

(c) Haroche Resonance

The experimental set-up is very similar to that of ordinary or multiple quantum transitions except for the direction of the pumping light beam which is now perpendicular to $\mathbf{H}_0$ (see Fig. 1.2(e)). An rf field is applied parallel to the pumping light. Keeping ω fixed, we vary ω_0 and look at

the absorbed light of the pumping light beam. No resonance appear for $\omega_0 = (2n + 1)\omega$. However, new resonances appear for $\omega_0 = 2n\omega$. They form an even spectrum, and may be detected on the various harmonics $2p\omega$ in the transmitted light beam. This type of resonance has been experimentally and theoretically investigated by Cohen-Tannoudji and Haroche (1965, 1967, 1969a,b).

On the other hand, Cohen-Tannoudji and Haroche have observed experimen tally (1965) that the Haroche resonance for $\omega_0 = 0$, namely the Hanle curve, is broadened by the oscillating rf field, and this broadening was interpreted as a change in the effective Lande g-factor for atoms strongly coupled to the oscillating field, i.e., the concept of "dressed atom" (1969a,b). Recently, Tsukada and Ogawa (1973a) showed that the broadening of the Hanle curve by the oscillating rf field can be interpreted as the variation of the position and shape of the Haroche resonances.

(d) Off-diagonal Resonance

The evolution of a magnetic moment in a system of paramagnetic particles optically oriented across a constant magnetic field $\mathbf{H}_0$ in the presence of a rotating rf field with frequency ω about $\mathbf{H}_0$ has been investigated independ-ently by Haroche (1971a,b), Aleksandrov and Sokorov (1972) and Tsukada et al (1972). They have shown that under these conditions a distinctive type of magnetic resonance may be realized, differing sharply from ordinary resonance. The resonance is characterized by the build up of a considerable moment with a mean value across the field $\mathbf{H}_0$. Formally, the difference between the ordinary resonance and this type of magnetic resonance reduces to a difference in the type of relaxation. Relaxation in the absence of a variable field leads to the establishment of the longitudinal magnetization. While the relaxation, in which the optical orientation process is included, tends to establish in the system a transverse magnetization. Since transverse

magnetization is associated in the theory with the off-diagonal elements of the density matrix, this type of magnetic resonance can be conventionally called "off-diagonal resonance" by Aleksandrov et al. (1972). All of the transverse resonances, i.e., the Hanle effect, parametric resonance and Haroche resonance, however, are due to the off-diagonal elements of the density matrix. We call "off-diagonal resonance" only for the transverse resonances which are caused by the rotating rf field (see Fig. 1.2 (f)).

A situation closes in principle to "off-diagonal" resonance arisen in the work of Dodd and Series (1961), in which the modulation of the emitted radiation of the excited mercury atoms was studied, for off-diagonal excitation in particular. However, it was not possible to observe the above resonance in the proper sence under the conditions of this work, because of the very large width of the excited levels; for which an over-powerful variable field would be required.

1.4. Outline of the Present Work

The remainder of the paper is organized into five sections and three Appendices. In Chapter 2, we review the equation of motion appropriate to the optically pumped atomic vapor system, and cast into the familiar Bloch equation. The relation between the Bloch equation and the density matrix of spin-1/2 system is studied briefly. We derive the excitation operator and the monitoring operator from considerations of the semiclassical correspondence and by the application of the Wigner-Eckart theorem. Bloch equation for the optical pumping case is adapted to the simple cases. We show that the Hanle effect (level crossing experiment) and the anticrossing experiment can easily be described with the Bloch equation.

In Chapter 3, we discuss the effects of the transverse pumping in the presence of the rotating rf field. The solution of the Bloch equation for

the case of a rotating rf field transverse to the static field predicts the new type resonances for the strong rf field. The same type of resonances have been treated by Haroche (1971a,b) and Aleksandrov and Sokorov (1972). This case is exactly solvable and the authors verify their calculations experimentally. We also solve the case of a rotating rf field, including misalignment effects of the pumping light beam. It is shown that the Hanle curve is broadened by a rotating rf field and is shifted towards high field region as the intensity of the rotating rf field is increased (Tsukada et al. 1972). We then consider the evolution of the magnetization of optically pumped atoms in the presence of two rotating rf fields with different frequencies. It is shown that the new type resonances which are due to the effect of the transverse pumping, together with the ordinary resonance and the multiple quantum resonances, are realized.

Chapter 4 is devoted to the discussions of the effects of the transverse pumping in the presence of an oscillating rf field. As described already, Cohen-Tannoudji and Haroche (1966, 1969b) and Pegg and Series (1970) have pointed out that the atomic g-factor is modified by the nonresonant rf field which is applied perpendicularly to the static magnetic field. We consider the more general case that the rf field is oriented in an arbitrary direction to the static magnetic field, and show by classical and quantum mechanical treatments that the g-factor is also modified by the oscillating rf field when the parametric resonances take place (Yabuzaki et al. 1972a). The anisotropy of the atomic g-factor (Landré et al. 1970) is also shown (Yabuzaki et al. 1972b).

In Chapter 5, we deal with the interaction between optically pumped atoms and the strong rf field. The calculation of the positions and shapes of the Haroche resonances for large intensity rf field, which differs from earlier work for weak rf field by Cohen-Tannoudji and Haroche (1965, 1967), are given

by use of Stenholm's technique (1973a). Then it is shown that the variation of the width of the Hanle curve by the oscillating rf field, i.e., the modification of the atomic g-factor, is due to the Haroche resonances (Tsukada and Ogawa 1973a,b).

We then treat the saturation effects for the more general case that the static magnetic field directs to an arbitrary direction with respect to the oscillating rf field. It is shown that the new type resonances similar to the Haroche resonance appear when the parallel component of the static field with respect to the oscillating rf field is equal to the integral multiple of the oscillating frequency (Tsukada and Ogawa 1973b, Tsukada, Koyama and Ogawa 1973a,b).

Finally, in Chapeer 6, we summarize our findings. The paper concludes with Appendices in which certain aspects of the calculation are clarified.

CHAPTER 2

BLOCH EQUATION AND MONITORING OPERATOR

2.1. Introduction

The theory of electron- and nuclear-spin resonance and the theory of the two level maser have in common the interaction of radiation with a two level system. We shall, first of all, give an identification between the density operator for the spin-1/2 system and the phenomenological Bloch equation. For the optical pumping case, the effects of relaxation or damping and population regeneration or excitation must be added to the equation of motion of the bulk magnetization.

By examining the Bloch equation, the characteristics and line shapes of several different magnetic resonance experiments may be seen.

The evaluation of the monitoring and the excitation operator for spin-1/2 ground state is made. It is well known that the amount of the absorption of the light beam by atoms is related to the component of the magnetization along the direction of the pumping light beam, and has been given by Dehmelt (1957).

In addition, we will consider the behaviors of the magnetic moment in the static field. The Hanle effect (level crossing) and the anticrossing experiment for zero frequency are investigated in detail.

2.2. The Bloch Equation and the Equation of Motion for the Density Operator

2.2.1. The Bloch Equation and the Density Matrix

In quantum statistical mechanics, the properties of a system are fully determined by the density matrix ρ. Its equation of motion is

$$i\hbar \frac{d\hat{\rho}}{dt} = [\hat{\mathcal{H}}, \hat{\rho}] , \tag{2.1}$$

and the average of a physical quantity, corresponding to an operator G, is given by the equation

$$\langle \hat{G} \rangle = \mathrm{Tr}[\hat{\rho}\,\hat{G}] . \tag{2.2}$$

From eqs.(2.1) and (2.2), it follows that the equation of motion of G is

$$i\hbar \frac{d\langle \hat{G} \rangle}{dt} = \langle [\hat{G}, \hat{\mathcal{H}}] \rangle . \tag{2.3}$$

The derivation we give here is for the spin-1/2 case, but it will be seen that it also holds for the general spin-S case. If the spin is in a constant external magnetic field $\mathbf{H}_0$ and an oscillating field $\mathbf{H}_1$, the spin Hamiltonian is

$$\hat{H} = -\frac{1}{2}\gamma\hbar\,(\boldsymbol{\sigma}\cdot\mathbf{H}_0 + \mathbf{H}_1) \tag{2.4}$$

where we have introduce the Pauli spin matrices,

$$\sigma_x = \begin{pmatrix} 0 & 1 \\ 1 & 0 \end{pmatrix}, \qquad \sigma_y = \begin{pmatrix} 0 & -i \\ i & 0 \end{pmatrix}, \qquad \sigma_z = \begin{pmatrix} 1 & 0 \\ 0 & -1 \end{pmatrix}, \tag{2.5}$$

to describe the spin vector of the spin-1/2 particle. If $\mathbf{S}_i$ is the spin vector of the spin-i, the total magnetization will be given by the equation

$$\mathbf{M} = \sum_i \gamma\hbar\,\mathbf{S}_i = N\gamma\hbar\langle \mathbf{S} \rangle , \tag{2.6}$$

where $\langle \ldots \rangle$ denotes an average. From eqs.(2.3) and (2.6) we get

$$\frac{d\mathbf{M}}{dt} = \frac{1}{2} N\gamma\hbar \frac{d\langle\boldsymbol{\sigma}\rangle}{dt} = \frac{N\gamma\hbar}{i\hbar} \langle [\boldsymbol{\sigma}, -\frac{1}{2}\gamma\hbar(\boldsymbol{\sigma}\cdot\mathbf{H}_0 + \mathbf{H}_1)] \rangle . \tag{2.7}$$

Using the commutation relation of the component of $\boldsymbol{\sigma}$, which in symbolic form can be written as follows,

$$[\boldsymbol{\sigma} \times \boldsymbol{\sigma}] = 2 i \boldsymbol{\sigma} \quad . \tag{2.8}$$

We find from eq.(2.7) that

$$\frac{d \mathbf{M}}{dt} = \gamma [\mathbf{M} \times \mathbf{H}] , \tag{2.9}$$

holds, where $\mathbf{H} = \mathbf{H}_0 + \mathbf{H}_1$.

2.2.2. Orientation as a Bulk Magnetization

In the case of the optical orientation it is reasonable to characterize the population differences among the magnetic sublevels of the system by a macroscopic magnetization. In addition, relaxation terms are present in the orientation expressions that describe the rate at which the atoms regain their normal Boltzmann distribution among the sublevels.

Since the ensemble of atoms can be characterized by a magnetization and by relaxation, it is reasonable that the macroscopic magnetic properties of the system can be described by expression similar to the phenomenological equation of Bloch (1946) which were formulated to describe the motion of nuclear moments in the presence of external magnetic fields. The solutions of these equations would then describe the behavior of the system of optically pumped atoms. The boundary values for the equations could be specified by a given set of experimental conditions.

In the absence of a pumping process or relaxation, the time variation of the magnetization $\mathbf{M}$ per unit volume of ensemble of atoms is given by eq.(2.9). In the case of nuclear magnetism, the Bloch equation is obtained by adding relaxation terms to eq.(2.9) which then becomes

$$\frac{d \mathbf{M}}{dt} = \gamma [\mathbf{M} \times \mathbf{H}] - \frac{M_x \mathbf{i} + M_y \mathbf{j}}{T_2} - \frac{M_z - M_0}{T_1} \mathbf{k} \tag{2.10}$$

Here **i**, **j**, **k** unit vectors in the laboratory coordinate system, and M_x, M_y and M_z are the components of **M** in this coordinate system. M_0 is the z-component value of the magnetization when the ensemble of magnetic moment has achieved a normal Boltzmann distribution. It is assumed that a steady external magnetic field is applied along the **k** direction. T_1 and T_2 are the longitudinal and the transverse relaxation times, respectively, and describe the rate at which the component of M relax along their respective directions.

The usual procedure is to solve eq.(2.10) for M_x, M_y and M_z with particular boundary conditions. These are usually dictated by the experimental conditions and the range of t in which one is interested **H** is generally composed of a steady magnetic field $\mathbf{H}_0$ (applied along the **k** direction) plus a magnetic field $\mathbf{H}_1(t)$ with the frequency ω are experimental variables contained in the expressions for M_x, M_y and M_z.

When optical pumping is also taking place the state populations and, hence, the magnetization are changed from the normal Boltzmann value. This change can be introduced by simply adding the contribution that comes from pumping. If the pumping is such that it changes the total z component of the angular momentum of the ensemble of atoms, the contributions to be added will be

$$\frac{M_0^p - M_z}{T_p} \mathbf{k} \ , \qquad (2.11)$$

where M_0^p is the maximum equilibrium value of M_z while pumping is taking place and T_p is the "optical pumping time" for this process to occur. It must be noted that M_0^p is a constant determined by three factors: T_1, the transition probabilities for excitation of the atom, and the intensity of light used for the pumping process. Usually M_0^p is much larger than the

normal Boltzmann distribution, which enables one to neglect the M_0 term for most problems. Equation (2.10) for the optical pumping case now becomes

$$\frac{d\mathbf{M}}{dt} = \gamma[\mathbf{M}\times\mathbf{H}] - \frac{M_x\,\mathbf{i} + M_y\,\mathbf{j}}{T_2} - \left(\frac{M_z}{T_1} + \frac{M_0^p - M_z}{T_p}\right)\mathbf{k} \quad . \tag{2.12}$$

If we assume that the longitudinal and the transverse relaxation times are equal to each other, i.e., $T_1 = T_2 = T$, eq.(2.12) becomes

$$\frac{d\mathbf{M}}{dt} = \gamma[\mathbf{M}\times\mathbf{H}] + \frac{\mathbf{M}_0' - \mathbf{M}}{\tau} \quad , \tag{2.13}$$

where

$$\mathbf{M}_0' = \frac{\tau}{T_p}\,\mathbf{M}_0^p \quad , \tag{2.14a}$$

$$\tau^{-1} = T_p^{-1} + T^{-1} \quad . \tag{2.14b}$$

Hereafter, we will use eq.(2.13) for investigation of the magnetic properties of various experimental configurations.

The eq.(2.13) have the same structure as the Bloch equation. In the Bloch equation, $\mathbf{M}_0'$ is the thermal equilibrium magnetization, given by Boltzmann factor, and usually parallel to the applied static field $\mathbf{H}_0$. For optical pumping case, usually $\mathbf{M}_0'$ is much larger than the normal Boltzmann distribution, which, as mentioned above, enables one to neglect $M_0\,\mathbf{k}$ term for most problems. Therefore, $\mathbf{M}_0'$ is essentially created by the optical pumping and is parallel to the pumping light. Namely, $\mathbf{M}_0'$ is not forced to be parallel to the static field $\mathbf{H}_0$. The fact that $\mathbf{M}_0'$ and $\mathbf{H}_0$ are not parallel to each other, i.e., the transverse optical pumping, is essential in the optical pumping experiments and leads the interesting effects. We will mainly investigate the effects of the transverse optical pumping in the following Chapters.

2.3. Monitoring Operator and the Exciting Operator

In optical double-resonance experiments, a bulk sample of particles, usually a vapour with suitable spectroscopic properties, is polarized by an optical pumping cycle represented by particular ρ^0. The monitoring process consists of observing the intensity of absorbed or emitted light which connected the ground states and excited states. The light itself has a polarization state represented by the vector **e**, which describes the direction and relative phase of the electric field component of the light. The monitoring beam for absorption experiments is usually derived from a discharge lamp, containing the same element as the sample, which emits an adequately strong line in electric dipole transition. After passing through the sample the partially scattered or absorbed beam is detected by a photodetector, which may either be sensitive only to quasistatic variations as the static field H_0 is varied through the resonance value, or may be tuned to the fundamental or harmonics of ω , and followed by a phase sensitive amplifier.

It is easy to find the form of the optical monitoring operator for experiments of this type from considerations of the semiclassical correspondence and by the application of the Wigner-Eckart theorem. There are a number of subtle points concerning the lifetime of the excited states and the spectral distribution of the light. These effects happily do not concern us in these examples if we consider that the spectral distribution of the light beam is sufficiently broad to cover or overlap the group of states of excited or ground, and this is the usual case because of the fact that the spectral distribution from the lamp is always as broad as, and usually broader than, that of the absorbing sample.

In this semiclassical model of absorption, the electric field of the incident light induces an electric dipole moment of the atom which is

proportional to the field and is represented by a dipole matrix element. The absorption on which our monitoring operator depends is proportional to the quantum mechanical transition rate, which is well known to be dependent on the square of the field or the square of the dipole matrix element. The form of the monitoring operator is

$$Q = K' \sum_{\mu} \langle m | \mathbf{e} \cdot \mathbf{P} | \mu \rangle \langle \mu | \mathbf{e}^* \cdot \mathbf{P} | m' \rangle \ , \tag{2.15}$$

where the individual brackets are the matrix elements of the electric dipole operator $\mathbf{P}$ or appropriate to the polarization $\mathbf{e}$ of the incident light, taken between the states m which are monitored, and a final state or states μ. This form for Q is applicable not only to absorption but also to emission because of the fact that both processes are proportional to the square of the electric dipole matrix element even though they differ in magnitude by the ratio of the Einstein B and A coefficients. The Q operator is identical to the $G \cdot G^*$ of Dodd and Series (1961).

To evaluate Q we make use of the matrix elements (Condon and Shortley 1951) written below for reference

$$\begin{aligned}
&\langle n,j,m \,|P|\, n',j+1,m\pm1 \rangle = \mp P_1(n,n',j,j') \, \tfrac{1}{2}[(j\pm m+1)(j\pm m+2)]^{1/2}(x \pm iy) \ , \\
&\langle j,m \,|P|\, j+1,m \rangle = P_1 \, [(j+1)^2 - m^2]^{1/2} \, z \ , \\
&\langle j,m \,|P|\, j,m\ 1 \rangle = P_0 \, \tfrac{1}{2} [(j \mp m)(j \pm m + 1)]^{1/2} \, (x \pm iy) \ , \\
&\langle j,m \,|P|\, j,m \rangle = P_0 \, m \, z \ , \\
&\langle j,m \,|P|\, j\ 1,m\ 1 \rangle = P_{-1} \, \tfrac{1}{2} [(j \mp m)(j \mp m - 1)]^{1/2} \, (x \pm iy) \ , \\
&\langle j,m \,|P|\, j-1,m \rangle = P_{-1} \, [j^2 - m^2]^{1/2} \, z \ .
\end{aligned} \tag{2.16}$$

These elements consist of a reduced matrix element depending on specific spectroscopic information involving the principle quantum number (shown in the first example and omitted from the notation in the remainder) and the

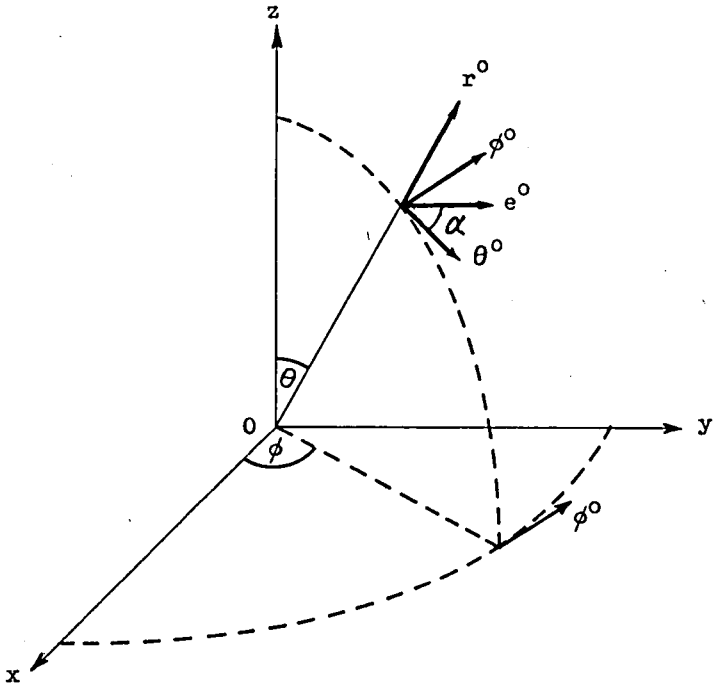

Fig. 2.1 The direction of the light beam and the electric vector.

spectroscopic configuration. This reduced matrix element is multiplied by Clebsh-Gordon coefficient depending only on the angular momentum. This separation is an example of the Wigner-Eckart theorem (for example Slichter 1963). It is convenient because we are concerned with transitions between a group of m levels and another group of μ levels, and can therefore absorb the reduced matrix element in the K' constant and find the form of Q from the angular momentum coefficients alone.

The evaluation of M_0' for spin-1/2 ground state is made. This case is of the most simple model: optical pumping for D_1 line of alkali atoms by neglecting the nuclear momentum: transition $^2S_{1/2} \leftrightarrow {}^2P_{1/2}$. It has been well known that the hypothetical alkali atom of zero nuclear spin behaves as a spin-1/2 particle. The calculation based on such a model has a particularly simple form and provides an adequate approximation to the behavior of real alkali atoms. The hypothetical alkali atom model is adopted for the evaluation of M_0' of D_1 optical pumping. Related energy levels of the atom in a weak magnetic field and relative transition probabilities between the Zeeman sublevels were already shown in Fig.1.1.

Let the electric field of the incident light at time t be $\mathbf{E}_i(t) = E_i(t)\, \mathbf{e}_i^0$, where $\mathbf{e}_i^0$ is a unit vector representing the direction of polarization. Let the direction of the light be specified by θ, ϕ, and let the electric vector make an angle α with the unit vector associated with θ as shown in Fig.2.1. Then

$$\begin{aligned} \mathbf{e}^0 = {} & \mathbf{i} \left(\cos\theta \cos\phi \cos\alpha - \sin\phi \sin\alpha \right) \\ & + \mathbf{j} \left(\cos\theta \sin\phi \cos\alpha + \cos\phi \sin\alpha \right) \\ & + \mathbf{k} \left(- \sin\theta \cos\alpha \right) . \end{aligned} \tag{2.17}$$

In eq.(2.15) the matrix $\mathbf{e}\cdot\mathbf{P}$ is written as

$$\langle n,1/2,m|\mathbf{e}\cdot\mathbf{P}|n',1/2,\mu\rangle \propto \langle n,1/2 \| P \| n',1/2\rangle \begin{vmatrix} e_z & e_- \\ e_+ & -e_z \end{vmatrix}, \tag{2.18}$$

where the components of the unit electric field polarization vector $\mathbf{e}$ are given by $e_{\pm} = e_x \pm ie_y = (\cos\theta\ \cos\alpha \pm i\sin\alpha\ )\exp(\pm i\phi\ )$, $e_z = -\sin\theta\ \cos\alpha$. For the case of arbitrary linear polarization,

$$\sum_{\mu} \langle m|\mathbf{e}\cdot\mathbf{P}|\mu\rangle\langle\mu|\mathbf{e}^*\cdot\mathbf{P}|m'\rangle \propto |\langle n,1/2\,\|\,P\,\|\,n',1/2\rangle|^2 \begin{vmatrix} 1 & 0 \\ 0 & 1 \end{vmatrix}. \tag{2.19}$$

Since the application of eq.(2.19) to $\mathbf{M}_0^p$ in eq.(2.14a) can produce no magnetization, i.e., $\mathbf{M}_0^p = 0$, no magnetic resonance is observed as the intensity of the static field $\mathbf{H}_0$ is varied. If one uses circularly polarized light, then the matrix of $\mathbf{e}\cdot\mathbf{P}$ (Gallagher et al. 1963) becomes

$$\begin{aligned} &\begin{vmatrix} e_z & e_- \\ e_+ & -e_z \end{vmatrix}_{\alpha=0} \pm i \begin{vmatrix} e_z & e_- \\ e_+ & -e_z \end{vmatrix}_{\alpha=90^\circ} \\ &= \begin{vmatrix} -\sin\theta & \cos\theta\ e^{-i\phi} \\ \cos\theta\ e^{i\phi} & \sin\theta \end{vmatrix} \pm i \begin{vmatrix} 0 & -ie^{-i\phi} \\ e^{i\phi} & 0 \end{vmatrix} \\ &= \begin{vmatrix} -\sin\theta & (\cos\theta \mp 1)e^{-i\phi} \\ (\cos\theta \pm 1)e^{i\phi} & \sin\theta \end{vmatrix}, \end{aligned} \tag{2.20}$$

and the matrix (2.15) now becomes

$$\begin{vmatrix} 1 \mp \cos\theta & \mp \sin\theta\ e^{i\phi} \\ \mp \sin\theta\ e^{-i\phi} & 1 \pm \cos\theta \end{vmatrix}, \tag{2.21}$$

which gives nonzero magnetization, and we can observe the magnetic resonance as the static field is varied, where the upper and lower signs refer to the circular polarization of the pumping light. Then we can obtain the components of $\mathbf{M}_0^p$ as follows;

$$M_{0x}^p = Q_{1/2,1/2} + Q_{-1/2,1/2} = \mp 2\sin\theta\ \cos\phi\ M_0^p\ , \tag{2.22a}$$

$$M_{0y}^p = i(Q_{-1/2,1/2} - Q_{1/2,-1/2}) = \mp 2\sin\theta\ \sin\phi\ M_0^p\ , \tag{2.22b}$$

$$M^{p}_{0z} = Q_{1/2,1/2} - Q_{-1/2,-1/2} = \mp 2 \cos\theta \; M^{p}_{0} \; . \qquad (2.22c)$$

These results are completely equivalent to the values which are easily expected by projecting the unit vector directed along the pumping light beam, specified by θ , ϕ, into the axes on the coordinate system.

It is well known that the amount of the absorption of the light beam by atoms is related to the component of the magnetization along the direction of the light beam, and given by the following equation (Dehmelt 1957)

$$S = K [1 - a (M_n / M'_0)]. \qquad (2.23)$$

Here K is the absorption coefficient for the unpolarized vapour, while a is a dimensionless constant depending on the degree of polarization attained and also on nuclear effects.

2.4. Behavior of the Magnetic Moment in a Static Field

2.4.1. The Hanle Effect

Let us start with a simple remark concerning the polarization that the light beam must have in order to achieve a transverse pumping. Let Oz be the direction of the field H_0 with the light beam propagated along Ox and having a right circularly polarized with respect to this direction (see Fig.2.2).

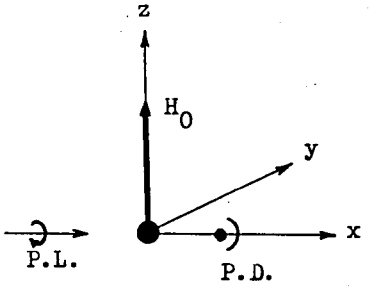

Fig. 2.2 Schematic diagram of the Hanle effect

A solar cell or photo detector PD measure the variation of the intensity of the light beam which transmitted through the sample cell. We investigate the variation with H_0 of optical signal S, i.e., M_x, when the value of H_0 vary near the value zero very slowly. We are interested in the steady state solution as a function of the magnitude of field H_0. For this case, the Bloch equation becomes as follows;

$$\frac{dM_x}{dt} = \omega_0 M_y + \frac{M_0'}{\tau} - \frac{M_x}{\tau} , \tag{2.24a}$$

$$\frac{dM_y}{dt} = -\omega_0 M_x - \frac{M_y}{\tau} , \tag{2.24b}$$

$$\frac{dM_z}{dt} = -\frac{M_z}{\tau} . \tag{2.24c}$$

At steady state, i.e., $dM_x/dt = dM_y/dt = dM_z/dt = 0$, we can immediately obtain the steady state solutions

$$M_x = \frac{1}{1 + (\omega_0 \tau)^2} M_0' , \tag{2.25a}$$

$$M_y = -\frac{\omega_0 \tau}{1 + (\omega_0 \tau)^2} M_0' , \tag{2.25b}$$

$$M_z = 0 . \tag{2.25c}$$

M_z remains always zero. The magnetic dipole of an atom which has been just pumped by the light beam of Fig.2.2, is pointing along the Ox direction. Immediately afterwards it begins to precess around H_0 at the Larmor frequency of the ground state ω_0. After a mean time τ, the atom undergoing a disorientating collision or absorbs another photon and it's orientation is destroyed or change completely.

In order to obtain the whole transverse magnetization of the vapour at a given time t_0, we have to take the resultant of all the dipoles which have

been pumped at time $t<t_0$ and which have not yet undergone a disorientating process at time t_0. All these dipoles form a kind of a fan, starting from the Ox axis and having an average angular spread is very small; the resultant has its maximum value and is directed along Ox. When ω_0 increase, the fan opens, the resultant decreases, and rotates: a M_y component appears. When $\omega_0\tau \gg 1$, the fan has become isotropic in the plane perpendicular to H_0 so that the resultant is now zero.

These predictions have been confirmed experimentally on the odd isotopes of Cd (Lehman and Cohen-Tannoudji 1964). This phenomenon is very similar to the Hanle effect (Hanle 1934, Mitchell and Zemansky 1934) which appears in the excited state.

For more general case that the pumping light beam makes an angle θ with respect to the static field H_0, the magnetization along the pumping light beam, M_n, is easily given in the same manner and is given in the form

$$M_n = \frac{1}{1 + (\omega_0\tau)^2} M_0' \sin^2\theta + M_0' \cos^2\theta. \qquad (2.26)$$

The first term on the right hand side of eq.(2.26) is due to the transverse pumping or the Hanle effect and the second term is due to the longitudinal pumping.

2.4.2. Anticrossing Experiment

We consider the variation of the magnetization in the sample cell which is optically pumped for the case that the field added to the ambient field is sweeping from negative to positive through zero in an arbitrary direction. As shown in Fig.2.3, we choose the sweeping field axis as z direction, and x axis is chosen in the direction of the component of the ambient field which exists on the perpendicular plane to the z axis. In Fig.2.3, P.L. shows the pumping light, H_z and H_r are Oz component and

xy plane component of the ambient field, respectively. ϕ is the angle between $\mathbf{H}_r$ and the projection on the xy plane of the pumping light direction and θ is the angle between z axis and the pumping light beam. The strength of the compositive field along the z axis becomes $H_s + H_z$.

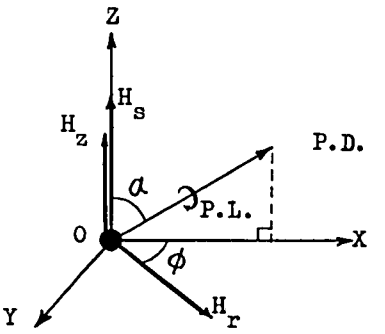

Fig. 2.3 Schematic diagram of the anticrossing experiment for zero frequency.

In this situation, the angle ζ between the pumping light beam and the total field direction which is the compositive vector of $\mathbf{H}_r$, $\mathbf{H}_z$ and $\mathbf{H}_s$ is given as follows;

$$\cos\zeta = \frac{H_r \cos\phi \sin\theta + H_s \cos\theta}{[\,(H_s + H_z)^2 + H_r^2\,]^{1/2}} \tag{2.27}$$

Substituting this into eq.(2.26), we can obtain

$$M_n = \frac{1}{1 + (\omega_0\tau)^2}\left[(\omega_r\tau)^2(\cos^2\phi \sin^2\theta - \cos^2\theta) + \omega_r \omega_s \tau^2 \cos\phi \sin 2\theta + (\omega_0\tau)^2\cos^2\theta + 1\right] M_0' , \tag{2.28}$$

where

$$\omega_0^2 = (\omega_s + \omega_z)^2 + \omega_r^2 \tag{2.29a}$$

$$\omega_s = \gamma H_s, \quad \omega_z = \gamma H_z, \quad \omega_r = \gamma H_r. \tag{2.29b}$$

For $\theta = 0$, M_n becomes as follows;

$$M_n = \frac{1 + (\omega_s + \omega_z)^2\tau^2}{1 + (\omega_0\tau)^2} M_0' . \qquad (2.30)$$

While, for $\theta = \pi/2$, M_n becomes

$$M_n = \frac{1}{1 + (\omega_0\tau)^2}[(\omega_r\tau)^2\cos^2\phi + 1] M_0' . \qquad (2.31)$$

Equation (2.30) has the same form as M_z of the ordinary resonance which will be descrived Sec. 3.2. The half width at half maximum of the lines of eqs.(2.30) and (2.31), $\delta\omega$, is given by

$$\delta\omega = [(\frac{1}{\tau})^2 + \omega_r^2]^{1/2} . \qquad (2.32)$$

Figures 2.4 show the line shapes of M_n calculated with eq.(2.28): (a) and (b) are for $\omega_r = 500$, $\tau = 1$, $\phi = 0$ and $\pi/4$, respectively, and (c) and (d) are for $\omega_r = 1$, $\tau = 1$, $\phi = 0$ and $\pi/4$, respectively.

Experimental results are shown in Fig.2.5. In this experiment, the axis of a double Helmholtz coil is nearly oriented to the direction of the geomagnetic field to minimize the anbient field H_r and the sweeping field H_s is created by the Helmholtz coil. The experimental results show a good agreement with the theoretical results in Fig.2.4(b).

By using the anticrossing curves, we may decide the field direction. Indeed, Aleksandrov , Bonch-Bruevich and Khodovoi (1967) show the posibilities of measuring weak magnetic fields by method of optical orientation of atoms. Their theoretical analysis shows that the optimum objects are alkali-metal atoms, and the optimum mode is that of extremely low intensities of the orienting light. It has also been shown that when the object and the optical-orientation regime are optimally chosen, their proposed method guarantees a maximum sensitivity not worse than 10^{-11} Oe at a recording-equipment bandwidth of 1 Hz.

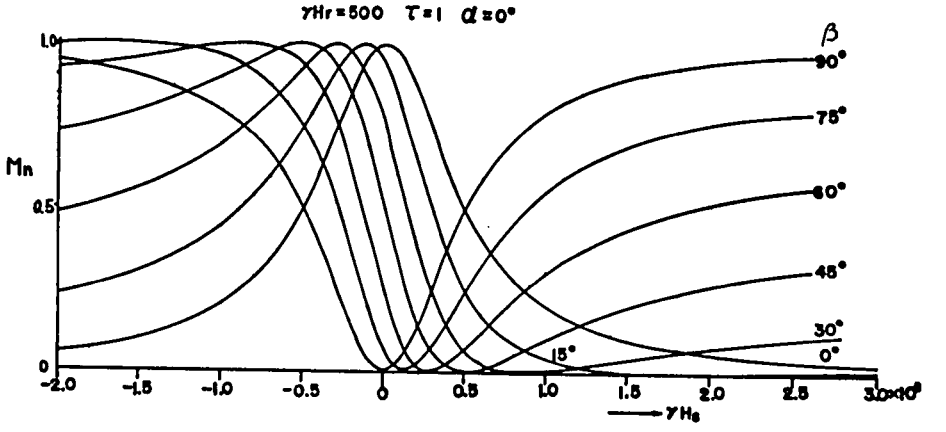

(a)

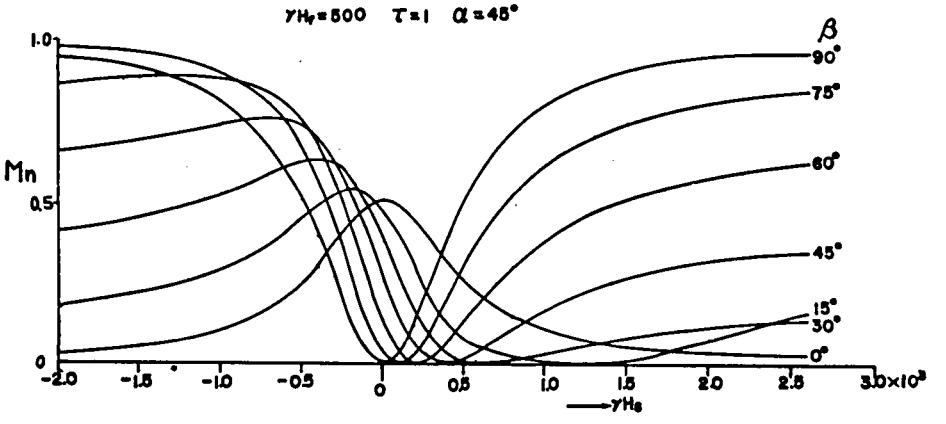

(b)

Fig. 2.4 (a), (b). For legend see P.34.

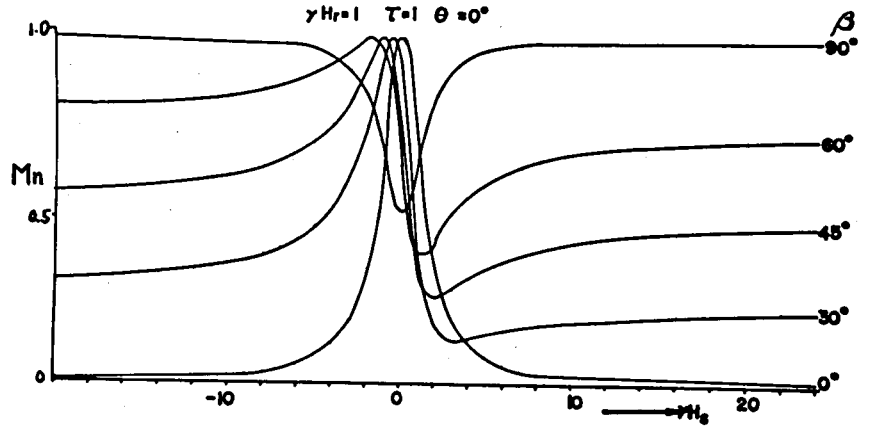

(c)

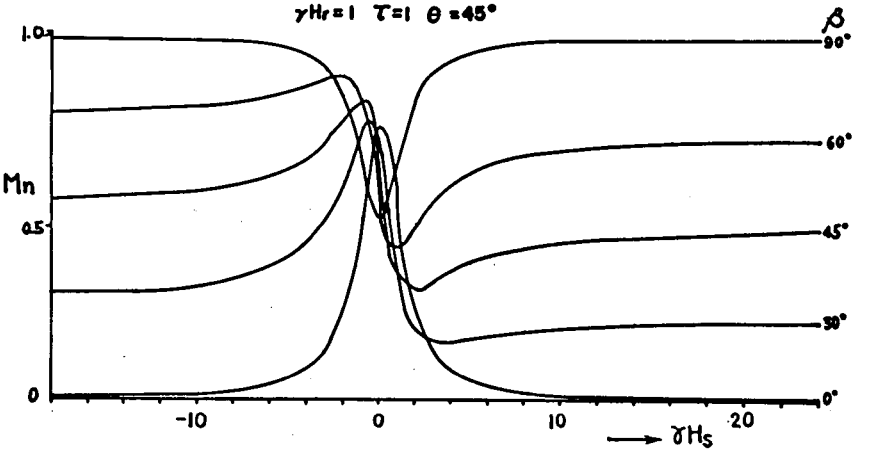

(d)

Fig. 2.4 Theoretical curves for the anticrossing experiment. (a) $\gamma H_r = 500$, $\tau = 1$, $\theta = 0^\circ$, (b) $\gamma H_r = 500$, $\tau = 1$, $\theta = 45^\circ$, (c) $\gamma H_r = 1$, $\tau = 1$, $\theta = 0^\circ$, (d) $\gamma H_r = 1$, $\tau = 1$, $\theta = 45^\circ$.

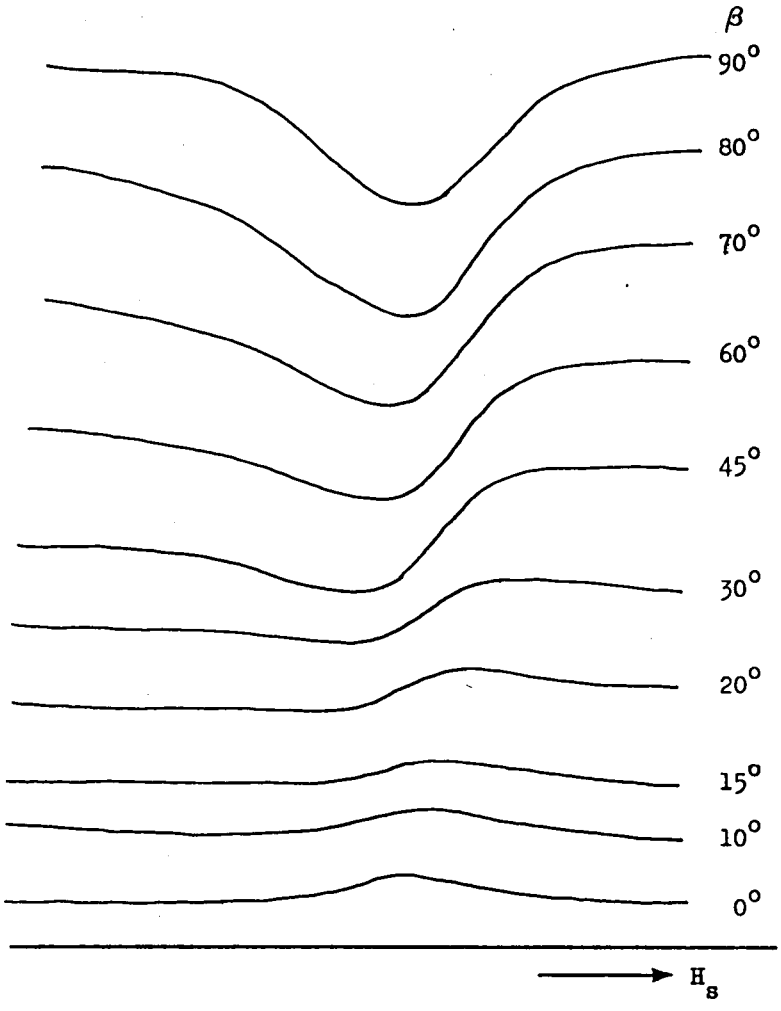

Fig. 2.5. Experimental recordings for anticrossing curves for zero frequency.

2.5. Conclusion

We have shown the equivalence between the equation of motion of the density matrix for spin 1/2 and the phenomenological Bloch equation. In the steady state resonance of the usual "bulk" magnetization we must include the effects of relaxation or damping, and of population regeneration. To this end, for the optical pumping case, the effects of relaxation or damping and population regeneration or excitation have been added to the equation of motion of the bulk magnetization in the magnetic field. By using the Bloch equation (2.13) obtained in 2.2.2, we will examine the characteristics and line shapes of the various magnetic resonances.

The evaluation of the monitoring and the excitation operator between $S_{1/2}$ and $P_{1/2}$ states has been given. It is well known that the amount of the absorption of the light beam by atoms is related to the component of the magnetization along the direction of the pumping light beam (Dehmelt 1957).

By using the Bloch equation (2.13), we have analyzed the behaviors of the magnetic moment in the static field. Two types of situations have analyzed. One corresponds to the level crossing or the Hanle experiment, and the other corresponds to the anticrossing experiment. The level crossing experiment is essentially an interference phenomenon. When the levels are degenerate, the intensity of the transmitted light increases. The anticrossing signal is the same as a double resonance signal, but in the one case the perturbation is static, and in the other, rf field H_1.

CHAPTER 3

EFFECTS OF THE TRANSVERSE PUMPING IN THE PRESENCE OF THE ROTATING RF FIELDS

3.1. Introduction

In the usual double resonance experiments atoms are subjected to the static magnetic field H_0 and the rf field $H_1(t)$ oscillating in the plane perpendicularly to the field H_0 with angular frequency ω , together with the circurarly porarized light beam which has two roles to create the magnetization in the ensemble of atoms along the direction of the light beam and to monitor the variation of this component of magnetization.

Workers in the magnetic resonance have often obtained solutions for spin flip transition probabilities by solving the corresponding classical problem of spinning dipole in a magnetic field using a rotating frame (Rabi, Ramsey and Schwinger 1954). Feynman et al.(1957) and terr Harr (1966) have in fact shown that the semiclassical Schrodinger equation for a two state system is mathematically equivalent to the phenomenological Bloch equation. Hence the Bloch equation may interpret the multiple quantum transitions, the Bloch-Siegert shift (Bloch and Siegert 1940) and other quantum mechanical effects.

At present, there exists an optical method of creation of magnetization which makes it possible to create magnetization in an arbitrary direction with respect to the magnetic field. In particular, a characteristic case is possible when magnetization is created across the static field by means of circurarly polarized light beam. It is obvious that when the rate of creation of magnetization is slow compared with the period of precession of the magnetization in the field,no significant magnetization will build up in the system. The situation, however, is changed when time

varing magnetic field is applied. An interesting case, called parametric resonance, arises when the oscillating rf field is parallel to the static field (Aleksandrov et al. 1966, Polonsky and Cohen-Tannoudji 1965).

Under the irradiation to an atomic vapor with optical and rf fields, Bell and Bloom (1957) have detected the modulation of the light at ω in cross-beam experiment. They have used a phenomenological model, based on Bloch equation, to interpret their experimental result. But the effect of the transverse optical pumping of the monitoring beam directed perpendicularly to $\mathbf{H}_0$ was neglected. Their treatment is justified only the case that the magnetic field $\mathbf{H}_0$ is much larger than the rf field $\mathbf{H}_1$. While in the case that the pumping beam and $\mathbf{H}_1$ are perpendicular to the field $\mathbf{H}_0$, the effect of the transverse pumping has been analyzed by using density matrix and iteration method by Cohen-Tannoudji and Haroche (1967). They have then observed the new type resonances in the modulation of the transmitted light beam with mercury vapor, and the resonances have been called " Haroche resonance " by Cohen-Tannoudji (1968). These resonances appear in the various even harmonics $2p\omega$ of the transmitted light when $H_0 = 2n\omega/\gamma$,(n=1,2,...) for weak rf field and are shifted but not broadened as the intensity of the rf field is increased.
Recently, we have analyzed the effect of the transverse pumping in the case that the direction of the pumping light beam and nonresonant rf field which is parallel to the pumping light beam, makes an arbitrary angle with respect to $\mathbf{H}_0$ (Yabuzaki et al. 1972a). And we have shown by classical and quantum mechanical treatments the fact that the atomic g-factor is modified by the nonresonant rf field when the Hanle effect and parametric resonance take place. This fact will be shown in chapter 4.

In section 3.2., we consider the situation that the direction of the pumping light beam makes an arbitrary angle θ with respect to the field

H_0 and the direction of the rf field is perpendicular to the field H_0 (Tsukada et al.1972). If the angle θ is chosen at 90°, this situation coincides with that of experiment by Cohen-Tannoudji and Haroche (1966, 1969a,b), and if θ is chosen at 0°, this situation coincides with that of the ordinary magnetic resonance. We analyze this situation by using the phenomenological Bloch equation which is obtained in chapter 2. We show that the Hanle effect and the new type resonances appear in the unmodulated or dc component and the component modulated at ω , in addition to the component modulated at 2ω predicted by the theory of Cohen-Tannoudji and Haroche (1967,1969a,b). It is shown theoretically and experimentally that the new type resonances are strongly broadened by increasing the rf field.

We carry out the experiments with optically pumped cesium vapor by using the effective field in a rotating system. Because the effective field can be easily made so weak that the transverse pumping plays an important role. We mainly investigated the character of the new type resonances which appear in the components modulated at ω and 2ω and dc component in the transmitted light.

In section 3.3., the evolution of the magnetization in a system of paramagnetic particles in the presence of two rotating rf fields with frequencies ω_a and ω_b is investigated with the phenomenological Bloch equation. In this case, the paramagnetic particles are optically oriented to an arbitrary direction to the static field H_0. Consequently, the results obtained here might be applicable to the special case that the rf field is elliptically polarized or linearly polarized. As one might expect, the multiple quantum transitions take place at $\omega_0 = 2\ \omega_a - \omega_b$, and $2\ \omega_b - \omega_a$ corresponding to the three photon process and at $\omega_0 = -2\,\omega_a + 3\,\omega_b$ correspond to the five photon process, in addition

to the ordinary magnetic resonances at $\omega_0 = \omega_a$ and ω_b. In addition to these resonances, the results of the calculation predict the new type resonances which are due to the effect of the transverse optical pumping. The new type resonances take place at $\omega_0 = 0, 2\omega_a, 2\omega_b, \omega_a \pm \omega_b$ and $\pm 2(\omega_a - \omega_b)$ etc. for the two rotating rf fields.

Since the maximum magnitude of the ordinary and the multiple quantum resonances are obtained when the pumping light beam is parallel to the static field H_0, these type of resonances can be conventionally called " longitudinal resonance ". On the other hand, the maximum magnitude of the new type resonances are obtained when the pumping light beam is perpendicular to H_0, therefore these type of resonance can be conventionally called " transverse resonance ". It is also shown that the transmitted light beam propagating through the system of atoms, or sample cell, contains the beat frequencies such as $\omega_a - \omega_b$, $\omega_a - 2\omega_b$, $2\omega_a - \omega_b$ and $2(\omega_a - \omega_b)$ etc., and the Hanle curve corresponding to the transverse resonance at $\omega_0 = 0$ is broadened by not only the oscillating rf field (Cohen-Tannoudji and Haroche 1969b) but also the rotating rf field.

3.2. Effects of the Transverse Pumping in the Presence of a Rotating RF Field

A theoretical and experimental study has been made of the effect of transverse optical pumping in the optical-rf double resonance. The solution of Bloch equation shows that the Hanle effect and the new type resonances, i.e., the off-diagonal resonance, become notable in the weak magnetic field or for strong rf field, as the effect of the transverse pumping. The new type resonances appear in the unmodulated component and the components modulated at the first and the second harmonics of the applied rf frequency in the pumping light beam transmitted through the vapor cell. It is pre-

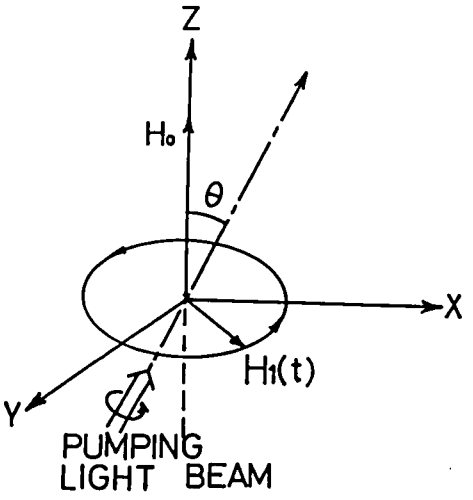

Fig. 3.1. Direction of the magnetic fields and of the pumping light beam for the situation to be considered.

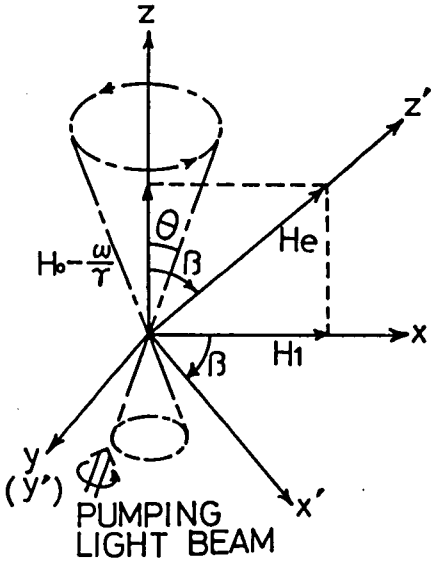

Fig. 3.2. Directions of the magnetic fields and of the pumping light beam in the coordinate system which rotates with the angular frequency ω. The direction of the pumping light beam rotates around Z axis with angular frequency $-\omega$.

dicted that the new type resonances are not only shifted but also broadened as the intensity of the rf field is increased. The shift, broadening and the amplitude for observed new type resonances are in good agreement with the theoretical prediction within the middle strength of the rf field.

3.2.1. Theory

We consider about the behaviors of the magnetization for the case of a rotating rf field transverse to the static field $\mathbf{H}_0$ (see Fig.3.1). A transformation to a system rotating about $\mathbf{H}_0$(Z axis) at a frequency ω makes magnetic field "time independent". In the Oxyz coordinate system as shown in Fig.3.2, the total magnetic field becomes an effective magnetic field $H_e = [(H_0 - \omega/\gamma)^2 + H_1^2]^{1/2}$ and the direction of the pumping light beam rotates with the angular frequency ω about the z axis. The direction of $\mathbf{H}_e$(z' axis) is given by the angle $\beta = \tan^{-1}[H_1/(H_0 - \omega/\gamma)]$ with respect to the x axis. Hence, by a further rotation of the coordinate system Oxyz about the y axis through the angle β the new z' axis is made to coincide with the direction of $\mathbf{H}_e$. In the Ox'y'z' coordinate system, we obtain the equations governing the motion of three components of the macroscopic magnetization $\mathbf{M}$ as follows;

$$\frac{d M_{x'}}{dt} = \frac{1}{\tau}(- M_0' \cos\theta \sin\beta + M_0' \sin\theta \cos\beta \cos\omega t - M_{x'}) + \omega_e M_{y'} , \tag{3.1a}$$

$$\frac{d M_{y'}}{dt} = \frac{1}{\tau}(M_0' \sin\theta \sin\omega t - M_{y'}) - \omega_e M_{x'} , \tag{3.1b}$$

$$\frac{d M_{z'}}{dt} = \frac{1}{\tau}(M_0' \cos\theta \cos\beta + M_0' \sin\theta \sin\beta \cos\omega t - M_{z'}), \tag{3.1c}$$

where

$$\omega_0 = \gamma H_0, \quad \Delta\omega = \omega_0 - \omega , \quad \omega_1 = \gamma H_1, \quad \omega_e = \gamma H_e, \tag{3.2a}$$

$$\omega_e = (\Delta\omega^2 + \omega_1^2)^{1/2} \quad , \quad \beta = \tan^{-1} (\omega_1/\Delta\omega). \qquad (3.2b)$$

Using the relation

$$M_{+'} = M_{x'} + i M_{y'} , \qquad (3.3)$$

we obtain the following two equations which are equivalent to three differential equations (3.1) in the form

$$\frac{d M_{+'}}{dt} = \frac{1}{\tau} (- M_0' \cos\theta \sin\beta + M_0' \sin\theta \cos\beta \cos\omega t + i M_0' \sin\theta \sin\omega t) - \frac{1}{\tau} (1 + i \omega_e \tau) M_{+'} , \qquad (3.4a)$$

$$\frac{d M_{z'}}{dt} = \frac{1}{\tau} (M_0' \cos\theta \cos\beta + M_0' \sin\theta \sin\beta \cos\omega t - M_{z'}) \qquad (3.4b)$$

Equations (3.4) can be solved and the steady state solutions are given as follows;

$$\begin{aligned} M_{+'} = & - \frac{M_0' \cos\theta \sin\beta}{1 + (\omega_e \tau)^2} + \frac{1}{2} \frac{M_0' \sin\theta (1 + \cos\beta)}{1 + (\omega_e + \omega)^2 \tau^2} \{ \cos\omega t + (\omega_e + \omega) \tau \sin\omega t \} \\ & - \frac{1}{2} \frac{M_0' \sin\theta (1 - \cos\beta)}{1 + (\omega_e - \omega)^2 \tau^2} \{ \cos\omega t - (\omega_e - \omega) \tau \sin\omega t \} \\ & + i \frac{M_0' \cos\theta \sin\beta}{1 + (\omega_e \tau)^2} + \frac{1}{2} \frac{M_0' \sin\theta (1+\cos\beta)}{1 + (\omega_e + \omega)^2 \tau^2} \{ \sin\omega t - (\omega_e + \omega) \tau \cos\omega t \} \\ & + \frac{1}{2} \frac{M_0' \sin\theta (1 - \cos\beta)}{1 + (\omega_e - \omega)^2 \tau^2} \{ \sin\omega t + (\omega_e - \omega) \tau \cos\omega t \}, \end{aligned} \qquad (3.5a)$$

$$M_{z'} = M_0' \cos\theta \cos\beta + \frac{M_0' \sin\theta \sin\beta}{1 + (\omega\tau)^2} (\cos\omega t + \omega\tau \sin\omega t). \qquad (3.5b)$$

The signal of the absorption of the transmitted light beam are proportional to S given by eq.(2.23). The value of M_n in eq.(2.23) is obtained by evaluating the time variation of the angles between the light beam and each axis of the Ox'y'z' coordinate system. If the quantities $\delta(t)$, $\eta(t)$

and $\xi(t)$ represent the angles between the light beam and x',y' and z' axes respectively, they are given by the following representations

$$\cos\delta(t) = \sin\theta\cos\beta\cos\omega t - \cos\theta\sin\beta \quad , \tag{3.6a}$$

$$\cos\eta(t) = \sin\theta\sin\omega t \quad , \tag{3.6b}$$

$$\cos\xi(t) = \sin\theta\sin\beta\cos\omega t + \cos\theta\cos\beta \quad . \tag{3.6c}$$

Then the total magnetic moment M_n which directs to the light beam becomes

$$M_n = M_{x'}\cos\delta(t) + M_{y'}\cos\eta(t) + M_{z'}\cos\xi(t). \tag{3.7}$$

When we substitute eqs.(3.5) and (3.6) into eq.(3.7), M_n is given in the form

$$M_n = M_n(0) + M_{n,s}(\omega)\sin\omega t + M_{n,c}(\omega)\cos\omega t + M_{n,s}(2\omega)\sin 2\omega t + M_{n,c}(2\omega)\cos 2\omega t, \tag{3.8}$$

where

$$M_n(0) = \left\{\frac{1}{1+(\omega_e\tau)^2}\sin^2\beta + \cos^2\beta\right\}M_0'\cos^2\theta + \left\{\frac{(1+\cos\beta)^2}{1+(\omega+\omega_e)^2\tau^2} + \frac{(1-\cos\beta)^2}{1+(\omega-\omega_e)^2\tau^2} + \frac{2\sin^2\beta}{1+(\omega\tau)^2}\right\}M_0'\sin^2\theta \quad , \tag{3.9a}$$

$$M_{n,s}(\omega) = \frac{1}{2}\left\{-\frac{(\omega+\omega_e)}{1+(\omega+\omega_e)^2\tau^2}(1+\cos\beta) + \frac{(\omega-\omega_e)}{1+(\omega-\omega_e)^2\tau^2}(1-\cos\beta) + \frac{2\omega\tau}{1+(\omega\tau)^2}\cos\beta + \frac{2\omega_e\tau}{1+(\omega_e\tau)^2}\right\}\sin\beta\, M_0'\sin\theta\cos\theta \quad , \tag{3.9b}$$

$$M_{n,c}(\omega) = \frac{1}{2}\left\{\frac{1}{1+(\omega+\omega_e)^2\tau^2}(1+\cos\beta) + \frac{1}{1+(\omega-\omega_e)^2\tau^2}(1-\cos\beta) + \frac{2}{1+(\omega\tau)^2}\cos\beta - \frac{2}{1+(\omega_e\tau)^2}\right\}\sin\beta\, M_0'\sin\theta\cos\theta \quad , \tag{3.9c}$$

$$M_{n,s}(2\omega) = -\frac{1}{4}\left\{\frac{(\omega+\omega_e)}{1+(\omega+\omega_e)^2\tau^2} + \frac{(\omega-\omega_e)}{1+(\omega-\omega_e)^2\tau^2} - \frac{2\omega\tau}{1+(\omega\tau)^2}\right\}\sin^2\beta\ M_0'\sin^2\theta\ , \tag{3.9d}$$

$$M_{n,c}(2\omega) = -\frac{1}{4}\left\{\frac{1}{1+(\omega+\omega_e)^2\tau^2} + \frac{1}{1+(\omega-\omega_e)^2\tau^2} - \frac{2}{1+(\omega\tau)^2}\right\}\sin^2\beta\ M_0'\sin^2\theta\ . \tag{3.9e}$$

The magnetic moment M_n contains the unmodulated component and the components modulated at ω and 2ω. The same results can be obtained by using the density operator and the monitoring operator (Carver and Partridge 1966) as shown in Appendix A. If θ is chosen to zero in eqs.(3.9), the effect of the transverse pumping disappears and only the ordinary magnetic resonance appears in the unmodulated component as one alters H_0. When θ is chosen to $\pi/2$ rad., the situation coincides with that of the experiment by Haroche (1971b), $M_n(0)$, $M_{n,s}(2\omega)$ and $M_{n,c}(2\omega)$ are not zero. For the condition that $\omega\tau \gg 1$, eqs.(3.9a), (3.9d) and (3.9e) become respectively as follows;

$$M_n(0) = \frac{1}{4}\ \frac{(1-\cos\beta)^2}{1+(\omega-\omega_e)^2\tau^2}\ M_0'\ , \tag{3.10a}$$

$$M_n(2\omega) = M_{n,s}(2\omega)\sin 2\omega t + M_{n,c}(2\omega)\cos 2\omega t = -\frac{1}{4}\ \frac{\sin^2\beta}{1+(\omega-\omega_e)^2\tau^2}\ M_0'\sin(2\omega t+\alpha)\ , \tag{3.10b}$$

where

$$\alpha = \tan^{-1}\ \frac{1}{(\omega-\omega_e)\tau} \tag{3.11}$$

Equations (3.10) show the resonances whose maximum appears for $\omega = \omega_e$, i.e.,

$$\omega_0 = \omega \pm \omega\left[1 - (\omega_1/\omega)^2\right]^{1/2}, \qquad (3.12)$$

and the maximum of the resonances are given in the form

$$M_n(0)^{max} = \frac{1}{4}\left[2\left\{1 - \left[1-(\omega_1/\omega)^2\right]^{1/2}\right\} - (\omega_1/\omega)^2\right] M_0', \qquad (3.13a)$$

$$M_n(2\omega)^{max} = \frac{1}{4}(\omega_1/\omega)^2 M_0'. \qquad (3.13b)$$

Equation (3.12) shows the resonances occur at $\omega_0 \sim 0$ and $\omega_0 \sim 2\omega$ for weak rf field and Bloch-Siegert (1940) type shift occurs as the magnitude of the rf field H_1 is increased. The resonance for $\omega_0 \sim 0$ shifts to the high field region and the resonance for $\omega_0 \sim 2\omega$ shifts to the low field region, i.e., both resonances move towards $\omega_0 = 0$. The maxima of the resonance of the component modulated at 2ω is proportional to H_1^2 as shown eq.(3.13b). On the other hand, if θ is chosen to $0 < \theta < \pi/2$, all of eqs.(3.9) are not zero. It should be noticed that the new type resonance may be detected not only in the unmodulated component and the component modulated at 2ω but also in the component modulated at ω of the transmitted light beam. For the condition that $\omega\tau \gg 1$, using eqs.(3.9a) and (3.9c) the component modulated at ω becomes as follows;

$$M_n(\omega) = M_{n,s}(\omega)\sin\omega t + M_{n,c}(\omega)\cos\omega t$$

$$= \frac{1}{4}\,\frac{(1-\cos\beta)\sin\beta}{\{1+(\omega-\omega_e)^2\tau^2\}^{1/2}}\,\sin 2\theta\, M_0'\sin(\omega t + \alpha). \qquad (3.14)$$

The variation of the position for the resonance peak is the same quantity as given by eq.(3.12) and the maximum can be represented as follows;

$$M_n(\omega)^{max} = \frac{1}{4}\frac{\omega_1}{\omega}\left\{1 - \left[1 - (\omega_1/\omega)^2\right]^{1/2}\right\}\sin 2\theta\, M_0'. \qquad (3.15)$$

The half width at half maximum $\Delta\omega_h$ of the new type resonances is given from eqs.(3.10) and (3.14) as follows;

$$\Delta\omega_h = \omega\left[\left\{\left(1 + \frac{1}{\omega\tau}\right)^2 - \left(\frac{\omega_1}{\omega}\right)^2\right\}^{1/2} - \left\{1 - \left(\frac{\omega_1}{\omega}\right)^2\right\}^{1/2}\right] \quad (3.16)$$

For the weak values of H_1, the linewidth $\Delta\omega_h$ becomes τ^{-1}, i.e., normal line width of the levels. When the magnitude of H_1 is increased, the linewidth becomes dependent not only on τ but also ω_1 and ω. The theoretical curves of the new type resonances calculated with eqs.(3.9a), (3.9d) and (3.9e) are shown in Fig.3.3. In Fig.3.3, (a) and (b) show the resonances of the unmodulated and the modulated at 2ω components, respectively. The maximum of the resonance in the unmodulated component is approximately given by eq.(3.13a) and the maximum of the component modulated at 2ω is proportional to H_1^2 as shown in eq.(3.13a). The magnitude of the shifts of both the unmodulated and the component modulated at 2ω are equal to each other; it is proportional to H_1^2 for the weak values of H_1 as shown in eq.(3.12).

The resonance of the component modulated at 2ω given in eq.(3.10b) may be the same as one of the resonances predicted by Haroche et al. (Cohen-Tannoudji and Haroche 1965, 1967), so called "Haroche Resonance" (Cohen-Tannoudji 1968). From their conclusion, it is expected that the resonances are shifted but not broadened, as the intensity H_1 is increased, and both the shift and the maximum of the resonance of the component modulated at 2ω are proportional to H_1^2; all the peaks of the resonance curves for various values of H_1 are thus on a straight line. Although all the peaks of the resonance curves of (b) in Fig.3.3, component modulated at 2ω, are on a straight line for weak H_1, the peaks deviate from the straight line for comparatively large H_1. The resonance curves of (a) and (b) in Fig.3.3 are broadened as the intensity of H_1 is increased. Haroche et al. have experimentally observed the saturation effect, i.e., the deviation of the peaks of the resonance from the straight line for large values of H_1,

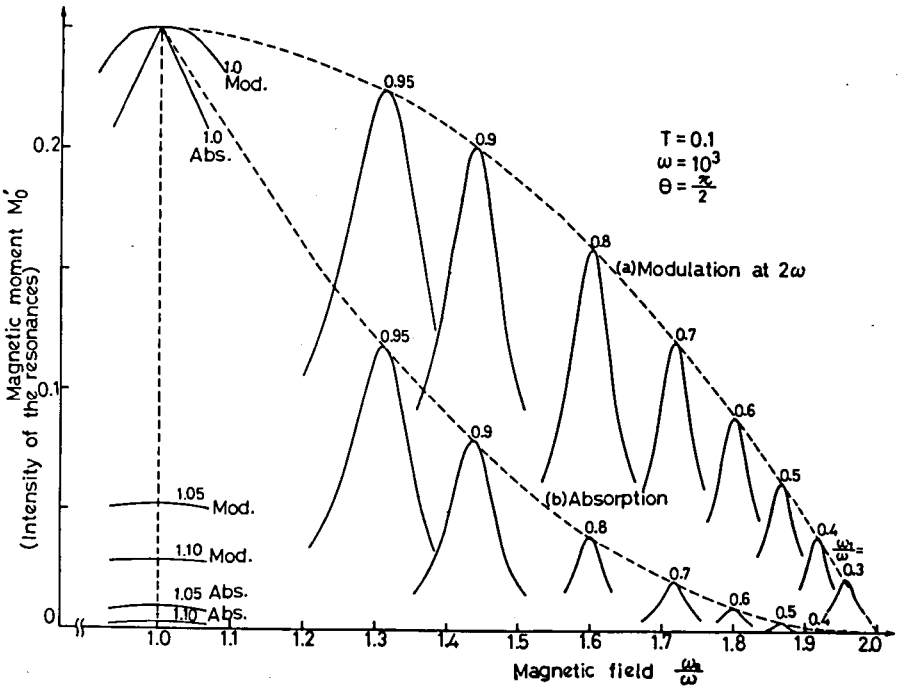

Fig. 3.3. Theoretical resonance curves obtained for $T = 0.1$, $\omega = 1000$ and $\theta = \pi/2$ from eqs.(3.9); (a) represents the unmodulated component, and (b) the component modulated at 2ω.

but they have not explained this effect in detail (Cohen-Tannoudji and Haroche 1965,1967). Recently, Haroche has explained this saturation effect in detail by using "dressed atom" theory (Haroche 1971a,b). The new type resonances which appear in the component modulated at ω have not been predicted by their theory, because only the case that $\theta = \pi/2$ has been treated in their theory.

If the conditions $\omega_0\tau \gg 1$ and $\omega_0 \gg \omega_1$ are satisfied, eqs.(3.9a~c) are expressed in the following form;

$$M_n(0) = \frac{1 + (\Delta\omega\tau)^2}{1 + (\Delta\omega\tau)^2 + (\omega_1\tau)^2} M_0' \cos^2\theta \quad , \tag{3.17a}$$

$$M_{n,s}(\omega) = \frac{1}{1 + (\Delta\omega\tau)^2 + (\omega_1\tau)^2} M_0' \sin\theta \cos\theta \quad , \tag{3.17b}$$

$$M_{n,c}(\omega) = -\frac{1}{1 + (\Delta\omega\tau)^2 + (\omega_1\tau)^2} M_0' \sin\theta \cos\theta \quad . \tag{3.17c}$$

It is seen that the intensities of resonances of the unmodulated component and the component modulated at ω are proportional to $\cos^2\theta$ and $\sin\theta\cos\theta$, respectively. The results of eqs.(3.17) are the same as that obtained by Abragam (1961) in nuclear magnetic resonance and by Bell and Bloom (1957) for "cross-beam" method in optical pumping, except for the angular dependency of θ .

If the rf field H_1 is removed, the magnetic moment M_n directed along the optical axis is given from eq.(3.8) as follows;

$$M_n = \frac{1}{1 + (\omega_0\tau)^2} M_0' \sin^2\theta + M_0' \cos^2\theta \quad . \tag{3.18}$$

The first term on the right hand side of eq.(3.18) is due to the transverse pumping or the Hanle effect (Hanle 1924, Mitchell and Zemansky 1934) and the second term is due to the longitudinal pumping. This result coincides

with that derived by using the Bloch equation (Lehman et al. 1964, Ito et al. 1968) and the density matrix (Brossel 1965) for the case that the rf field is absent.

Thus, it is shown that eq.(3.8) gives a comprehensive theoretical description for the behavior of the ensemble of the optically pumped atoms which undergo the double resonance.

3.2.2. Experiments and Discussion

For the purpose to confirm the conclusions of the theory, experiments were made with optically pumped cesium atoms. An absorption cell with wall coated with paraffin, containing saturated vapor of cesium at temperature about 25°C, was situated at the center of a set of Helmholtz coils which produced a constant magnetic field $H_s \sim 0.5$ gauss. To observe the effect of the transverse pumping, the experiments must be carried out in a weak magnetic field. Therefore we used the effective field in the rotating coordinate system as a static field H_0 in the theory. The rf field $\mathbf{h}_0 \cos \Omega t$ with frequency $\Omega/2\pi = 175$ KHz was applied perpendicularly to the field $\mathbf{H}_s$ and the another rf field $\mathbf{H}_1 \cos \omega t$ with frequency $\omega/2\pi = 3$ KHz, oscillating in the direction of the $\mathbf{H}_s$, was produced by a low frequency generator. The optical pumping was done by means of circularly polarized light beam from an electrodeless cesium lamp, propagating along $\mathbf{H}_s$.

When the frequency Ω is set at near resonance condition of the ordinary magnetic resonance, i.e., $\Omega \sim \gamma H_s$, the direction of the effective field in the rotating coordinate system which rotates about z axis with angular frequency Ω makes an angle $\beta = \tan^{-1}(\gamma h_0/(\gamma H_s - \Omega))$ to $\mathbf{H}_s$(z axis) and its magnitude is $H_e = \{(H_s - \Omega/\gamma)^2 + h_0^2\}^{1/2}$ as shown in Fig.3.4. The rotating coordinate system is then equivalent to the situation which is discussed in the theory by considering that $H_0 = H_e$ and $\theta = \beta$, and by neglecting the counter-rotating component of the oscillating rf field $\mathbf{H}_1$.

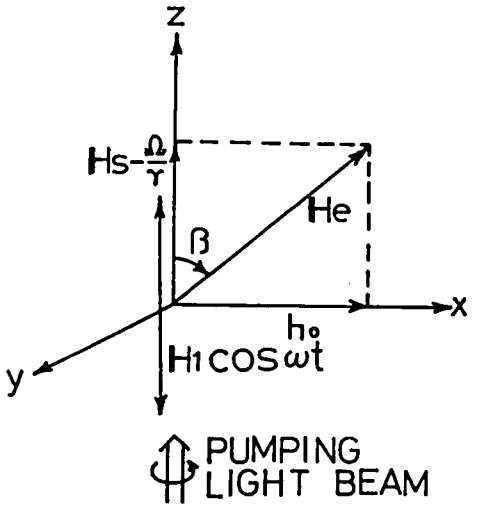

Fig. 3.4. Experimental situation on the coordinate system which rotates around $\mathbf{H}_s$ with angular frequency ω.

At first, the angle β was set at just $\pi/2$ rad., i.e., $\Omega = \gamma H_s$. The change of the transmitted light intensity obtained for this case can be calculated with eq.(3.8) by setting the angle θ to $\pi/2$ rad. In this case the resonances are expected in the unmodulated component from the second term of the right hand side of eq.(3.9a) and the component modulated at 2ω from eqs.(3.9d,e), but the component modulated at ω disappears.

Resonances in the unmodulated component and the component modulated at 2ω in the light beam transmitted through the absorption cell were recorded by an X-Y recorder as the amplitude h_0, i.e., H_0 in the theory, was varied continuously. The recorder traces of the resonance appearing in the unmodulated component are shown in Fig.3.5, where each resonance corresponds to a different value of H_1. We can see in Fig.3.5 that the maxima of the resonance for $\omega_0 \sim 2\omega$ move towards the low field region, as H_1 is increased. The resonance for $\omega_0 \sim 0$ expected from eq.(3.12) can not be

observed, because in the experiments the oscillating rf field was used instead of the rotating rf field. The sudden increase of the transmitted light near $h_0 = 0$ is associated with the Hanle effect in the rotating coordinate system. The effect of "dressed atom" (Cohen-Tannoudji and Haroche 1969a,b) is seen in the resonance curves, especially the resonance curve for $V_1 = 22$ millivolt, where V_1 is proportional to H_1, shows the remarkably broadened Hanle curve. The curve for $V_1 = 0$ shows the normal Hanle curve in the absence of the rf field. Figure 3.6 shows the recorder traces of the component modulated at 2ω. The resonance for $\omega_0 \sim 2\omega$ shifts towards the same direction and by the same quantity as the resonances which appear in the unmodulated component. The peaks of the resonance curves are on a straight line for weak rf field and the saturation effect appears in the region of the relatively large H_1 as expected by the theory. The half width at half maximum of the resonance is nearly equal to the inverse of the relaxation time τ for the weak rf field H_1, but it is remarkably broadened by increasing the intensity of H_1. Figure 3.7 shows the maxima of the resonances for $\omega_0 \sim 2\omega$ of the unmodulated component as a function of H_1, in which the solid line is the theoretical value and the cross points are the experimental results. In Fig.3.8, the solid line shows the theoretical value of the maxima of the component modulated at 2ω and the circle points show the experimental results. The shift of the center of the resonance curves is shown in Fig.3.9 as a function of H_1. The solid line shows the theoretical result. and the cross points and the circular points show the experimental results. The agreement between the experimental and the theoretical results is excellent in the case that $\omega_1 = \gamma H_1$ does not exceed ω. When the value of ω_1 goes over ω, our theory becomes invalid, because the counter-rotating component of the oscillating rf field H_1 becomes important for such a large value of ω_1. If the rotating rf field is used

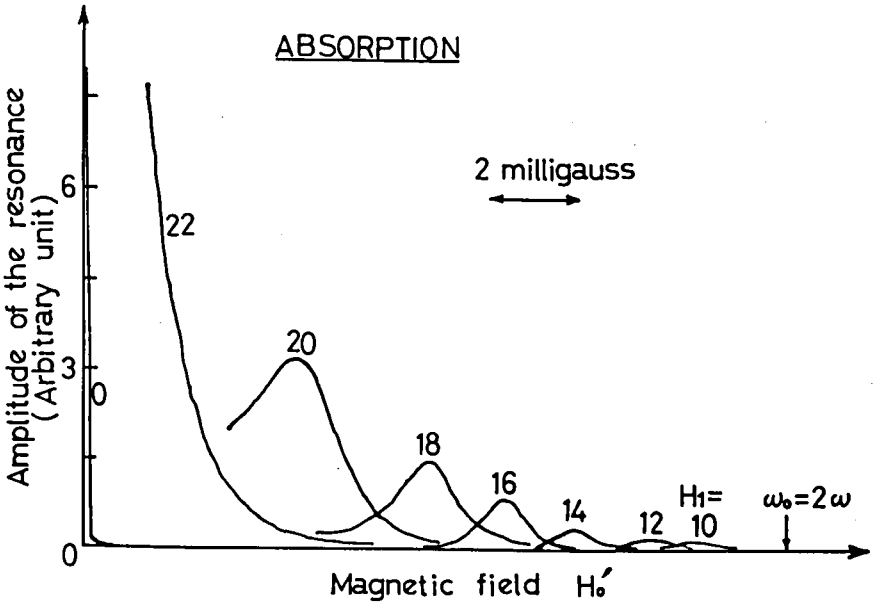

Fig. 3.5. Recorder traces of the resonance curves for $\omega_0 = 2\omega$ in the unmodulated component as a function of h_0. The rf field h_0 is varied from zero to 20 milligauss. A number written in each trace is the input voltage V_1 of rf coils (in millivolt), which is proportional to H_1.

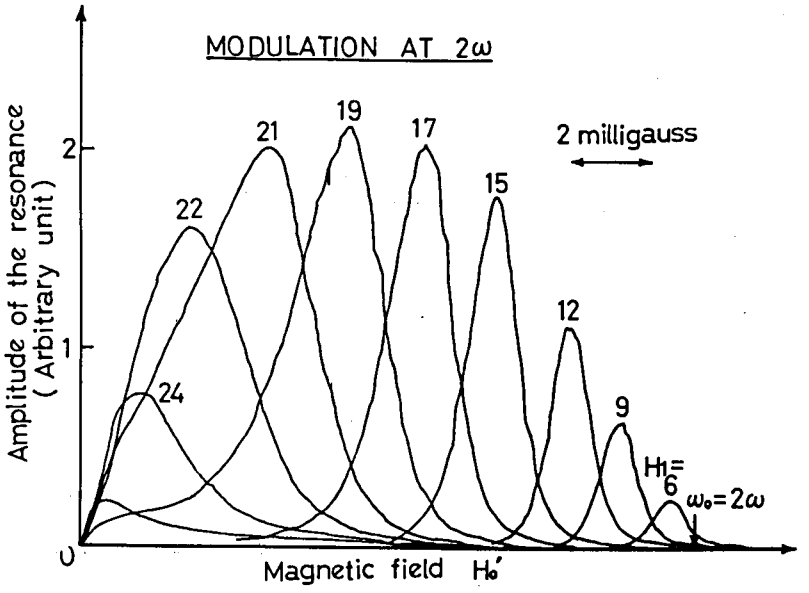

Fig. 3.6. Recorder traces of the resonance curves of the component modulated at 2ω for $\omega_0 = 2\omega$. A number written in each trace is the input voltage V_1 of the rf coils (in millivolt), which is proportional to H_1.

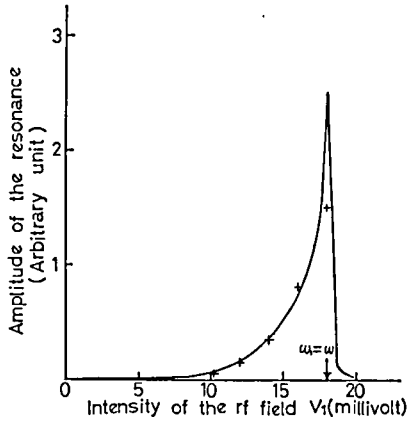

Fig. 3.7. The variation of the resonance maxima of the unmodulated component as a function of V_1. Experimental points are shown by the crosses and the solid line is the theoretical value.

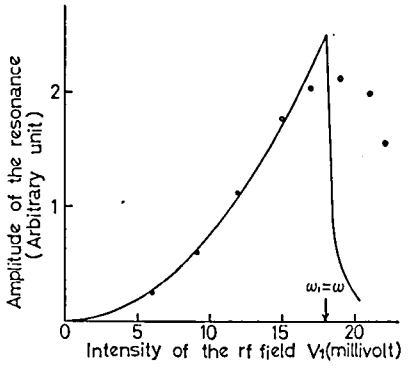

Fig. 3.8. The variation of the resonance maxima of the component modulated at 2ω as a function of V_1. Experimental points are shown by the circles and the solid line is the theoretical value.

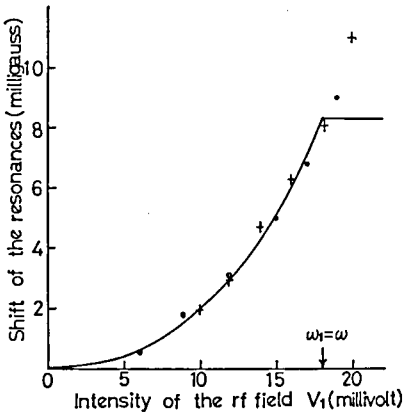

Fig. 3.9. Position of the center of the resonances as a function of V_1. The points are experimental results: the crosses represent the unmodulated component, and encircled points represent the component modulated at 2ω and the solid line represents the theoretical value.

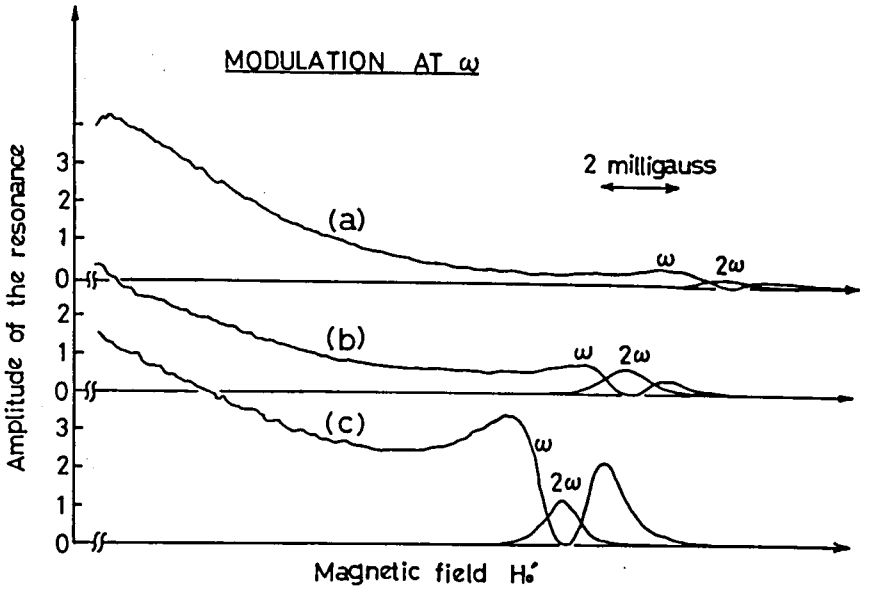

Fig.3.10. Resonance curves in the component modulated at ω; (a), (b) and (c) correspond to the cases that the intensity of H_1 is small, medium and large, respectively. The resonance curves in the component modulated at 2ω are also shown.

in the experiments the theory is rigorous without the restriction for the intensity of the rf field, and the resonance for $\omega_0 \sim 0$ may appear. The new type resonance which appears in the component modulated at ω is also observed for the case that the angle β differs from $\pi/2$ rad. Figure 3.10 shows the resonance curves for small, medium and large values of H_1, in which the resonances in the component modulated at 2ω are also shown. The resonance curves situate on the slope of the ordinary magnetic resonance curve in the component modulated at ω, the center of which is at $\omega_0 = \omega$. When the value of H_1 is increased, it shifts towards the same direction and by the same magnitude as the resonances which appear in the unmodulated component and the component modulated at 2ω.

It has been shown by Cohen-Tannoudji and Haroche (1969a,b) that the new type resonances are due to the crossing of the energy levels of the system, which consists of an atom and the rf photon. Their theory shows that the linewidth of the new type resonance or Haroche resonance is determined only by the natural width of the crossing energy levels and is independent of the amplitude of H_1. However, as we have shown theoretically and experimentally, the new type resonances are actually broadened by the rf field H_1. This fact can be explained from the point of view of the crossing of the energy levels. When the magnitude of static field H_0 is varied, the region of H_0 where the energy levels are crossed is independent not only on the natural line width of these levels but also on the angle between the crossing energy levels which is determined by the atomic g-factor. The angle is perturbed by the anticrossing of the energy levels which is associated with the ordinary magnetic resonance. The variation of the angle can be considered as an effect of the modification of the atomic g-factor by the rf photon..Accordingly, when the amplitude of H_1 is increased, the crossing point of the energy levels, i.e., the center of the resonance, shifts accompanying the

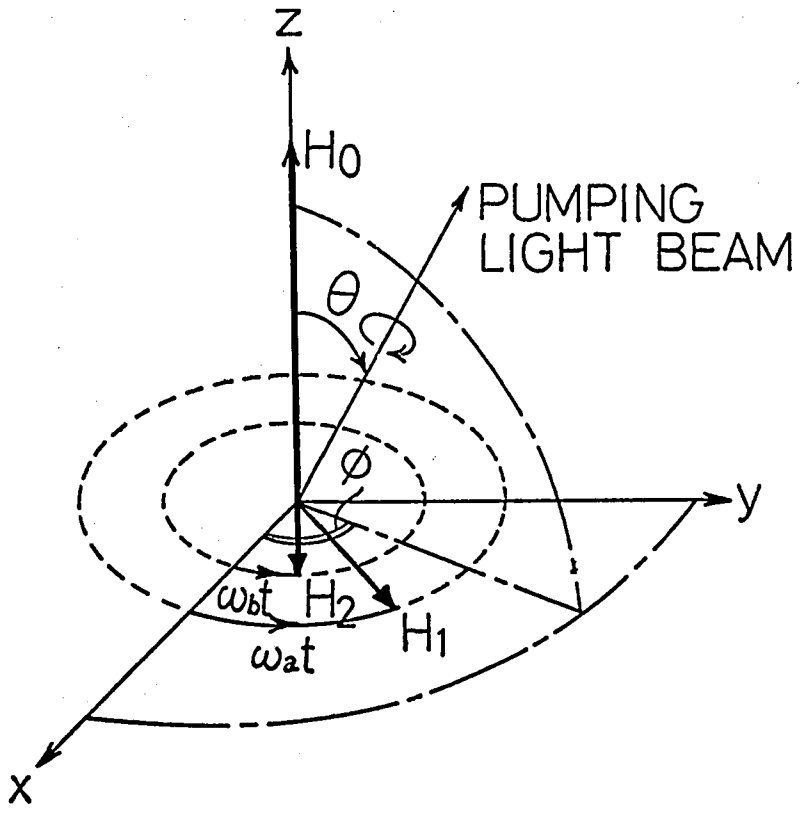

Fig. 3.11. Directions of magnetic fields and pumping light beam in the laboratory coordinate system ($S^{(0)}$ frame).

broadening of the resonance line. It must be emphasized that the broadening of the new type resonance is due to the fact that the atomic g-factor is modified by the rf field H_1.

3.3. Effects of the Transverse Pumping in the Presence of Two Rotating RF Fields

The evolution of the magnetization of the optically pumped atoms in the presence of two rotating rf fields with different frequencies is investigated by using the Bloch equation. It is shown that the new type resonances which are due to the effect of the transverse pumping together with the ordinary magnetic resonance and the multiple quantum resonances are realized undergoing the influences of two rotating rf fields. It is also shown that the Hanle curve is broadened by the rotating rf field in the same manner as by the oscillating rf field, and is shifted towards high field region as the intensity of the rotating rf field is increased. The results obtained are applicable to the case of an elliptically rotating rf field, which is superposition of two rotating rf fields.

3.3.1. Theory

(a) Transformation of the Magnetic Fields

We investigate the evolution of a magnetization $\mathbf{M}$ acted upon a static field $\mathbf{H}_0$ and the two rotating rf fields H_1 and H_2, which rotate about H_0 with angular frequency ω_a and ω_b, respectively, as shown in Fig.3.11. The magnetic fields in the laboratory frame S^0 are represented as follows;

$$\mathbf{H}^0(t) = H_1(\mathbf{i}\cos \omega_a t + \mathbf{j}\sin \omega_a t) + H_2(\mathbf{i}\cos \omega_b t + \mathbf{j}\sin \omega_b t) + \mathbf{k}\, H_0 \tag{3.19}$$

In the absence of H_2, it has been shown that the ordinary magnetic resonance at $\omega_0 = \omega_a$ and the transverse resonance at $\omega_0 = 2\,\omega_a$ occur

(Aleksandrov and Sokorov 1972, Tsukada et al. 1972). It now remains to see how the presence of H_2 rotating at frequency ω_b affects the evolution of magnetic moment. This problem can easily be analyzed by the use of rotating frames. Consider the problem from the point of view of a frame rotating with angular frequency ω_a. This transformation makes the field H_1 to rest, and the frequency of field H_2 to $\omega_b - \omega_a$. This succeeds in removing resonant terms leaving only a small off-resonant field. If we were to neglect the off-resonant field, we would obtain the usual "zeroth order" approximation which predicts the ordinary resonance at $\omega_0 = \omega_a$ and the transverse resonance at $\omega_0 = 2\omega_a$. A more accurate solution which includes all of the first order effects of H_2 is given by the following successive transformations (Abragam 1961, Rewis 1969),

$$R_1(S^0 \leftrightarrow S^1) = \begin{pmatrix} \cos\omega_b t & \sin\omega_b t & 0 \\ -\sin\omega_b t & \cos\omega_b t & 0 \\ 0 & 0 & 1 \end{pmatrix}, \qquad (3.20a)$$

$$R_2(S^1 \leftrightarrow S^2) = \begin{pmatrix} \cos\delta & 0 & -\sin\delta \\ 0 & 1 & 0 \\ \sin\delta & 0 & \cos\delta \end{pmatrix}, \qquad (3.20b)$$

$$R_3(S^2 \leftrightarrow S^3) = \begin{pmatrix} \cos(\omega_a - \omega_b)t & \sin(\omega_a - \omega_b)t & 0 \\ -\sin(\omega_a - \omega_b)t & \cos(\omega_a - \omega_b)t & 0 \\ 0 & 0 & 1 \end{pmatrix}, \qquad (3.20c)$$

$$R_4(S^3 \leftrightarrow S^4) = \begin{pmatrix} \cos\beta & 0 & -\sin\beta \\ 0 & 1 & 0 \\ \sin\beta & 0 & \cos\beta \end{pmatrix}. \qquad (3.20d)$$

The first transformation (3.20a) represents that of the rotating field H_2 to rest. This transformation is accomplished by introducing a system S^1 that rotates with the angular frequency ω_b about the z axis of the laboratory frame S^0. The magnetic field in the frame S^1 becomes as follows;

$$\mathbf{H}^1(t) = H_1[\mathbf{i}\cos(\omega_a - \omega_b)t + \mathbf{j}\sin(\omega_a - \omega_b)t] + \mathbf{i}H_2 + \mathbf{k}(H_0 - \omega_b/\gamma). \qquad (3.21)$$

Next transformation (3.20b) represents that the direction of the static part of this field is chosen as the z^2 axis in the S^2 frame, therefore

$$\mathbf{H}^2(t) = H_1[\mathbf{i}\cos\delta\cos(\omega_a - \omega_b)t - \mathbf{j}\sin(\omega_a - \omega_b)t + \mathbf{k}\sin\delta\cos(\omega_a - \omega_b)t] + \mathbf{k}\left[(H_0 - \omega_b/\gamma)^2 + H_2^2\right]^{1/2} . \tag{3.22}$$

The direction z^2 is given by the angle δ with respect to the z^1 axis. The angle δ is defined by

$$\tan\delta = H_2/(H_0 - \omega_b/\gamma) . \tag{3.23}$$

We once again rotate the frame S^2 about the z^2 axis at frequency $\omega_a - \omega_b$ by the transformation (3.20c). Then in this frame S^3, the magnetic field becomes as

$$\mathbf{H}^3(t) = H_1[-\mathbf{i}\sin^2(\delta/2)\cos 2(\omega_a - \omega_b)t - \mathbf{j}\sin^2(\delta/2)\sin 2(\omega_a - \omega_b)t + \mathbf{k}\sin\delta\cos(\omega_a - \omega_b)t] + \mathbf{i}H_1\cos^2(\delta/2) + \{[(H_0 - \omega_b/\gamma)^2 + H_2^2]^{1/2} - (\omega_a - \omega_b)/\gamma\}\mathbf{k} , \tag{3.24}$$

and we again choose the direction of the static part as the z^4 axis by using the transformation (3.20d). The magnetic field in the frame S^4 becomes as

$$\mathbf{H}^4(t) = H_1[-\mathbf{i}\{\sin^2(\delta/2)\cos\beta\cos 2(\omega_a - \omega_b)t - \sin\delta\sin\beta\cos(\omega_a - \omega_b)t\} - \mathbf{j}\sin^2(\delta/2)\sin 2(\omega_a - \omega_b)t - \mathbf{k}\{\sin^2(\delta/2)\sin\beta\cos 2(\omega_a - \omega_b)t + \sin\delta\cos\beta\cos(\omega_a - \omega_b)t\}] + \mathbf{k}(\Omega/\gamma) . \tag{3.25}$$

The static field is now

$$\Omega/\gamma = [(H_0 - \omega_b/\gamma)^2 + H_2^2]^{1/2} = \gamma^{-1}(\omega_a - \omega_b)^2 + H_1^2\cos^4(\delta/2)^{1/2} . \tag{3.26}$$

The angle β is defined by

$$\tan\beta = \frac{H_1\cos^2(\delta/2)}{[(H_0 - \omega_b/\gamma)^2 + H_2^2]^{1/2} - (\omega_a - \omega_b)/\gamma} \tag{3.27}$$

The field $H^4(t)$ contains only small fields of order of $H_1(H_2/H_0)$ and $H_1(H_2/H_0)^2$ at frequency $\omega_a - \omega_b$ and $2(\omega_a - \omega_b)$, if the condition $H_0 \gg H_1, H_2$ is satisfied. We can obtain a useful approximation by neglecting the effect of the time dependent fields, keeping only the static field Ω/γ .

(b) The Bloch Equation and the Orientation Parameter $\mathbf{M}_0'$ in the Frame S^4

We investigate the evolution of a magnetization $\mathbf{M}$ in the frame S^4 by means of a system of the phenomenological Bloch equation. In this frame S^4, the magnetic field can be represented approximately by a static field Ω/γ under the condition $H_0 \gg H_1, H_2$, but the orientation parameter $\mathbf{M}_0'$ by means of circularly polarized light is no longer time independent. The orientation parameter $\mathbf{M}_0'^4$ in the frame S^4 is obtained by accomplishing the similar successive rotations (3.20). The components of the orientation parameter $\mathbf{M}_0'^4$ are then given as follows;

$$M_{0x}'^4 = M_0' \{ A_x^0 + \sum_{n=1}^{4} (B_x^n \cos \omega_n t + C_x^n \sin \omega_n t) \quad , \tag{3.28a}$$

$$M_{0y}'^4 = M_0' \{ A_y^0 + \sum_{n=1}^{4} (B_y^n \cos \omega_n t + C_y^n \sin \omega_n t) \quad , \tag{3.28b}$$

$$M_{0z}'^4 = M_0' \{ A_z^0 + \sum_{n=1}^{4} (B_z^n \cos \omega_n t + C_z^n \sin \omega_n t) \quad , \tag{3.28c}$$

with

$$\omega_1 = \omega_a, \quad \omega_2 = \omega_b, \quad \omega_3 = \omega_a - \omega_b, \quad \omega_4 = \omega_a - 2\omega_b, \tag{3.29}$$

where

$$A_x^0 = -\cos\theta \sin\beta \cos\delta \quad ,$$

$$B_x^1 = 2^{-1} \sin\theta \cos\phi \cos\beta (1 + \cos\delta),$$

$$B_x^2 = -\sin\theta \cos\phi \sin\beta \sin\delta \quad ,$$

$$B_x^3 = -\cos\theta \cos\beta \sin\delta \quad ,$$

$$B_x^4 = -2^{-1} \sin\theta \cos\phi \cos\beta (1 - \cos\delta),$$

$$C_x^1 = 2^{-1}\sin\theta\ \sin\phi\ \cos\beta\ (1 + \cos\delta\ ),$$

$$C_x^2 = -\sin\theta\ \sin\phi\ \sin\beta\ \sin\delta\ ,$$

$$C_x^4 = 2^{-1}\sin\theta\ \sin\phi\ \cos\beta\ (1 - \cos\delta\ ),$$

$$B_y^1 = 2^{-1}\sin\theta\ \sin\phi\ (1 + \cos\delta\ ),$$

$$B_y^4 = 2^{-1}\sin\theta\ \sin\phi\ (1 - \cos\delta\ ),$$

$$C_y^1 = -2^{-1}\sin\theta\ \cos\phi\ (1 + \cos\delta\ ),$$

$$C_y^3 = \cos\theta\ \sin\delta\ ,$$

$$C_y^4 = 2^{-1}\sin\theta\ \cos\phi\ (1 - \cos\delta\ ),$$

$$A_z^0 = \cos\theta\ \cos\beta\ \cos\delta\ ,$$

$$B_z^1 = 2^{-1}\sin\theta\ \cos\phi\ \cos\beta\ (1 + \cos\delta\ ),$$

$$B_z^2 = \sin\theta\ \cos\phi\ \cos\beta\ \sin\delta\ ,$$

$$B_z^3 = -\cos\theta\ \sin\beta\ \sin\delta\ ,$$

$$B_z^4 = -2^{-1}\sin\theta\ \cos\phi\ \sin\beta\ (1 - \cos\delta\ ),$$

$$C_z^1 = 2^{-1}\sin\theta\ \sin\phi\ \sin\beta\ (1 + \cos\delta\ ),$$

$$C_z^2 = \sin\theta\ \sin\phi\ \cos\beta\ \sin\delta\ ,$$

$$C_z^4 = 2^{-1}\sin\theta\ \sin\phi\ \sin\beta\ (1 - \cos\delta\ ),$$

$$C_x^3 = A_y^0 = B_y^2 = B_y^3 = C_y^2 = C_z^3 = 0. \qquad (3.30)$$

Using the eqs.(3.26) and (3.28), we obtain the Bloch equation governing the motion of the three components of the magnetization $\mathbf{M}^4$ in the frame S^4 as follows;

$$\frac{d\,M_x^4}{dt} = \Omega\,M_y^4 - \frac{1}{\tau}\,M_x^4 + \frac{1}{\tau}\,M_{0x}^4\ , \qquad (3.31a)$$

$$\frac{d\,M_y^4}{dt} = -\Omega\,M_x^4 - \frac{1}{\tau}\,M_y^4 + \frac{1}{\tau}\,M_{0y}^4\ , \qquad (3.31b)$$

$$\frac{d M_z^4}{dt} = -\frac{1}{\tau} M_z^4 + \frac{1}{\tau} M_{0z}^4 . \tag{3.31c}$$

Using the relation

$$M_+^4 = M_x^4 + iM_y^4 , \tag{3.32}$$

we obtain the following two equations which are equivalent to the three diferential equations (3.31) in the form

$$\frac{d M_+^4}{dt} = -i\Omega M_+^4 - \frac{1}{\tau} M_+^4 + \frac{1}{\tau} (M_{0x}^4 + iM_{0y}^4), \tag{3.33a}$$

$$\frac{d M_z^4}{dt} = -\frac{1}{\tau} M_z^4 + \frac{1}{\tau} M_{0z}^4 . \tag{3.33b}$$

Since the system of eqs.(3.33) are linear differential equations, we can get exact solutions

$$M_+^4 = 2^{-1}\{2M_x^0 + \sum_{n=1}^{4} (M_x^{nc}\cos \omega_n t + M_x^{ns}\sin \omega_n t)\}$$
$$+ i2^{-1}\{2M_y^0 + \sum_{n=1}^{4} (M_y^{nc}\cos \omega_n t + M_z^{ns}\sin \omega_n t)\} , \tag{3.34a}$$

$$M_z^4 = M_z^0 + \sum_{n=1}^{4} (M_z^{nc}\cos \omega_n t + M_z^{ns}\sin \omega_n t) , \tag{3.34b}$$

in which

$$M_x^0 = \frac{1}{1 + (\Omega\tau)^2} A_x^0 ,$$

$$M_x^{nc} = \frac{1}{1 + (\Omega + \omega_n)^2\tau^2}\{(B_x^n + C_y^n) - (\Omega + \omega_n)\tau (C_x^n - B_y^n)\}$$
$$+ \frac{1}{1 + (\Omega - \omega_n)^2\tau^2}\{(B_x^n - C_y^n) + (\Omega + \omega_n)\tau (C_x^n + B_y^n)\} ,$$

$$M_x^{ns} = \frac{1}{1 + (\Omega + \omega_n)^2\tau^2}\{(C_x^n - B_y^n) + (\Omega + \omega_n)\tau (B_x^n + C_y^n)\}$$
$$+ \frac{1}{1 + (\Omega - \omega_n)^2\tau^2}\{(C_x^n + B_y^n) - (\Omega - \omega_n)\tau (B_x^n - C_y^n)\} ,$$

$$M_y^0 = -\frac{\Omega\tau}{1+(\Omega\tau)^2}\,A_x^0 ,$$

$$M_y^{nc} = \frac{1}{1+(\Omega+\omega_n)^2\tau^2}\{(-C_x^n+B_y^n)-(\Omega+\omega_n)\tau(B_x^n+C_y^n)\}$$

$$+\frac{1}{1+(\Omega-\omega_n)^2\tau^2}\{(C_x^n+B_y^n)+(\Omega-\omega_n)\tau(-B_x^n+C_y^n)\} ,$$

$$M_y^{ns} = \frac{1}{1+(\Omega+\omega_n)^2\tau^2}\{(B_x^n+C_y^n)+(\Omega+\omega_n)\tau(-C_x^n+B_y^n)\}$$

$$+\frac{1}{1+(\Omega-\omega_n)^2\tau^2}\{(-B_x^n+C_y^n)-(\Omega-\omega_n)\tau(C_x^n+B_y^n)\} ,$$

$$M_z^0 = A_z^0 ,$$

$$M_z^{nc} = \frac{1}{1+(\omega_n\tau)^2}(B_z^n-\omega_n\tau C_z^n) ,$$

$$M_z^{ns} = \frac{1}{1+(\omega_n\tau)^2}(C_z^n+\omega_n\tau B_z^n) . \qquad (3.35)$$

(c) Absorption of the Pumping Light Beam

It is well known that the amount of the absorption of the light beam by atoms is related to the component of the magnetization along the direction of the light beam, and given by eq.(2.23). Since the values of the components of the magnetization in the frame S^4 was given by eqs.(3.34), M_n is obtained by transforming back to the laboratory frame S^0 with eqs.(3.20). Thus M_n becomes

$$M_n = M_0^{'-1}(M_x^4 M_{0x}^{'4} + M_y^4 M_{oy}^{'4} + M_z^4 M_{0z}^{'4}) . \qquad (3.36)$$

The magnetization M_n contains the unmodulated or D.C. component and the components which are modulated at ω_a, ω_b, $\omega_a \pm \omega_b$, $2\omega_a$, $2(\omega_a - \omega_b)$, etc. It should be also noticed that the beat frequencies such as $\omega_a - \omega_b$, $2(\omega_a - \omega_b)$, $\omega_a - 2\omega_b$, $2\omega_a - \omega_b$, etc. appear.

Table 3.1. Resonance functions and the resonance positions.

Resonance Function	Resonance Position	Dependency of θ
Ω	ω_a , $2\omega_b - \omega_a$	$\cos^2\theta$
$\Omega + \omega_a$	$2\omega_a$, $2(\omega_b - \omega_a)$	$\sin^2\theta$
$\Omega - \omega_a$	0 , $2\omega_b$	$\sin^2\theta$
$\Omega + \omega_b$	$\omega_a + \omega_b$, $-\omega_a + \omega_b$	$\sin^2\theta$
$\Omega - \omega_b$	$\omega_a - \omega_b$, $3\omega_b - \omega_a$	$\sin^2\theta$
$\Omega + (\omega_a - \omega_b)$	$2\omega_a - \omega_b$, $-2\omega_a + 3\omega_b$	$\cos^2\theta$
$\Omega - (\omega_a - \omega_b)$	ω_b ,	$\cos^2\theta$
$\Omega + (\omega_a - 2\omega_b)$	$2(\omega_a - \omega_b)$, $-2(\omega_a - \omega_b)$	$\sin^2\theta$
$\Omega - (\omega_a - 2\omega_b)$	$2\omega_b$, 0	$\sin^2\theta$

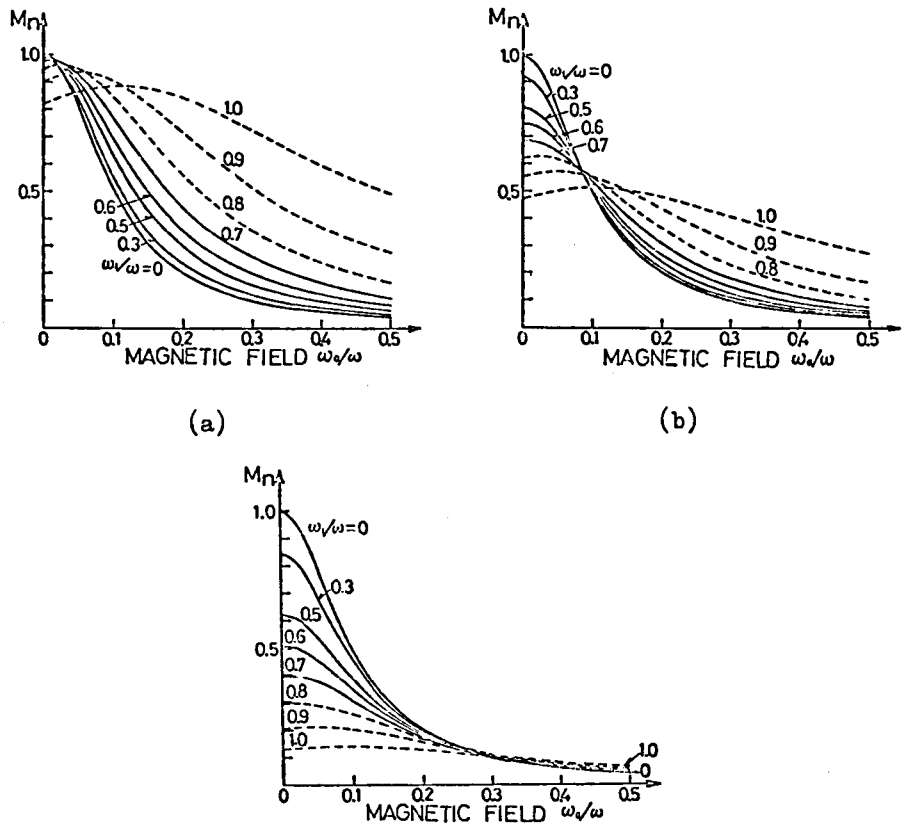

Fig. 3.12. Broadening of the Hanle curve by the linearly oscillating rf field; (a), (b) and (c) show the calculation results for the cases $\phi = 0$, $\pi/4$ and $\pi/2$ rad, respectively.
Parameters for the theoretical curves:
$T = 0.01$ sec, $\omega = 1000$ rad sec^{-1} and $\theta = \pi/2$.

The strengths of the resonances contained in the various modulated components are not all the same; they depend on some power series of H_1/H_0 and H_2/H_0 and on the angle θ .

Unmodulated component M_n^0 in eq.(3.36) is given by substituting eqs.(3.28), (3.34) into eq.(3.36) and given as follows;

$$M_n^0 = M_x^0 A_x^0 + M_z^0 A_z^0 + \frac{1}{2} \sum_{n=1}^{4} (M_x^{nc} B_x^n + M_x^{ns} C_x^n + M_y^{nc} B_y^n + M_y^{ns} C_y^n + M_z^{nc} B_z^n + M_z^{ns} C_z^n). \quad (3.37)$$

This expression is complicated, but it is possible to expect the resonance positions from the expressions of the components of the magnetic moment in eqs.(3.35). Resonances may occur when the quantities Ω , $\Omega \pm \omega_a$, $\Omega \pm \omega_b$, $\Omega \pm(\omega_a - \omega_b)$ and $\Omega \pm(\omega_a - 2\omega_b)$ pass through the minimum values. The positions of the resonances for the case H_1/H_0, $H_2/H_0 \ll 1$ are shown in Table 3.1. It is known that the transverse resonances i.e., the components which are proportional to $\sin^2\theta$, occur at $\omega_0 = 0$, $2\omega_a$, $2\omega_b$, $\omega_a \pm \omega_b$, $-(\omega_a \pm \omega_b)$, $\pm 2(\omega_a - \omega_b)$ etc. The transverse resonance at $\omega_0 = 0$ represents the Hanle effect and the resonances at $\omega_0 = 2\omega_a$, $2\omega_b$ are just those reported in previous section 3.2. The longitudinal resonances at $\omega_0 = \omega_a$, ω_b correspond to the ordinary magnetic resonance, and at $\omega_0 = 2\omega_a - \omega_b$, $2\omega_b - \omega_a$ correspond to the multiple quantum resonance of three photon process, and at $\omega_0 = -2\omega_a + 3\omega_b$ corresponds to the five photon process. These results agree well with those obtained previously by Winter (1959). It should be noticed that the line width of the longitudinal resonances depends on the intensity of H_1 and is remarkably broadened as the H_1 is increased, but the width of the transverse resonances is almost determined by only the relaxation time τ for small H_1. Namely, the width of the transverse resonances is narrower than that of the longitudinal resonances. For the case $\tau = \infty$, the transverse resonances may disappear,

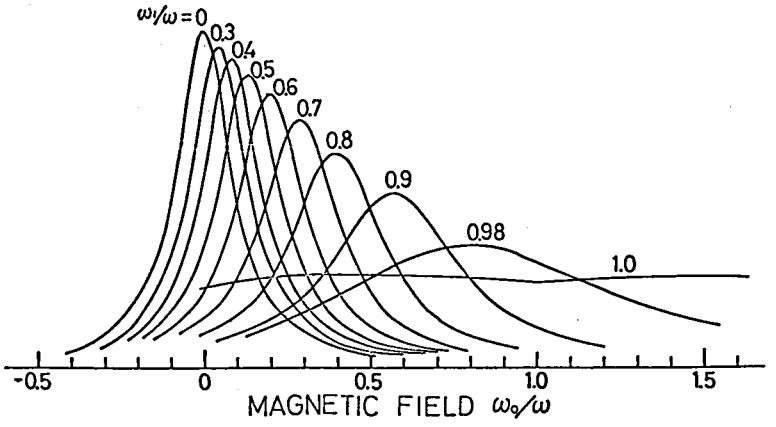

Fig. 3.13. Broadening and shift of the Hanle curve by the rotating rf field. Parameters for the theoretical curves: T = 0.01 sec, ω = 1000 rad sec^{-1} and $\theta = \pi/2$.

and only the longitudinal resonances are detectable; the relaxation time is the essential factor for the appearance of the transverse resonance.

3.3.2. Special Cases and Discussion

For the case of $\omega_a = -\omega_b = \omega$ and $H_1 = H_2 = h_1$, the two rotating rf fields become an oscillating rf field. In this case the longitudinal resonances occur at $\omega_0 = (2n + 1)\omega$; these resonances correspond to the ordinary and the multiple quantum transitions as mentioned above. On the other hand, the transverse resonances occur at $\omega_0 = 2n\omega$. The shift of the resonances at $\omega_0 = n\omega$ can be obtained from eq.(3.35) as $\omega_0 \approx \pm\omega \left[1 - \frac{1}{4}(\gamma h_1/\omega)^2\right]$, $\omega_0 \approx \pm 2\omega \left[1 - \frac{1}{3}(\gamma h_1/\omega)^2\right]$ and $\omega_0 \approx \pm 3\omega \left[1 - \frac{1}{8}(\gamma h_1/\omega)^2\right]$, etc. The resonances at $\omega_0 \approx \pm\omega\left[1 - \frac{1}{4}(\gamma h_1/\omega)^2\right]$ are ordinary, or fundamental resonance and the quantity of the shift of the resonance frequency coincides with the result which has been first derived theoretically for magnetic resonance by Bloch and Siegert (1940) and is often refered to as the Bloch-Siegert shift.

The width of the Hanle curve due to zero field level crossing is remarkably broadened by the linearly oscillating rf field. Figures 3.12(a)~(c) show the results of the calculation with eq.(3.37). Figures 3.12(a)~(c) correspond to the values $\phi = 0$, $\pi/4$ and $\pi/2$ rad. respectively. The cases for $\phi = 0$ and $\pi/2$ rad. correspond to the cases that h_1 is parallel and perpendicular to the pumping light beam, respectively. The shift towards the high field region of the Hanle curves for large values of h_1, which are drown with the dashed lines, may be caused by the fact that the condition $\delta \approx 0$, i.e., $\omega \ll \gamma h_1$, is nomore satisfied. It should be noticed that the peaks of the Hanle curves for $\phi = 0$ remain nearly the same magnitude as the intensity of rf field h_1 is increased, but for $\phi = \pi/4$ and $\pi/2$ rad. peaks of the Hanle curves are remarkably decreased as the intensity of h_1 is increased. If we observe the Hanle curve in the case

of $\phi = \pi/2$ rad., its magnitude decreases as h_1 is increased and finally will disappear.

The broadenning of the Hanle curve by the linearly oscillating rf field has also be interpreted by the shifts of the energy levels of "dressed atom" which has been analyzed quantum mechanically by Cohen-Tannoudji and Haroche (1969a,b), semiclassically by Pegg et al. (1970), and classically by Yabuzaki et al. (1972a). Their results indicate that the frequency of the precession of the magnetization around the static field H_0, and hence g-factor of the atom, are modified to be $g_0 J_0(\gamma h_1/\omega)$, where g_0 is unperturbed value of g-factor and $J_0(\gamma h_1/\omega)$ is the Bessel function of the zeroth order and the first kine, when the angular frequency ω of the rf field is much larger than ω_0. But they have not consider on the variation of the Hanle curves for the various values of ω_1.

If we put the value H_2 to zero in eq.(3.37), we can easily obtain the Hanle curves for the rotating rf field as a parameter of the intensity of H_1. As the intensity of the rotating rf field is increased, the Hanle curve is not only broadened but also shifted as shown in Fig.3.13. When the rotating rf field is absent, the transverse pumping creates a magnetization only for the weak field, but the transverse pumping is able to create the magnetization even for strong static field when the intensity of the rotating rf field increases. The peaks of the Hanle curves decrease as the intensity of H_1 is increased. Observation of the Hanle curves with the rotating rf field has been reported by Series (1970) and Haroche (1971a,b). Series has observed the shift of the Hanle curve due to the rotating rf field. But his data can not endure to discuss about the broadening and the decreasing of the peak of the Hanle curve, because of the deformation of the Hanle curve, caused by the appearance of resonances for the antirotating field when the rf field is strong. More recently, Haroche (1971 b) has observed

the shifts of the Hanle curve due to the rotating rf field. His results agree well with our theory.

The broadening of the Hanle curve by the rotating rf field may also be interpreted by considering the energy levels of "dressed atom", and may effectively be expressed in terms of the variation of the atomic g-factor. The g-factor of the atom in the oscillating rf field is given by the Bessel function as mentioned above, and varies in a somewhat complicated way. However, the effective g-factor in the rotating rf field decreases monotonously to the value of zero as the intensity is increased.

The ground state of alkali atoms consists of two hyperfine levels $F = I + 1/2$ and $F' = I - 1/2$, where I is nuclear spin of the atom. Since the signs of the gyromagnetic ratio of the two hyperfine levels F and F' are opposite each other, the zero field level crossing or the Hanle curves in the presence of the rotating rf field are displaced in opposite directions for the two hyperfine levels as shown in Fig.3.14.

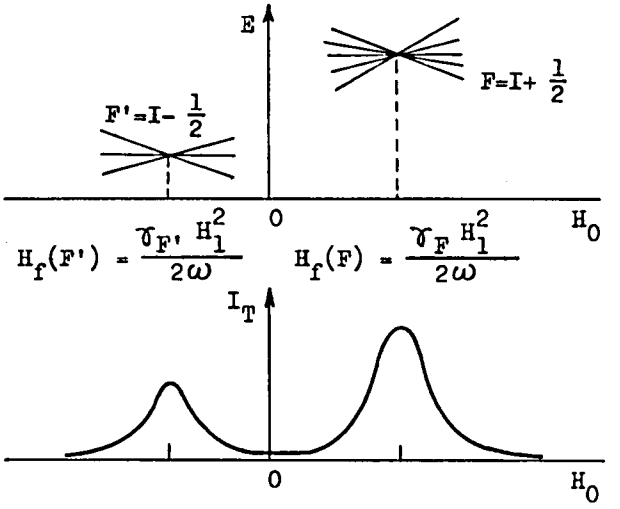

Fig. 3.14. Zeeman hyperfine diagram of alkali atoms perturbed by a rotating rf field. The fictitious fields $H_f(1)$ and $H_f(2)$ are of opposite signs.

3.4. Misalignment Effects of a Rotating RF Field

By means of a theoretical approach recently developed by Pegg and Series (Pegg and Series 1970,1973, Pegg 1973a,b), the consequences of misalignment of the rotating rf field in the magnetic resonance are investigated. For the longitudinal pumping case, the resultant equation becomes the same result obtained by Pegg (1973a). The effects of the transverse pumping are also included in the Bloch equation. The effects of the transverse pumping appeared in the resultant equation are very complicated. The rotating rf field is regarded as a static fictitious field $H_f = \gamma H_1^2/2\omega$.

3.4.1. Theory

We shall allow the plane of rotation to be at an arbitrary angle to the static field by considering the field configuration

$$\mathbf{H} = H_1 \cos\omega t(\cos\theta\,\mathbf{i} + \sin\theta\,\mathbf{k}) + H_1 \sin\omega t\,\mathbf{j} + H_s\mathbf{k}\,. \qquad (3.38)$$

When $\theta = 0$, the normal configuration which has been considered in section 3.2 is regained. A non-zero θ allows for field misalignment. Equation (3.30) can be written as

$$\begin{aligned}\mathbf{H} = {} & (H_1/2)(1+\cos\theta)(\cos\omega t\,\mathbf{i} + \sin\omega t\,\mathbf{j}) \\ & - (H_1/2)(1-\cos\theta)(\cos\omega t\,\mathbf{i} + \sin\omega t\,\mathbf{j}) + H_1\sin\theta\cos\omega t\,\mathbf{k} \\ & + H_s\mathbf{k}\,. \end{aligned} \qquad (3.39)$$

This is the sum of a rotating, a counter-rotating, an oscillating and a static component. Normally $\gamma H_1 \ll \omega$, which is just the necessary condition for the application of the procedure of Pegg and Series (1970, 1973). This procedure involves the transformation to a reference frame in which the oscillating component vanishes. Under this transformation the rotating fields become a series of rotating components with different amplitudes and frequencies. A further transformation can then be

made to the frame in which any one of these components is static. Under these transformations, the static component becomes as follows;

$$\tilde{H}_0^p = (\bar{H}_0^p, \quad 0 \quad , H_s - (p + 1) \omega / \gamma), \tag{3.40}$$

where

$$\bar{H}_0^p = (H_1/2) \{ J_{-p}(a)(1 + \cos \theta) - J_{-p-2}(a)(1 - \cos \theta) \}, \tag{3.41}$$

$a = \gamma H_1 \sin \theta / \omega$ and p is an integer, positive negative or zero, specifying the rotating component selected.

Ignoring the non-static components (for zeroth-order approximation) reduces the problem to that of normal magnetic resonance in the usual rotating frame, but now with $H_s - (p + 1) \omega / \gamma$ and $\bar{H}_0^p$ in place of $H_s - \omega/\gamma$ and H_1 in (3.2b), giving as the total field in the new frame

$$\tilde{H}_0^p = \left[\{H_s - (p + 1) \omega / \gamma\}^2 + (\bar{H}_0^p)^2 \right]^{1/2}. \tag{3.42}$$

While the excitation components in this frame are given as

$$\tilde{M}_{0x}^p = M_{0x}^{'} \cos \beta \cos \Phi (t) + M_{0y}^{'} \cos \beta \sin \Phi (t) - M_{0z}^{'} \sin \beta \ , \tag{3.43a}$$

$$\tilde{M}_{0y}^p = - M_{0x}^{'} \sin \Phi (t) + M_{0y}^{'} \cos \Phi (t) \ , \tag{3.43b}$$

$$\tilde{M}_{0z}^p = M_{0x}^{'} \sin \beta \cos \Phi (t) + M_{0y}^{'} \sin \beta \sin \Phi (t) + M_{0z}^{'} \cos \beta \ , \tag{3.43c}$$

where

$$\Phi(t) = a \sin \omega t + (p + 1) \omega t \ , \tag{3.44a}$$

$$\beta = \tan^{-1} \frac{\bar{H}_0^p}{H_s - (p + 1) \omega / \gamma} \ , \tag{3.44b}$$

and $M_{0x}^{'}$, $M_{0y}^{'}$ and $M_{0z}^{'}$ are excitation components in the laboratory frame, which have been given in eqs.(2.22). Substituting eqs.(3.42) and (3.43)

into the Bloch equation (2.13), we obtain the equations governing the motion of three components of the magnetization in the oscillating-rotating frame as follows;

$$\frac{d\tilde{M}_x^p}{dt} = \tilde{\omega}_0^p \tilde{M}_y^p - \frac{1}{\tau}\tilde{M}_x^p + \frac{1}{\tau}\tilde{M}_{0x}^p \quad , \tag{3.45a}$$

$$\frac{d\tilde{M}_y^p}{dt} = -\tilde{\omega}_0^p \tilde{M}_x^p - \frac{1}{\tau}\tilde{M}_y^p + \frac{1}{\tau}\tilde{M}_{0y}^p \quad , \tag{3.45b}$$

$$\frac{d\tilde{M}_z^p}{dt} = -\frac{1}{\tau}\tilde{M}_z^p + \frac{1}{\tau}\tilde{M}_{0z}^p \quad , \tag{3.45c}$$

where

$$\tilde{\omega}_0^p = \gamma \tilde{H}_0^p \quad . \tag{3.46}$$

Using the relation

$$\tilde{M}_+^p = \tilde{M}_x^p + i\tilde{M}_y^p \quad , \tag{3.47}$$

we obtain the following two equations which are equivalent to the three differential equations (3.45) in the forms

$$\frac{d\tilde{M}_+^p}{dt} = -i\tilde{\omega}_0^p \tilde{M}_+^p - \frac{1}{\tau}\tilde{M}_+^p + \frac{1}{\tau}(\tilde{M}_{0x}^p + \tilde{M}_{0y}^p), \tag{3.48a}$$

$$\frac{d\tilde{M}_z^p}{dt} = -\frac{1}{\tau}\tilde{M}_z^p + \frac{1}{\tau}\tilde{M}_{0z}^p \quad . \tag{3.48b}$$

Equations (3.48) can be completely be solved and the steady state solutions are given as follows;

$$\tilde{M}_x^p = -\frac{1}{1+(\tilde{\omega}_0^p \tau)^2} M_{0z}' \sin\beta$$

$$+ \frac{1}{4}\sum_{n=-\infty}^{\infty} J_n(a) \sum_{i=+,-} \Big\{ F_i(n+p+1)\big[M_{0x}'\{\cos\beta\, f_i(n+p+1) - 1\}$$

$$+ M'_{0y}\{\sin\beta + f_i(n+p+1)\}]\sin(n+p+1)\omega t$$

$$+ F_i(n+p+1)[M'_{0x}\{\cos\beta + f_i(n+p+1)\}$$

$$+ M'_{0y}\{1 - \sin\beta\, f_i(n+p+1)\}]\cos(n+p+1)\omega t$$

$$(-1)^n F_i(n-p-1)[M'_{0x}\{1 + \cos\beta\, f_i(n-p-1)\}$$

$$+ M'_{0y}\{f_i(n-p-1) - \sin\beta\}]\sin(n-p-1)\omega t$$

$$(-1)^n F_i(n-p-1)[M'_{0x}\{\cos\beta - f_i(n-p-1)$$

$$+ M'_{0y}\{1 + \sin\beta\, f_i(n-p-1)\}]\cos(n-p-1)\omega t\,, \qquad (3.49a)$$

$$\tilde{M}_y^p = \frac{\tilde{\omega}_0^p \tau}{1 + (\tilde{\omega}_0^p \tau)^2} M'_{0z}\sin\beta$$

$$+ \frac{1}{4}\sum_{n=-\infty}^{\infty} J_n(a) \sum_{i=+,-}\{\pm F_i(n+p+1)[M'_{0x}\{\cos\beta + f_i(n+p+1)\}$$

$$+ M'_{0y}\{1 - \sin\beta\, f_i(n+p+1)\}]\sin(n+p+1)\omega t$$

$$+ F_i(n+p+1)[\pm M'_{0x}\{1 - \cos\beta\, f_i(n+p+1)$$

$$\mp M'_{0y}\{\sin\beta + f_i(n+p+1)\}]\cos(n+p+1)\omega t$$

$$\pm (-1)^n F_i(n-p-1)[M'_{0x}\{\cos\beta - f_i(n-p-1)\}$$

$$+ M'_{0y}\{1 + \sin\beta\, f_i(n-p-1)\}]\sin(n-p-1)\omega t$$

$$\mp (-1)^n F_i(n-p-1)[M'_{0z}\{1 + \cos\beta\, f_i(n-p-1)\}$$

$$\pm M_{0y}\{\sin\beta - f_i(n-p-1)\}]\cos(n-p-1)\omega t, \qquad (3.49b)$$

$$M_z^p = M'_{0z}\cos\beta$$

$$+ \frac{1}{2}\sum_{n=-\infty}^{\infty} J_n(a)\sin\beta[G(n+p+1)\{M'_{0x}\, g(n+p+1) + M'_{0y}\}\sin(n+p+1)\omega t$$

$$+ G(n+p+1)\{M'_{0x} - M'_{0y}\, g(n+p+1)\}\cos(n+p+1)\omega t$$

$$+ G(n-p-1)\{M'_{0x}\, g(n-p-1) - (-1)^n M'_{0y}\}\sin(n-p-1)\omega t$$

$$+ G(n-p-1)\{(-1)^n M'_{0x} - g(n-p-1)\, M'_{0y}\}\cos(n-p-1)\omega t\,, \qquad (3.49c)$$

with

$$F_{\pm}(q) = \frac{1}{1 + (q\omega \pm \tilde{\omega}_0^p)^2\tau^2} \quad , \tag{3.50a}$$

$$f_{\pm}(q) = (q\omega \pm \tilde{\omega}_0^p)\tau \quad , \tag{3.50b}$$

$$G(q) = \frac{1}{1 + (q\omega\tau)^2} \quad , \tag{3.50c}$$

$$g(q) = q\omega\tau \quad , \tag{3.50d}$$

where the upper and the lower signs refer to i = + and −, respectively. When the transformation is made back to the laboratory frame the components of the magnetization are given as

$$M_z^p = (\tilde{M}_x^p \cos\beta + \tilde{M}_z^p \sin\beta) \cos\Theta(t) - \tilde{M}_y^p \sin\Theta(t), \tag{3.51a}$$

$$M_y^p = (\tilde{M}_x^p \cos\beta + \tilde{M}_z^p \sin\beta) \sin\Theta(t) + \tilde{M}_y^p \cos\Theta(t), \tag{3.51b}$$

$$M_z^p = - \tilde{M}_x^p \sin\beta + \tilde{M}_z^p \cos\beta \; . \tag{3.51c}$$

3.4.2. The Case of the Longitudinal Pumping

Let us at first consider the longitudinal pumping case, i.e., $M'_{0x} = M'_{0y} = 0$ and $M'_{0z} = M'_0$. For this case, eqs.(3.49) become

$$M_x^p = - \frac{1}{1 + (\tilde{\omega}_0^p \tau)^2} M'_0 \sin\beta \quad , \tag{3.52a}$$

$$M_y^p = \frac{1}{1 + (\tilde{\omega}_0^p \tau)^2} M'_0 \sin\beta \quad , \tag{3.52b}$$

$$M_z^p = M'_0 \cos\beta \; . \tag{3.52c}$$

By using eqs.(3.61), we can obtain the magnetization M_z along the pumping light beam as

$$M_z^p = \frac{1}{1 + (\tilde{\omega}_0^p \tau)^2} M'_0 \sin^2\beta + M'_0 \cos^2\beta \; . \tag{3.53}$$

Substituting eq.(3.44) into eq.(3.53), M_z^p becomes as

$$M_z^p = \left[1 - \frac{(\gamma \bar{H}_0^p \tau)^2}{1 + (\gamma \bar{H}_0^p \tau)^2 + \{\gamma H_s - (p + 1)\omega\}^2 \tau^2} \right] M_0' . \quad (3.54)$$

For $\theta = \pi/2$ rad. and p = -1, eq.(3.54) become

$$M_z^p = \left[1 - \frac{(\gamma \bar{H}_0^p \tau)^2}{1 + (\gamma \bar{H}_0^p \tau)^2 + (\gamma H_s \tau)^2} \right] M_0' , \quad (3.55)$$

where

$$\bar{H}_0^p = J_1 (\gamma H_1/\omega) \omega_1/\gamma \quad (3.56)$$

Since we are restricting the problem to $|\gamma H_1| \ll \omega$, i.e.,

$$J_1(\gamma H_1/\omega) \approx (1/2)(\gamma H_1/\omega), \quad (3.57)$$

eq.(3.55) become

$$M_z^p = \left[1 - \frac{(\omega_1^2/2\omega)^2}{(1/\tau)^2 + (\gamma H_s)^2 + (\omega_1^2/2\omega)^2} \right] M_0' . \quad (3.58)$$

This expression clearly exhibits that the rotating rf field which is rotating in the plane containing the static field H_s acts as a static fictitious field H_f perpendicularly to the rotating plane and its magnitude is $\omega_1^2/2\omega$.

3.4.3. The Case of the Transverse Pumping

Since the general expression of the magnetization for the transverse pumping has a very complicated form, we consider only the D.C. component of the magnetization for near zero field. We can obtain the following expression for $\theta = \pi/2$ rad. and for the pumping of x-direction, by neglecting the higher order Bessel function $J_n(a) = 0$, where n = 1, 2, ...,

$$M_x = J_0^2 \left(\frac{\omega_1}{\omega} \right) \left\{ \frac{1}{1 + (\tilde{\omega}_0 \tau)^2} M_0' \cos^2\beta + M_0' \sin^2\beta \right\}, \qquad (3.59)$$

where

$$\beta = \tan^{-1} \frac{\bar{H}_0^p}{H_s} , \qquad (3.60a)$$

$$\tilde{\omega}_0 = \gamma (H_s^2 + \bar{H}_0^p)^{1/2} . \qquad (3.60b)$$

By using eqs.(3.56) and (3.57), eq.(3.59) can be rewritten as

$$M_x = J_0^2 (\omega_1/\omega) \left\{ 1 - \frac{(\gamma H_s)^2}{(1/\tau)^2 + (\gamma H_s)^2 + (\omega_1/2\omega)^2} \right\} M_0' . \qquad (3.61)$$

From eqs.(3.58), (3.61) and (3.12), we can see that the rotating rf field acts as a static fictitious field $H_f = (\gamma H_1^2)/2\omega$, which is parallel to the rotating axis. Fig.3.15 shows the configurations of the static field H_s and the rotating rf field, and also shows the fictitious field due to the rotating rf field.

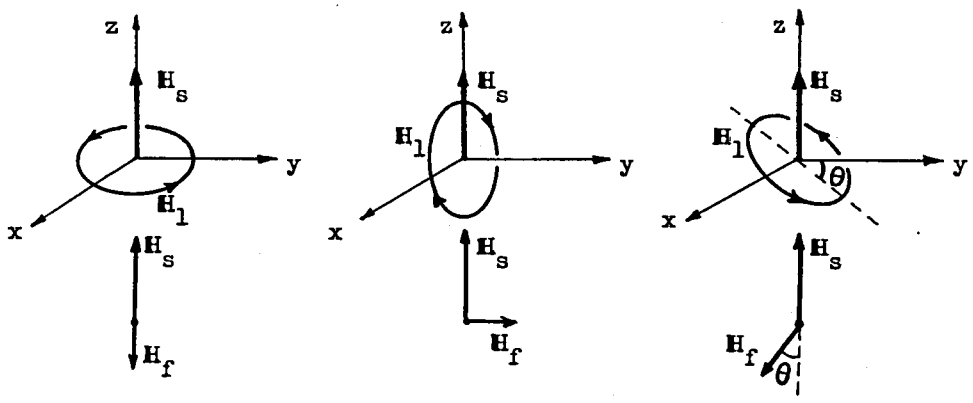

(a) (b) (c)

Fig. 3.15. Fictitious field due to the rotating rf field for various configurations.

3.5. Conclusion

The effects of the transverse optical pumping in the presence of rotating rf fields have been taken into account for the phenomenological Bloch equation used by Bell et al.(1957). The new type resonances which appear in the unmodulated component and the components modulated at ω and 2ω in the transmitted light beam have been predicted and verified experimentally in section 3.2. Quantitative characters of the observed new type resonances agree with the theoretical calculations. The new type resonances are shifted and broadened as the intensity of the rf field increases.

We have treated the rf field H_1 as a rotating rf field in the theory but used an oscillating (linearly) rf field in the experiments, so that the rigorous comparison between the theory and the experimental results is restricted within the condition that $\omega_1 < \omega$ is satisfied. It should be noted that eq.(3.9) gives a comprehensive description for the behavior of the ensemble of the optically pumped atoms without the restriction, if we use a rotating rf field instead of the oscillating rf field.

The evolution of the magnetization of the paramagnetic particles in the presence of the two rotating rf fields with frequencies ω_a and ω_b has been investigated in section 3.3. It has been shown that the longitudinal resonances occur at $\omega_0 = \omega_a$, ω_b, $2\omega_a - \omega_b$, and $2\omega_b - \omega_a$, etc., and the transverse resonances occur at $\omega_0 = 0$, $2\omega_a$, $2\omega_b$, $\omega_a \pm \omega_b$ and $\pm 2(\omega_a - \omega_b)$, etc. The longitudinal resonances at $\omega_0 = \omega_a$, ω_b correspond to the ordinary magnetic resonance and those at $\omega_0 = 2\omega_a - \omega_b$, $2\omega_b - \omega_a$ correspond to the multiple quantum transitions which are due to three photon process. The transverse resonances at $\omega_0 = 0$, $2\omega_a$, $2\omega_b$ can be expected from our previous paper (Tsukada et al. 1972), and those at $\omega_0 = \omega_a \pm \omega_b$, $\pm 2(\omega_a - \omega_b)$ etc., which correspond to the

new type resonance for the case of the two rotating rf fields, have been first shown by Tsukada, Yabuzaki and Ogawa (1973). We have also shown that the transmitted light beam passed through the sample cell contains the beat frequencies such as $\omega_a - \omega_b$, $2(\omega_a - \omega_b)$, $\omega_a - 2\omega_b$ and $2\omega_a - \omega_b$ etc. Moreover, it has been shown that the Hanle curve is broadened not only by the oscillating rf field but also by the rotating rf field. As the intensity of the rotating rf field is increased, the Hanle curve shifts towards $\omega_0 = \omega$ and its peak is decreased. The peak of the Hanle curve is also remarkably decreases with the intensity of the oscillating rf field, if the pumping light beam is perpendicular to h_1 and H_0.

In section 3.4, we have investigated the effects of misalignment of the rotating rf field in the magnetic resonance by means of a theoretical approach developed by Pegg and Series (1970). The effects of the transverse pumping appeared in the resultant equations (3.49) are very complicated. For weak static field, the rotating rf field is regarded as a static fictitious field $H_f = \gamma H_1^2/2\omega$.

CHAPTER 4

EFFECTS OF THE TRANSVERSE PUMPING IN THE PRESENCE OF AN OSCILLATING RF FIELD

4.1. Introduction

In the usual magnetic resonance experiments with optically pumped atoms, the atoms are subjected to the static magnetic field $\mathbf{H}_0$ and the rf field which is linearly oscillating, rather than rotating, in the plane perpendicular to the static field $\mathbf{H}_0$, together with the circularly polarized light beam which has two roles to create the magnetization in the ensemble of atoms along the direction of the light beam and to monitor the variation of this component of the magnetization. In common with these experiments, the angular frequency of the rf field is set near the Zeeman splitting $\gamma H_0 = g_0 \beta H_0$ of the ground state, where g_0 is the atomic g-factor and β is Bohrmagneton, and its amplitude is, in general, weak enough not to saturate the Zeeman transitions.

The interest in the effects of the strong oscillating rf field on the optically pumped atoms has been increased. In the case that the rf field is oriented parallel to the field $\mathbf{H}_0$, the parametric resonance takes place when the integral multiple of the angular frequency of the rf field coincides with the Zeeman splitting. Semiclassical (Aleksandrov et al. 1963, Favrė and Geneux 1964) and quantum mechanical treatments (Polonsky and Cohen-Tannoudji 1965c) on the parametric resonance have been given, and demonstrating experiments have been made by observing the modulation of the fluorescence with cadmium vapor and observing the absorption of the pumping light beam propagating perpendicularly to the field $\mathbf{H}_0$ with mercury vapor. We show the theoretical analysis for the parametric resonance in Appendix B.

On the other hand, when the oscillating rf field is oriented perpen-

dicularly to the field $\mathbf{H}_0$ and the integral multiple of its angular frequency coincides with the Zeeman splitting, studies have been made on the shifts of the resonance frequency and the multiple quantum transitions between Zeeman sublevels (Cohen-Tannoudji and Haroche 1969a,b). Recent interest has been given to the effects of the strong rf field, whose frequency is nonresonant for the atomic transitions. Cohen-Tannoudji and Haroche (1969a, b) have analyzed this case by quantizing the rf field and by introducing a new concept that the atom is "dressed" by the rf photons. One of the important effects of the "dressed atom" is that the frequency of the precession of the magnetic moment around the field $\mathbf{H}_0$, and hence the g-factor of the atom, is drastically modified by the rf photons, when the angular frequency of the rf field is much higher than γH_0 (Cohen-Tannoudji and Haroche 1969b, Haroche and Cohen-Tannoudji 1970).

Recently, Pegg and Series (1970) have considered semiclassically the case that the static magnetic field $\mathbf{H}_0$ has weak component $H_\perp$ perpendicular to the oscillating rf field $\mathbf{H}_1(t) = \mathbf{H}_1 \cos \omega t$, and the component $H_{/\!/}$ parallel to $\mathbf{H}_1$ whose magnitude is equal to $n\omega/\gamma$, where $n = 0, \pm 1, \pm 2, \cdots$. The theoretical results have been cheked partly by Chapman (1970) by observing themodulation in the fluorescence of mercury vapor.

In the case that the pumping light beam and the oscillating rf field $\mathbf{H}_1$ with an angular frequency ω are perpendicular to the static field $\mathbf{H}_0$, the effects of the transverse pumping have been analyzed by using the density matrix and iteration method (Cohen-Tannoudji and Haroche 1967) and by use of quantum mechanics (Cohen-Tannoudji and Haroche 1969a). Cohen-Tannoudji and Haroche (1965,1967) have observed the new type of resonances in the modulation of the transmitted light beam propagated through the mercury vapor and the resonances have been named "Haroche's resonance" by Cohen-Tannoudji (1968). They concluded that these resonances appear in

the various even harmonics $2p\omega$, where p is an integer, of the transmitted light beam when $H_0 = 2n\omega/\gamma$, where n is an integer, for weak rf field and shifted but not broadened as the intensity of the rf field is increased. They have also mentioned that their experimental results for the components modulated at 2ω and 4ω show the saturation effect in the resonance intensity for large intensity of the rf field. We show that the Haroche resonance is strongly power broadened and is seen to move towards low field region more rapidly than their perturbation results. Saturation effects in their experiments appear to be consistent with our theoretical results, but their presented data (Cohen-Tannoudji and Haroche 1965) are not so many enough to allow a detail comparison. Indeed, we have already shown in section3.2 that the Haroche like resonances for the rotating rf field are not only shifted but also broadened as the intensity of the rf field is increased.

In section 4.2, we generalize the case treated by Pegg and Series (1970) and Cohen-Tannoudji and Haroche (1966) to the situation that the static magnetic field $\mathbf{H}_0$ is oriented in an arbitrary direction with respect to the oscillating field $\mathbf{H}_1$. In that case the circularly polarized light beam is applied along the direction of $\mathbf{H}_1$. We analyze the behavior of the optically pumped atoms in these static and oscillating magnetic field, in terms of the macroscopic magnetization. In the classical theory, we can easily introduce the effects of the relaxation process and of the pumping light beam, and can obtain the shapes of the line of the Hanle curve and the parametric resonances, which take place respectively $H_{//} = 0$ and $H_{//} = n\omega/\gamma$, where n is an integer, when the magnetic field $H_\perp$ is weak. We show that the angular frequency of the Larmor precession of the magnetization around the field $H_\perp$ is drastically modified by the rf field when the Hanle effect or the parametric resonance occurs. This fact can be also obtained by the

quantum mechanical treatment (Yabuzaki et al. 1972a).

In order to verify the theory, we carry out the experiments with respect to the ground state of cesium atoms, in which we observed the secular change of the transmitted light intensity. In addition, the effects of the non-resonant oscillating rf field on optically pumped alkali vapor magnetometer are investigated.

In section 4.3, we investigate the behaviors of the magnetization undergoing the influences of both the transverse and the longitudinal pumping. We study, by use of the theoretical approach recently developed by Pegg (1973a, b), the case that the misaligned oscillating rf field can be regarded as a perturbation on the static field. It is shown for this case that two types of resonances, i.e., the longitudinal and the transverse resonances, appear simultaneously at integral multiples of the oscillating rf field frequency. Some experimental results are also shown.

4.2. Modification of the Atomic g-factor by the Oscillating RF Field

In this section, we deal with the interaction between atoms in the ground state and a relatively strong rf field. Behavior of the optically pumped atoms in the oscillating rf field is analyzed classically in terms of the macroscopic magnetization, in the case that the static magnetic field has components both parallel and perpendicular to the rf field. The theory predicts that the g-factor is modified by the rf field when the Hanle effect and the parametric resonance take place, and that the effect makes its appearance in the variation of width and maxima of lines of the Hanle effect and the parametric resonance. The modification of the g-factor is also derived by the quantum mechanical treatment. The theoretical predictions are quantitatively verified by the experiments with cesium vapor.

4.2.1. Theory

(a) Phenomenological Description of Spin System

The directions of the magnetic fields and of the pumping light beam are shown in Fig.4.1.

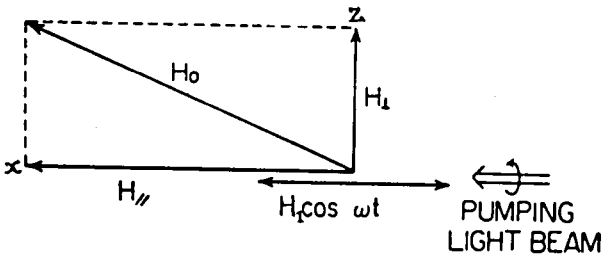

Fig. 4.1. Illustration of the situation to be considered.

From eq.(2.13), we obtain the equations governing the motion of three components of **M** as follows;

$$\frac{d M_x}{dt} = -\frac{1}{\tau} M_x + \frac{1}{\tau} M_0' - \omega_\perp M_y, \tag{4.1a}$$

$$\frac{d M_y}{dt} = -\frac{1}{\tau} M_y - (\omega_{//} + \omega_1 \cos \omega t) M_z + \omega_\perp M_x , \tag{4.1b}$$

$$\frac{d M_z}{dt} = -\frac{1}{\tau} M_z + (\omega_{//} + \omega_1 \cos \omega t) M_y , \tag{4.1c}$$

where

$$\omega_{//} = g_0 \beta H_{//} , \quad \omega_\perp = g_0 \beta H_\perp , \quad \omega_1 = g_0 \beta H_1 . \tag{4.2}$$

It is well known that the amount of the absorption of the circularly polarized light beam by atoms is related to the component of the magnetization along the direction of the light beam. Then in this case the signal to be observed is determined by the x-component of **M**, i.e., M_x, so that we have to solve eqs.(4.1) for M_x. It is usual in analysis to

transform the variables M_x, M_y and M_z to the component of $\mathbf{M}$ along the static magnetic field, i.e. $\mathbf{H}_0$ in this case, and two components rotating around the static magnetic field. This transformation has actually been used by Novikov et al.(1968). However, in order to get approximate solution, the restriction that $\omega_1 \sin\theta / \omega \ll 1$ is required in this transformation.

In our treatment of the oscillating rf field it is very helpful to refer the motion of the magnetization, not to the fixed coordinate system of the laboratory but to a coordinate system that rotates about $\mathbf{H}_0$ with the modulated angular frequency $(\omega_1/\omega)\sin\omega t$, in which the oscillating rf field is reduced to zero (Pegg and Series 1970). In this frame, however, the static magnetic field $\mathbf{H}_0$ in the laboratory frame is no longer time-independent. The field in the frequency modulated rotating frame is the sum of the various harmonics of ω of rotating rf field and become as follows;

$$\tilde{\mathbf{H}} = H_\perp \sum_{n=-\infty}^{\infty} J_n(\omega_1/\omega)\{\mathbf{J}_z \cos n\omega t + \mathbf{J}_y \sin n\omega t\} . \qquad (4.3)$$

Considering the motion of the magnetization in the rotating frame, we think of that the geometrical configuration of the magnetic fields and the pumping light beam is the case of the ordinary magnetic resonance with many rotating rf fields. When $|\gamma H_\perp / \omega| \ll 1$ and $\omega \gg \Gamma$ are satisfied, it is a good approximation to consider that only one of the rotating rf fields with the angular frequency $n\omega$, affects the motion of the magnetization near $\gamma H_{//} = n\omega$. Therefore, the variation of the transmitted light intensity is given as follows;

$$M_x^n = \sum_{n=-\infty}^{\infty} \frac{1 + (\omega_{//} + n\omega)^2 \tau^2}{1 + (\omega_{//} + n\omega + \Delta\omega_n)^2 \tau^2 + \{\omega_\perp J_n(\omega_1/\omega)\tau\}^2} \qquad (4.4)$$

where we have included the term $\Delta\omega_n$, yet to be determined, to allow for

possible resonance shifts due to higher order effects of the neglected rotating components.

Since we are restricting the problem to $|\gamma H_1| \ll \omega$, it is sufficient to consider only those effects derivable by second order perturbation theory applied, for example, after incorporating the rotating components in a Floquet matrix (Shirley 1965). Elementary shifts due to each component will therefore be added. Each rotating fields component gives rise to a Bloch-Siegert type shift $\{\gamma H_1 J_m(\omega_1/\omega)\}^2/2m\omega$. The total shift is thus

$$\Delta\omega_n = \frac{(\gamma H_1)^2}{2\omega} \sum_{\substack{m=-\infty \\ m\neq n}}^{\infty} J_m^2\left(\frac{\omega_1}{\omega}\right) \frac{1}{n-m} \quad . \tag{4.5}$$

This expression is the same one as that obtained by Allegrini and Arimond (1971) and by Pegg (1972a).

When the variables ω_1, ω and $\omega_\perp$ are fixed, eq.(4.4) shows that M_x as a function of $\omega_{//}$ is expressed by the superposition of the Lorentzian functions, the center of which is given by $\omega_{//} = -n\omega$. When the value of ω satisfies the condition

$$\omega^2 \gg \omega_\perp^2 + (1/\tau)^2, \tag{4.6}$$

each Lorentzian function is well resolved. Hereafter we consider the case that ω satisfies the above condition.

First we will consider the particular case that $\omega_{//} = 0$, i.e. the off-resonant rf field $H_1(t)$ whose angular frequency ω satisfies the condition (4.6) is applied perpendicularly to the static magnetic field $H_\perp$. In this case the secular component (or D.C. component) of the magnetization along the direction of H_1 becomes from eq.(4.4), neglecting the term $\Delta\omega_n$ in eq. (4.4), as follows;

$$M_x^0 = \frac{(1/\tau)^2}{\{\omega_\perp J_0(\omega_1/\omega)\}^2 + (1/\tau)^2} M_0' \quad . \tag{4.7}$$

In the absence of H_1, eq.(4.7) gives rise to the usual Hanle effect which can be obtained by sweeping $H_\perp$ around the value of zero. We can see from eq.(4.7) that the broadening of the Hanle curve due to the field $H_\perp$ is drastically modified by the rf field H_1, which leads to the concept that the angular frequency of the Larmor precession around $H_\perp$ is modified by H_1. In general it may be expected that the medium in the relatively strong rf field is no more isotropic, and hence the g-factor perpendicular to the field H_1, i.e. $g_\perp$ is modified as follows;

$$g_\perp = g_0 J_0(\omega_1/\omega). \tag{4.8}$$

Equation (4.8) is exactly the same as the result obtained by Cohen-Tannoudji and Haroche (1966) who have analized by quantizing the rf field, and by Pegg and Series (1970). However, in their analysis, the disorientation process due to the thermal relaxation and the pumping light beam was neglected so that the condition to obtain the eq.(4.8) was that $\omega \gg \omega_\perp$ instead of the inequality (4.6).

On the other hand, by varing $\omega_{//}$ in the vicinity of $-\omega$, -2ω, $\cdots$, eq.(4.4) gives rise to the effects of the parametric resonances. The minimum of M_x^n for the n-th resonance are given by

$$M_{x,\min}^n = \frac{(1/\tau)^2}{\omega_\perp J_n(\omega_1/\omega)^2 + (1/\tau)^2} M_0' , \tag{4.9}$$

and its half width $\delta_{//}^n$ is given by

$$\delta_{//}^n = (1/\tau)^2 + \{\omega_\perp J_n(\omega_1/\omega)\}^2 \quad . \tag{4.10}$$

Generally the parametric resonance is characterized by the absence of

the broadening due to the rf field, but in our case the width of the n-th resonance depends on the amplitude of H_1. This is due to the existence of the weak magnetic field $H_\perp$ perpendicular to the field H_1. Then in the extreme case that $\omega_\perp \ll |\tau^{-1} J_n(\omega_1/\omega)|$, eq.(4.9) gives the pure effect of the parametric resonance.

Consequently, when $\omega_{//}$ is in the region where $|\omega_{//} + n\omega| \ll 1/\tau + \omega_\perp$, we are again led to the new concept that the angular frequency of the precession around the field $H_\perp$ is modified, i.e. $g_\perp$ becomes

$$g_\perp = g_0 J_n(\omega_1/\omega). \tag{4.11}$$

It should be noted that an essential difference exists between the modifications of $g_\perp$ represented by eqs.(4.8) and (4.11). in each other. Namely in eq. (4.8) the angular frequency ω is nonresonant, but in eq.(4.11) the integral multiple of ω is resonant to the static field H_0, approximately to $H_{//}$.

When we set $\omega_{//}$ to the center of the n-th resonance, and sweep $\omega_\perp$, we can get the Lorentzian curve which is analogous to the Hanle curve represented by eq.(4.7). The half width for the n-th resonance is given by

$$\delta_\perp^n = \{\tau J_n(\omega_1/\omega)\}^{-1}. \tag{4.12}$$

(b) Quantum Mechanical Treatment of the Modification of g-Factor

Modification of the value of $g_\perp$ due to the rf field, which is represented by eq.(4.11), can be also obtained by the quantum mechanical treatment, in which the rf field is quantized. Here we analyze along the line of the theory by Cohen-Tannoudji and Haroche (1969b), who have treated the case $H_{//} = 0$. We neglect the thermal relaxation process and assume that the total electronic angular momentum **J** in the ground state of an atom is 1/2 and then the ground state consists of the two Zeeman substates $|+\rangle$ and $|-\rangle$. If the effect of the pumping light is neglected, the total Hamiltonian of the system can be

written as

$$\mathcal{H} = \omega_{\perp} J_z + \omega_{//} J_x + \omega\, a^{+}a + \lambda J_x (a + a^{+}) , \qquad (4.13)$$

where J_x and J_z are the components of the angular momentum of an atom along the x and z axes respectively, and a^{+} and a are the creation and annihilation operators of the rf photon ω. The first and second terms on the right hand of eq.(4.13) represent the magnetic dipole coupling with static magnetic fields $H_{\perp}$ and $H_{//}$,respectively. The first term has eigenstates $|+\rangle_z$ and $|-\rangle_z$ with eigenvalues $\pm$ 1/2 $\omega_{\perp}$, and the second term has eigenstates $|+\rangle_x$ and $|-\rangle_x$ with eigenvalues $\pm$ 1/2 $\omega_{//}$. The third term is the Hamiltonian of the rf field only, the eigenstate being represented by $|n\rangle$, where n is the number of the rf photons. The last term represents the interaction between the atoms and rf photons, λ being the coupling coefficient which is given by Cohen-Tannoudji and Haroche (1969a) as

$$\lambda = \frac{\omega_1}{2\sqrt{\bar{N}}} , \qquad (4.14)$$

where $\bar{N}$ is the average number of the rf photons.

In eq.(4.13), the second term is considered to be a small perturbation, thus we adopt the perturbation theory. Equation (4.13) can then be written as follows;

$$\mathcal{H} = \mathcal{H}_0 + \omega_{\perp} J_z , \qquad (4.15)$$

where

$$\mathcal{H}_0 = \omega_{//} J_x + \omega\, a^{+}a + \lambda J_x (a + a^{+}). \qquad (4.16)$$

The eigenstates and eigenvalues of $\mathcal{H}_0$ have already been obtained (Polonsky et al. 1965) and given by

$$\mathcal{H}_0 |+\rangle_x |\bar{n}_+\rangle = (\omega_{//}/2 + n\omega - \lambda^2/4\omega) |+\rangle_z |\bar{n}_+\rangle , \qquad (4.17a)$$

$$\mathcal{H}_0 |->_x |\bar{n}'_-\rangle = (-\omega_{//}/2 + n'\omega - \lambda^2/4\omega) |->_x |\bar{n}'_-\rangle , \qquad (4.17b)$$

with

$$|\bar{n}_\pm\rangle = D (\mp \lambda/\omega) |n\rangle , \qquad (4.18)$$

where $D(\pm \lambda/\omega)$ is the displacement operator (Glauber 1963).

Equations (4.17) indicate that the eigenstates $|+\rangle_x |\bar{n}_+\rangle$ and $|-\rangle_x |\bar{n}_-\rangle$ have the same energy, when the condition $(n - n')\omega = \omega_{//}$ is satisfied. This is the condition for which the parametric resonance takes place. This degeneracy is removed by the perturbation $\omega_\perp J_z$.

The effects of the perturbation of $\omega_\perp J_z$ can be obtained by finding the matrix element in the base of $|\pm\rangle_x |\bar{n}_\pm\rangle$, i.e. eigenstates of $\mathcal{H}_0$. The matrix element is

$$_x\langle +|\langle \bar{n}_+|\omega_\perp J_z |\bar{n}'_-\rangle|->_x = \omega_\perp \langle \bar{n}_+|\bar{n}'_-\rangle_x \langle +|J_z|->_x \quad . \qquad (4.19)$$

For the large value of n, the matrix element $\langle \bar{n}_+|\bar{n}'_-\rangle$ is given by $J_{n-n'}(\omega_1/\omega)$. The matrix $_x\langle +|J_z|->_x$ can be diagonalized by a rotation of the coordinate system of $\pi/2$ about Oy, then we have new energies $\pm (1/2)\omega_\perp J_{n-n'}(\omega_1/\omega)$. Consequently, if we measure the g-factor in the direction of the z axis, $g_\perp$ is predicted to modified as represented by eq.(4.12).

4.4.2. Experiments and Discussion

In the experiment, the situation is slightly different from that discussed in the theory; the atoms are subjected to the rf field $\mathbf{h}$ (t) rotating in the Y-Z plane with the amplitude h and the angular frequency Ω , in addition to the static magnetic field $\mathbf{H}_s$ and the oscillating rf field $\mathbf{H}_1(t)$ which are oriented in the X axis, as shown in Fig.4.2(a). Thus in the present case , the coordinate system rotating about X axis synchronously to

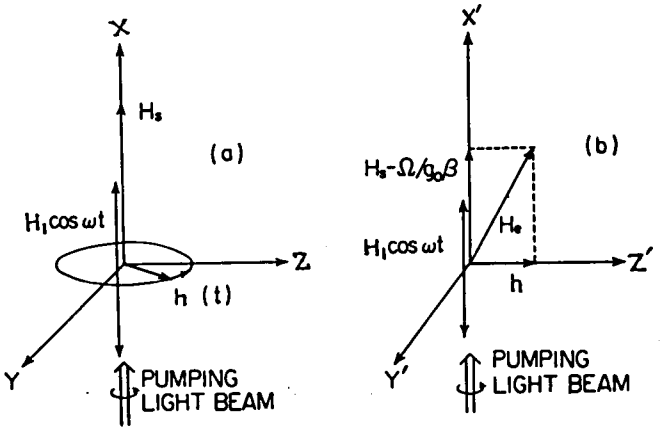

Fig. 4.2. Directions of magnetic fields and pumping light beam in the laboratory coordinate system (a) and in the coordinate system rotating synchronously to the rf field h(t)(b).

the field h(t) becomes important. As shown in Fig.4.2(b), in the rotating coordinate system, the static magnetic field is the effective field $\mathbf{H}_e$, and its components parallel and perpendicular to the direction of $\mathbf{H}_1(t)$ can be varied independently. Thus the rotating coordinate system is equivalent to the situation discussed in the theory by considering that

$$\mathbf{H}_0 = \mathbf{H}_e,\ H_{//} = H_s - \Omega/g_0\beta\ ,\ H_\perp = h\ . \tag{4.20}$$

Since the direction of observation, i.e. the direction of the pumping light beam, is kept unchanged by the rotation of coordinate system, it results that the change in $M_x^n(0)$ to be observed in the present experiment gives the change in $M_x^n(0)$ derived in the theory.

The optical system consists of an electrodeless rf cesium lamp, a circular polarizer, an absorption cell containing cesium vapor, and a solar cell.

Resonance radiation from the cesium lamp propagating in the X direction was passed through a circular polarizer, and was focussed by a quartz lens onto an absorption cell which was situated at the center of the Helmholtz coils to produce the static magnetic field $\mathbf{H}_s$. The magnitude of the field $\mathbf{H}_s$ was about 0.5 gauss. The sylindrical absorption cell with coated walls has diameter of 5 cm and length of 5 cm, and contained the saturated cesium vapor at the temperature of about 30°C. The rf fields $\mathbf{h}(t)$ and $\mathbf{H}_1(t)$ were provided by the rf coils of 10 cm in diameter wound around the absorption cell. The light beam transmitted through the absorption cell was focussed onto the solar cell in order to detect the secular or D.C. change in the X component of the magnetization $\mathbf{M}$. In the following experimemt, we set the frequencies $\Omega/2\pi$ and $\omega/2\pi$ to 175 KHz and 3 KHz, respectively.

In order to demonstrate the Hanle effect and the parametric resonance in the rotating coordinate, the magnetic field $\mathbf{H}_s$ was swept through the

resonance of about 0.5 gauss and the output of the solar cell was amplified by a D.C. amplifier and displayed on the X-Y recorder, as a function of H_s. The typical recorder traces in the case that the amplitude h is set about 0.2 milligauss are shown in Fig.4.3, where the amplitude H_1 is varied as a parameter.

It is noted that these recorder traces give the variation of the quantity $\Delta M_x^n = M_0'(1 - M_x^n)$, which is represented in eq.(4.4), due to the field amplitude h. In Fig.4.3, we can see that two resonance lines appear when H_s is swept near $(\Omega + n\omega)/g_0\beta$, where n is zero or an integer. The appearance of the two resonance lines is due to the fact that the rf field $\mathbf{h}(t)$ is not circularly polarized but elliptically polarized, so that the resonances of two hyperfine levels, F = 4 and 3, in the ground state of the cesium atom are induced. In the following discussion, we will give a particular attention to the larger line which is due to the resonance of the F = 4. In Fig.4.3, we can see that the width of each resonance line is almost independent of the amplitude H_1. This feature can easily be explained by the theory, by assuming $\omega_1 < 1/\tau$ in eq.(4.10). This assumption is valid in this case, since $\omega_1/2\pi$ is about 70 Hz and the value of $1/2\pi\tau$ estimated from the width of the resonance line is about 120 Hz.

From eq.(4.10), it is expected that the width of each resonance line is broadened by the rf field $\mathbf{H}_1(t)$ for the large value of ω_1. This can be seen in Fig.4.4, which shows the recorder traces in the case $h \simeq 3.4$ milligauss, i.e. $\omega_1 \simeq 10/\tau$.

The variation of the maximum of the n-th resonance line due to the amplitude H_1 was automatically obtained by setting the value of H_s to the center of the n-th resonance, i.e. $(\Omega + n\omega)/g_0\beta$ and sweeping the amplitude H_1 from the value of zero. The line appearing at $H_s = \Omega/g_0\beta$ is not due to the resonance, but to the Hanle effect in the rotating coordinate and we will call it zeroth resonance.

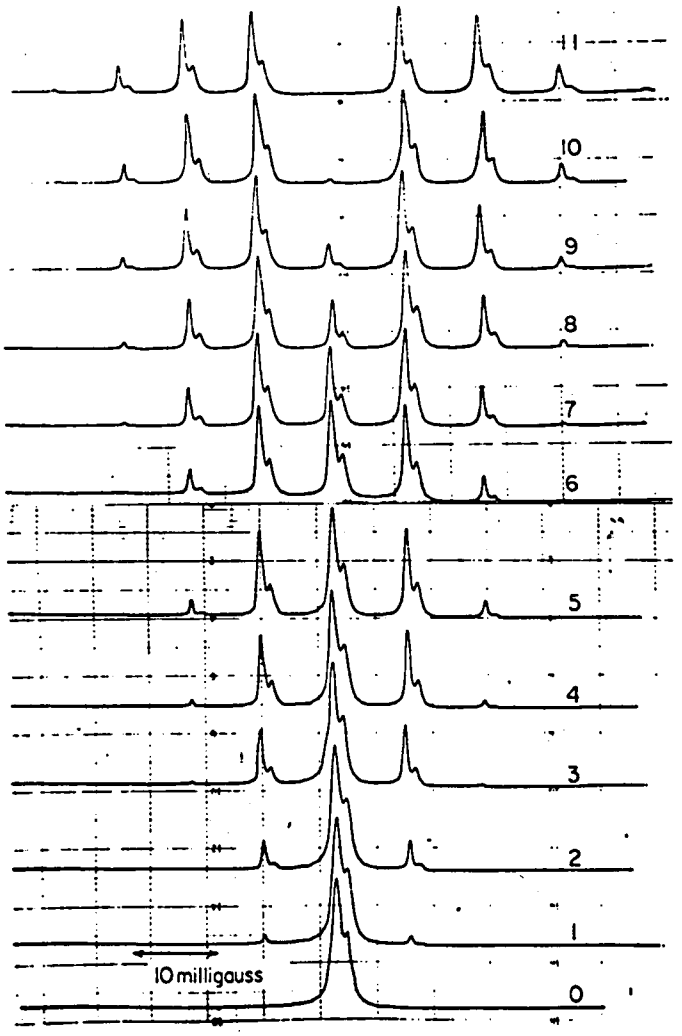

Fig. 4.3. Recorder traces showing the Hanle effect and parametric resonances in the case $h \simeq 0.2$ milligauss. The static magnetic field H_s is swept near 0.5 gauss and the amplitude H_1 of the rf field $H_1(t)$ is varied as a parameter. A number written in each trace gives the value of H_1; H_1 = number x 1.9 milligauss.

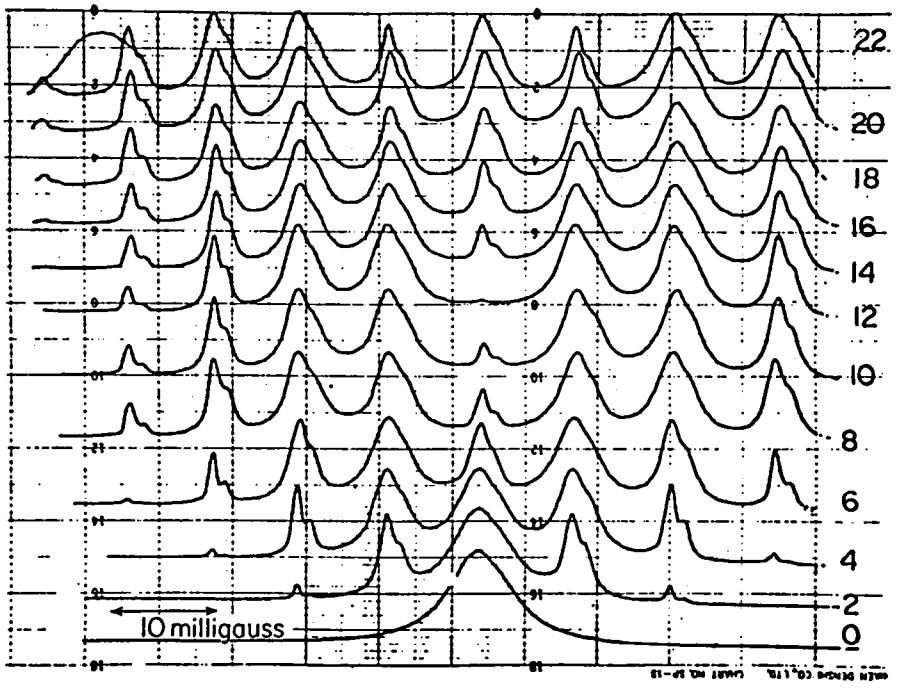

Fig. 4.4. Recorder traces showing the Hanle effect and parametric resonances in the case $h \simeq 3.4$ milligauss. A number written in each trace gives the value of H_1; H_1 = number x 1.9 milligauss.

Typical results for zeroth, first and second resonances are shown in Fig.4.5. Although the drifts of the base lines exist in these recorder traces, we can confirm that these experimental results agree with the theory given by eq.(4.9).

Recent demonstrating experiment (Cohen-Tannoudji and Haroche 1969b) on the modification of the g-factor due to the nonresonant rf field has been carried out by measuring the width of the Hanle curve, which is determined by the quantity $g_\perp \beta H_\perp \tau$ as shown in eq.(4.7). In order to obtain experimentally the similar Hanle curve in the rotating coordinate, based on the relations (4.20), we set H_s to the zeroth resonance, i.e. to $\Omega / g_0 \beta$, and varied the value of h near zero. The variation of the maximum of the zeroth resonance is shown in Fig.4.6(a), where the amplitude H_1 is varied as a parameter. The vertical axis in this figure is drawn downward, since the increase of the maximum of the zeroth resonance corresponds to the decrease of $M_x^n(0)$. Figure 4.6(a) shows apparently the variation of the width of the Hanle curve due to H_1 and this variation is the same as that of $\delta_\perp^{(0)}$ due to ω_1 in eq.(4.12). As the result, we can confirm experimentally that the value of $g_\perp$ is modified as seen in eq.(4.8).

The similar experiments were carried out by setting H_s to the first and second resonances. The results are shown in Fig.4.6(b) and (c). We see that the shape of the curves in Fig.4.6(b) and (c) are quite analogous to that of the Hanle curves shown in Fig.4.6(a), and the widths also vary considerably with the field amplitude H_1. The variation of the widths of the curves in Fig.4.6(b) and (c) due to H_1 shows a good agreement with that of $\delta_\perp^{(1)}$ and $\delta_\perp^{(2)}$ due to ω_1 in eq.(4.12), and then it can be said that the value of $g_\perp$ becomes $g_0 J_1(\omega_1/\omega)$ and $g_0 J_2(\omega_1/\omega)$ when $\omega_{//} = \omega$ and $\omega_{//} = 2\omega$, respectively. In this way the varidity of eq.(4.11) can be proved experimentally.

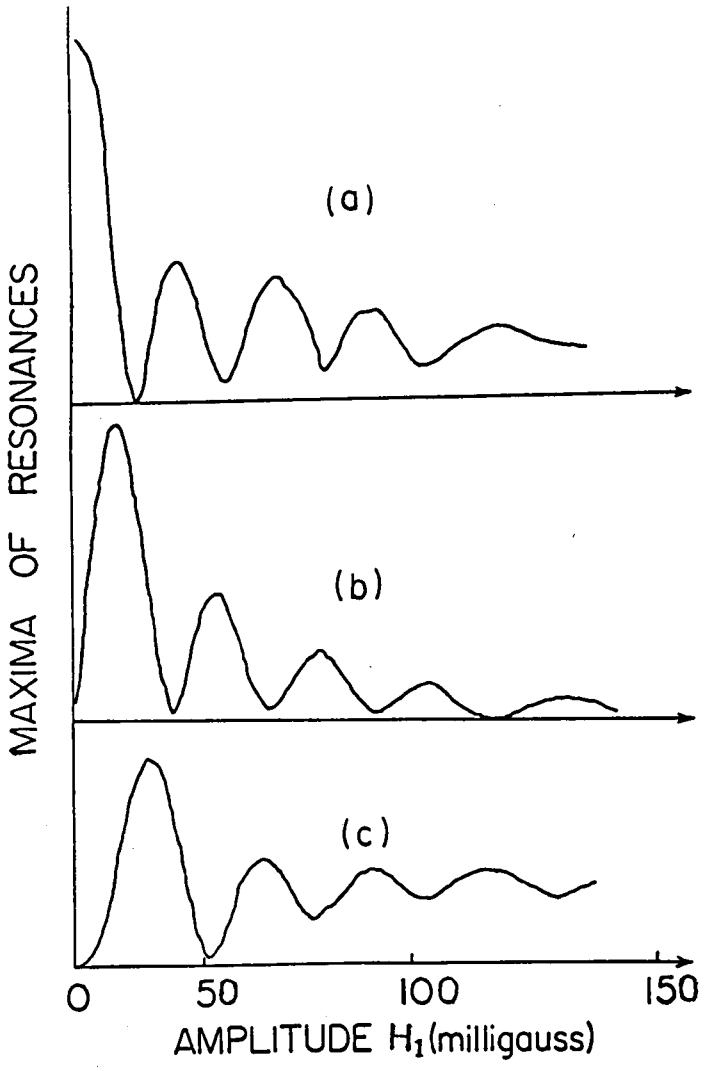

Fig. 4.5. Level crossing experiment as a function of H_1. Recorder traces showing the variation of the maxima of the zeroth resonance (a), the first resonance (b), and the second resonance (c) due to the amplitude H_1. The amplitude h is about 1 milligauss, i,e. $\omega_1/2\pi =$ 350 Hz.

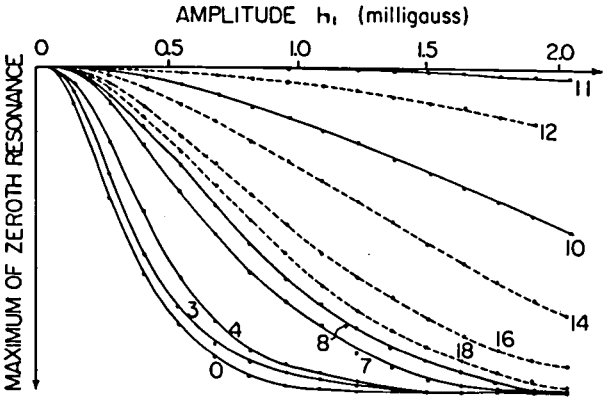

Fig. 4.6. (a). Variation of the maximum of the zeroth resonance due to the amplitude h with a parameter of the amplitude H_1. A number written by each curve gives the value of H_1 in the unit of 1.9 milligauss.

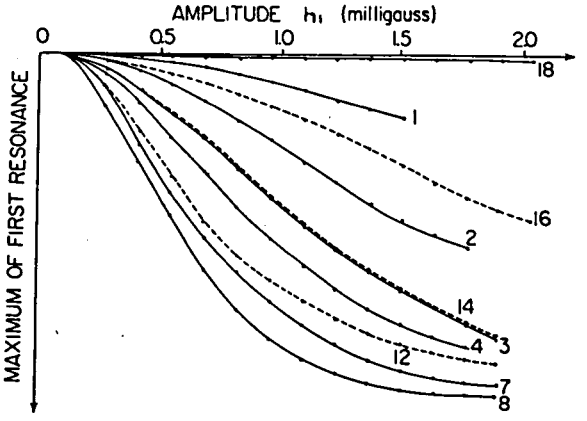

Fig. 4.6. (b). Same as for Fig.4.6(a), but for the maximum of the first resonance.

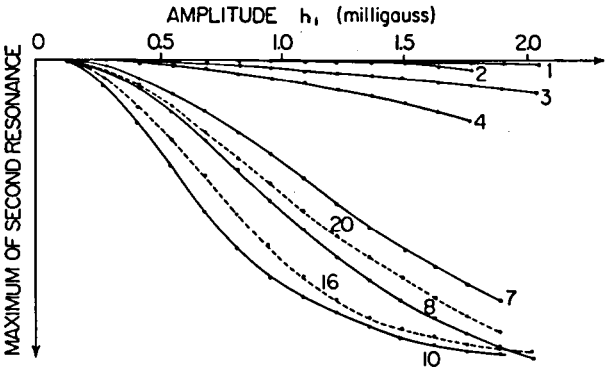

Fig. 4.6. (c). Same as for Fig.4.6(a), but for the maximum of the second resonance.

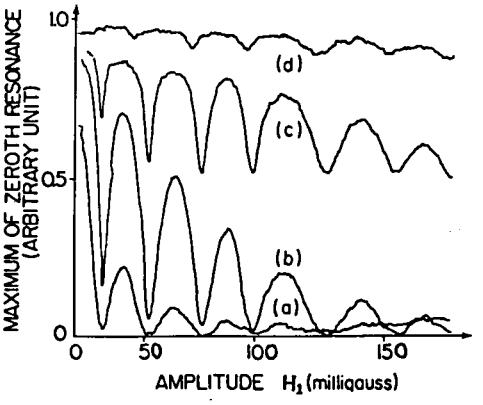

Fig. 4.7. Level crossing curves as a function of H_1 for various values of h. Recorder traces showing the variation of the maximum of the zeroth resonance due to the amplitude H_1. The amplitude h is varied as a parameter; (a), (b), (c) and (d) are the cases that h = 0.7 milligauss, 2.0 milligauss, 6.2 milligauss and 18.2 milligauss, respectively.

The theory shows that the modification of g occurs when the condition (4.6) is satisfied. Then it might be worthwhile to consider the condition (4.6) from the experimental point of view. Figure 4.7 shows the recorder traces representing the maximum of the zeroth resonance as a function of the amplitude H_1, while the amplitude h, i.e. $H_\perp$, is varied as a parameter. In Fig.4.7, (a),(b), (c) and (d) are the cases $\omega_\perp/2\pi \simeq 240$ Hz, 720 Hz, 2160 Hz and 6480 Hz, respectively. Since the values of $\omega/2\pi$ and $1/2\pi\tau$ are respectively 3 KHz and 120 Hz in these cases, it can be said that (a) is the case that the condition (4.6) is satisfied and the case (d) is entirely out of the condition. In this figure, we can see that the maximum of the zeroth resonance in the case (a) is exactly expressed by the quantity ΔM_x^n. For the larger values of $\omega_\perp$, the maximum does not fall to zero even when the value of $J_0(\omega_1/\omega)$ becomes zero, as seen in Fig.4.4(c) and (d), and then it can be no more expressed by ΔM_x^n. This fact may be understood by considering the effects of the other resonance lines expressed by ΔM_x^n with $n \neq 0$. Since these lines are broadened by the field H_1 as seen in Fig.4.4, the effects of the slopes of these lines on the zeroth resonance increase with the value of $\omega_\perp$. As the results, the maximum of the zeroth resonance becomes independent of the amplitude H_1 for the large values of $\omega_\perp$. This fa t may imply that the value of $g_\perp$ cannot be expressed by eq.(4.11), but is expected to be g_0 for large value of $\omega_\perp$.

4.2.3. Frequency Shift due to the Nonresonant RF Field

We deal with the shift of the output frequency of the optically pumped alkali vapor magnetometer due to the nonresonant rf field, whose direction is arbitrary with respect to the static magnetic field to be measured. It has been known that the magnetometer does not respond to the rf field with the frequency much higher than the inverse of the relaxation time of the alkali vapor, and hence the influence of such rf field has not been considered

yet. Recently, Landre' et al. (1970) have shown that the atomic g-factor is severely modified by the strong rf field when the angular frequency of this field is much higher than the Zeeman splitting of the atom. However, when we study the shift of the optically pumped alkali vapor magnetometer quantitatively, their results cannot directly be applied to our case, since they have treated the special case that the oscillating nonresonant rf field is oriented perpendicular to the static magnetic field.

In previous section, we analyzed the behavior of the optically pumped atoms in the nonresonant rf field in terms of the macroscopic magnetization. When the oscillating nonresonant rf field $H_1(t)$ with the angular frequency ω and a circularly polarized pumping light beam are oriented in the same axis (X axis) and the static magnetic field H_0 is oriented in an arbitrary direction, the secular component of the magnetization along the X axis can be written as

$$M_x(0) = \frac{(g_0\beta H_\perp)^2 + (1/\tau)^2}{g_0\beta H_\perp J_0(\gamma_0 H_1/\omega)^2 + (g_0\beta H_{//})^2 + (1/\tau)^2} M_0' , \quad (4.21)$$

if the condition $\omega^2 \gg (g_0\beta H_0)^2 + (1/\tau)^2$ is satisfied. In eq.(4.21), M_0' is the equilibrium magnetization when the fields H_0 and H_1 are absent, $g_0\beta$ the gyromagnetic ratio of the ground state of the atom, τ the relaxation time including the optical pumping time, H_1 the amplitude of the field $H_1(t)$. Comparing eq.(4.21) and $M_x(0)$ in the case that $H_1 = 0$, we can expect

$$g_\theta = \sqrt{(g_\perp\beta\sin\theta)^2 + (g_{//}\beta\cos\theta)^2} , \quad (4.22)$$

where

$$g_{//} = g_0 , \quad g_\perp = g_0 J_0(\omega_1/\omega) , \quad \theta = \tan^{-1}(H_{//}/H_\perp) . \quad (4.23)$$

From eqs.(4.22) and (4.23), it can be said that the medium irradiated by the strong nonresonant rf field is nomore isotropic, and the gyromagnetic ratio

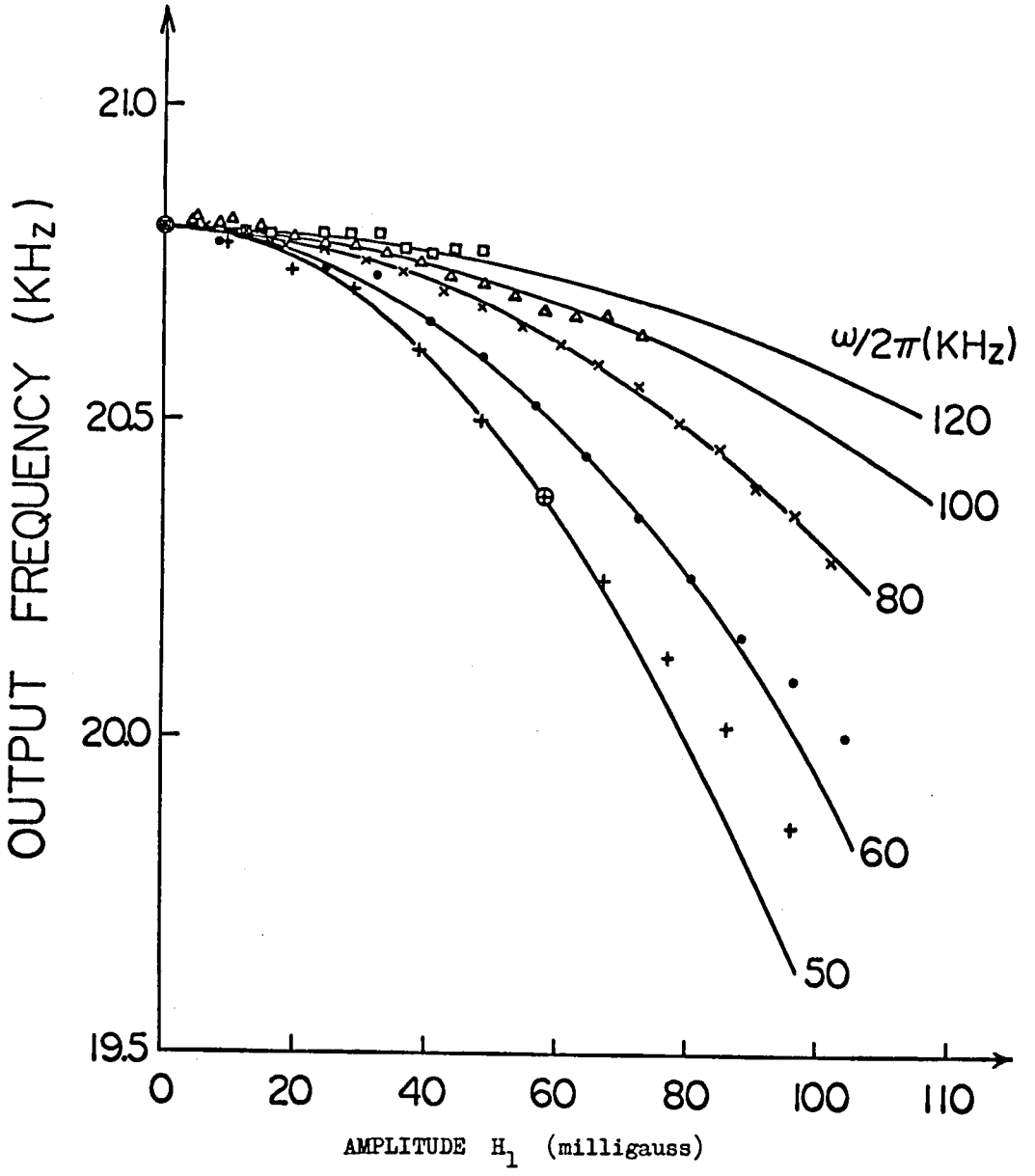

Fig. 4.8. The output frequency of the magnetometer as a function of the amplitude H_1 of the nonresonant rf field. The frequency $\omega/2\pi$ of the field H_1 is varied as a parameter. The solid lines are the theoretical curves calculated from eq.(4.26), and two circles indicate the values which are used to determine the absolute values of H_1.

becomes a tensorial quantity. The output frequency of the magnetometer is given by the quantity $g_\theta \beta H_0/2\pi$, since it gives rise to the Zeeman splitting of the atom in the nonresonant rf field. When $g_0 \beta H_1 \ll \omega$, the shift $\Delta\omega_0$ of the output frequency is given by

$$\Delta\omega_0/\omega_0 \simeq -(g_0\beta H_1 \sin\theta/2\omega)^2. \qquad (4.24)$$

In order to verify the theoretical prediction, we carried out the experiment with a self-oscillating magnetometer with cesium vapor. The static magnetic field H_0 was fixed to about 0.06 gauss and θ was chosen about 45°. The output frequency of the magnetometer as a function of the amplitude H_1 is shown in Fig.4.8, where the frequency $\omega/2\pi$ of the field $H_1(t)$ is varied as a parameter. In this figure, we can see that the shift obtained agrees approximately with eq.(4.24). The discrepancy between the theory and the experimental results for the large value of H_1 is due to the direct coupling between the field $H_1(t)$ and the photodetector circuit in the magnetometer.

In general, we can easily obtain the anisotropy of the atomic g-factor for the case that $\omega_{//} = n\omega$. At $\omega_{//} = n\omega$, the gyromagnetic ratio g_θ^n

$$g_\theta^n = g_0 \sqrt{\cos^2\theta + J_n^2(\omega_1/\omega)\sin^2\theta}\ , \qquad (4.25)$$

here we assumed that the additional small magnetic field makes an angle θ with respect to the oscillating rf field and $\omega_{//}$.

4.3. Mixture of the Longitudinal Resonance and the Transverse Resonance

By means of a theoretical approach recently developed by Pegg and Series (1970), the consequences of misalignment of an oscillating rf field in optical-rf double resonances are investigated. Effects of both the longitudinal pumping and the transverse pumping are considered. We show that the ordinary or

multiple quantum resonanees and the transverse resonances appear at integral multiples of the oscillating rf field frequency simultaneously. It is also shown that there is no essential difference between the parametric resonance and the Haroche resonance, namely the transverse resonance becomes the parametric resonance for misalignment angle $\theta = 90^{\circ}$ and becomes the Haroche resonance for $\theta = 0^{\circ}$.

4.3.1. Theory

We study the behavior of the magnetization $\mathbf{M}$ of spin 1/2 atom in the field

$$\mathbf{H} = H_1 \cos\theta \cos\omega t\, \mathbf{i} + (H_1 \sin\theta \cos\omega t + H_0)\, \mathbf{k} , \qquad (4.26)$$

by use of Bloch equation taking into account the effects of both the longitudinal pumping and the transverse pumping. Equation (4.26) can be rewritten as

$$\mathbf{H} = (1/2)\, H_1 \cos\theta \ (\cos\omega t\, \mathbf{i} + \sin\omega t\, \mathbf{j}) + (\cos\omega t\, \mathbf{i} + \sin\omega t\, \mathbf{j}) + (H_1 \sin\theta \cos\omega t + H_0)\, \mathbf{k} . \qquad (4.27)$$

This is the sum of a rotating, a counter-rotating, an oscillating and a static component. We consider the case of $|\gamma H_1 \cos\theta| \ll \omega$, which is the necessary condition for the application of the procedure of Pegg and Series (1970,1973) This procedure involves the transformation to a reference frame in which the oscillating component vanishes. The magnetic field in the reference frame, which rotates with angular frequency $a\sin\omega t + (p + 1)\omega t$ about z axis, where p is any integer, positive, negative or zero, specifying the rotating component selected, and $a = 2\omega_1 \sin\theta / \omega$, becomes

$$\mathbf{H} = \{ \omega_0/\gamma - (p + 1)\omega/\gamma \}\, \mathbf{k} + \omega_1 \cos\theta / 2\gamma \{ \mathbf{i} \cos(-a\sin\omega t - p\omega t) + \mathbf{j} \sin(-a\sin\omega t - p\omega t) \} + \omega_1 \cos\theta / 2\gamma \{ \mathbf{i} \cos[-a \sin\omega t - (p + 2)\omega t]$$

$$+ \mathbf{j} \sin[- a \sin \omega t - (p + 2) \omega t]\} , \qquad (4.28)$$

where $\omega_1 = \gamma H_1$ and $\omega_0 = \gamma H_0$. The last two terms can be Fourier analyzed in terms of Bessel functions as

$$\bar{\omega}_p = \sum_{m=-\infty}^{\infty} (\omega_1/2) \{ J_m(a) + J_{m-2}(a)\} \cos\theta \times \{\cos(-p - m)\omega t \, \mathbf{i} + \sin(-p - m)\omega t \, \mathbf{j}\} , \qquad (4.29)$$

and the static component is

$$\overline{\omega}_p^{(0)} = \gamma \bar{H}_p^{(0)} = (\omega_1/2) \{ J_{-p}(a) + J_{-p-2}(a)\} \cos\theta . \qquad (4.30)$$

Ignoring the non-static component, the Bloch equation in this frame is given as follows;

$$\frac{d \bar{M}_x}{dt} = X \bar{M}_y - \frac{1}{\tau} \bar{M}_x + \frac{1}{\tau} \bar{M}_{0x} , \qquad (4.31a)$$

$$\frac{d \bar{M}_y}{dt} = - \bar{M}_x - \frac{1}{\tau} \bar{M}_y + \frac{1}{\tau} \bar{M}_{0y} , \qquad (4.31b)$$

$$\frac{d \bar{M}_z}{dt} = - \frac{1}{\tau} \bar{M}_z + \frac{1}{\tau} \bar{M}_{0z} , \qquad (4.31c)$$

where

$$X = \left[\{\omega_0 - (p + 1)\omega\}^2 + \overline{\omega}_p^{(0)2} \right]^{1/2} , \qquad (4.32)$$

$\bar{M}_{0x}$, $\bar{M}_{0y}$ and $\bar{M}_{0z}$ are the orientation parameters in the reference frame:

$$\bar{M}_{0x} = M_{0x} \cos\beta \cos\{ a \sin \omega t + (p + 1) \omega t\} + M_{0y} \cos\beta \sin\{ a \sin \omega t + (p + 1) \omega t\} - M_{0z} \sin\beta , \qquad (4.33a)$$

$$\bar{M}_{0y} = - M_{0x} \sin\{ a \sin \omega t + (p + 1) \omega t\}$$

$$+ M_{0y}\cos\{ a \sin\omega t + (p + 1)\omega t \}, \tag{4.33b}$$

$$\bar{M}_{0z} = M_{0x}\sin\beta \cos\{ a \sin\omega t + (P + 1)\omega t\}$$
$$+ M_{0y}\sin\beta \sin\{ a \sin\omega t + (p + 1)\omega t\}$$
$$+ M_{0z}\cos\beta \ , \tag{4.33c}$$

with

$$\beta = \tan^{-1} \frac{\overline{\omega}_p(0)}{\omega_0 - (p + 1)\omega} \tag{4.34}$$

Using the relation

$$\bar{M}_+ = \bar{M}_x + i\,\bar{M}_y \ , \tag{4.35}$$

we obtain the equation which is equivalent to the diffrential equations (4.31a) and (4.31b),

$$\frac{d\,\bar{M}_+}{dt} = - i\,X\,\bar{M}_+ - \frac{1}{\tau}\bar{M}_+ + \frac{1}{\tau}(\bar{M}_{0x} + i\,\bar{M}_{0y}) \ . \tag{4.36}$$

The equations (4.31c) and (4.36) are linear differential equations, and they admit exact solutions

$$\bar{M}_z = \exp(- \frac{t}{\tau}) \int_{-\infty}^{t} \frac{1}{\tau}\bar{M}_{0z} \exp(\frac{1}{\tau})\, t\, dt \ , \tag{4.37a}$$

$$\bar{M}_+ = \exp(- iX - \frac{1}{\tau})t \int_{-\infty}^{t} \frac{1}{\tau}(\bar{M}_{0x} + i\,\bar{M}_{0y})$$
$$\exp(i\,X + \frac{1}{\tau})t\, dt. \tag{4.37b}$$

Using the well-known relations

$$\sin(a \sin\omega t + p\,\omega t) = \sum_{n=-\infty}^{\infty} J_n(a) \sin(n + p)\omega t \ , \tag{4.38a}$$

and

$$\cos(a \sin\omega t + p\,\omega t) = \sum_{n=-\infty}^{\infty} J_n(a) \cos(n + p)\omega t, \tag{4.38b}$$

the solutions of the equations (4.37a) and (4.37b) can be obtained and the final expressions of $\bar{M}_x$, $\bar{M}_y$ and $\bar{M}_z$ becomes as follows;

$$\bar{M}_x = \frac{1}{2}\sum_{m=-\infty}^{\infty} J_{m-p-1}(a)\Big[\frac{\cos\beta + 1}{1+(m\omega + X)^2\tau^2}\{M_{0x} - M_{0y}(m\omega + X)\tau\} + \frac{\cos\beta - 1}{1+(m\omega - X)^2\tau^2}\{M_{0x} + M_{0y}(-m\omega + X)\tau\}\Big]\cos m\omega t + \frac{1}{2}\sum_{m=-\infty}^{\infty} J_{m-p-1}(a)\Big[\frac{\cos\beta + 1}{1+(m\omega + X)^2\tau^2}\{M_{0y} + M_{0x}(m\omega + X)\tau\} + \frac{\cos\beta - 1}{1+(m\omega - X)^2\tau^2}\{M_{0y} + M_{0x}(m\omega - X)\tau\}\Big]\sin m\omega t - \frac{1}{1+(X\tau)^2} M_{0z}\sin\beta \quad , \tag{4.39a}$$

$$\bar{M}_y = \frac{1}{2}\sum_{m=-\infty}^{\infty} J_{m-p-1}(a)\Big[-\frac{\cos\beta + 1}{1+(m\omega + X)^2\tau^2}\{M_{0y} + M_{0x}(m\omega + X) + \frac{\cos\beta - 1}{1+(m\omega - X)^2\tau^2}\{M_{0y} + M_{0x}(m\omega - X)\tau\}\Big]\cos m\omega t + \frac{1}{2}\sum_{m=-\infty}^{\infty} J_{m-p-1}(a)\Big[\frac{\cos\beta + 1}{1+(m\omega + X)^2\tau^2}\{M_{0x} - M_{0y}(m\omega + X)\tau\} - \frac{\cos\beta - 1}{1+(m\omega - X)^2\tau^2}\{M_{0x} - M_{0y}(m\omega - X)\tau\}\Big]\sin m\omega t + \frac{1}{1+(X\tau)^2} M_{0z}\sin\beta \quad , \tag{4.39b}$$

$$\bar{M}_z = \sum_{m=-\infty}^{\infty} J_{m-p-1}(a)\Big\{\frac{\sin\beta}{1+(m\omega\tau)^2}(M_{0x} - m\omega\tau M_{0y})\Big\}\cos m\omega t + \sum_{m=-\infty}^{\infty} J_{m-p-1}(a)\Big\{\frac{\sin\beta}{1+(m\omega\tau)^2}(M_{0y} + m\omega\tau M_{0x})\Big\}\sin m\omega t + M_{0z}\cos\beta \quad . \tag{4.39c}$$

It is well known that the variation of the absorption of the light beam by atoms is proportional to the component of the magnetic moment along the

light beam, M_n. In general, M_n is given as

$$M_n = (\bar{M}_x \bar{M}_{0x} + \bar{M}_y \bar{M}_{0y} + \bar{M}_z \bar{M}_{0z}) M_0^{-1} \quad , \tag{4.40}$$

with

$$M_0^2 = M_{0x}^2 + M_{0y}^2 + M_{0z}^2 = \bar{M}_{0x}^2 + \bar{M}_{0y}^2 + \bar{M}_{0z}^2 \quad . \tag{4.41}$$

Substituting equations (4.33) and equations (4.39) into equation (4.40), the magnetic moment along the light beam in the laboratory frame, $\mathbf{M}_n$, can be obtained, but we are interested in only the unmodulated component $M_n^p(0)$ in M_n. After some tedious treatments, we obtain $M_n^p(0)$ in the form

$$\begin{aligned} M_n^p(0) = \frac{1}{4} \sum_{m=-\infty}^{\infty} J_{m-p-1}^2(a) \Bigg\{ & \frac{(\cos\beta + 1)^2}{1 + (m\omega + X)^2 \tau^2} \\ & + \frac{(\cos\beta - 1)^2}{1 + (m\omega - X)^2 \tau^2} + \frac{2 \sin^2\beta}{1 + (m\omega\tau)^2} \Bigg\} \cdot \frac{M_{0x}^2 + M_{0y}^2}{M_0} \\ & + J_{-p-1}(a) \cdot \frac{2 (X\tau)^2 \sin\beta \cos\beta}{1 + (X\tau)^2} \cdot \frac{M_{0x} M_{0y}}{M_0} \\ & + \left\{ \frac{1}{1 + (X\tau)^2} \sin^2\beta + \cos^2\beta \right\} \cdot \frac{M_{0z}^2}{M_0} \quad . \end{aligned} \tag{4.42}$$

It contains two types of resonance functions. One of them is the function $m\omega \pm X$ contained in the denominators of the first term in the right side and the other is the function X contained in the denominators of the second and the third terms.. If we set $M_{0x} = M_{0y} = 0$ and $M_{0z} = M_0$, i.e., for the longitudinal pumping, equation (4.42) becomes

$$M_n^p(0) = \left\{ \frac{1}{1 + (X\tau)^2} \sin^2\beta + \cos^2\beta \right\} \cdot M_0 \quad . \tag{4.43}$$

This can be rewritten by using equations (4.32) and (4.34) as

$$M_n^p(0) = \frac{1 + \{\omega_0 - (p+1)\omega\}^2 \tau^2}{1 + (\omega_p^{(0)} \tau)^2 + \{\omega_0 - (p+1)\omega\}^2 \tau^2} M_0 \quad . \tag{4.44}$$

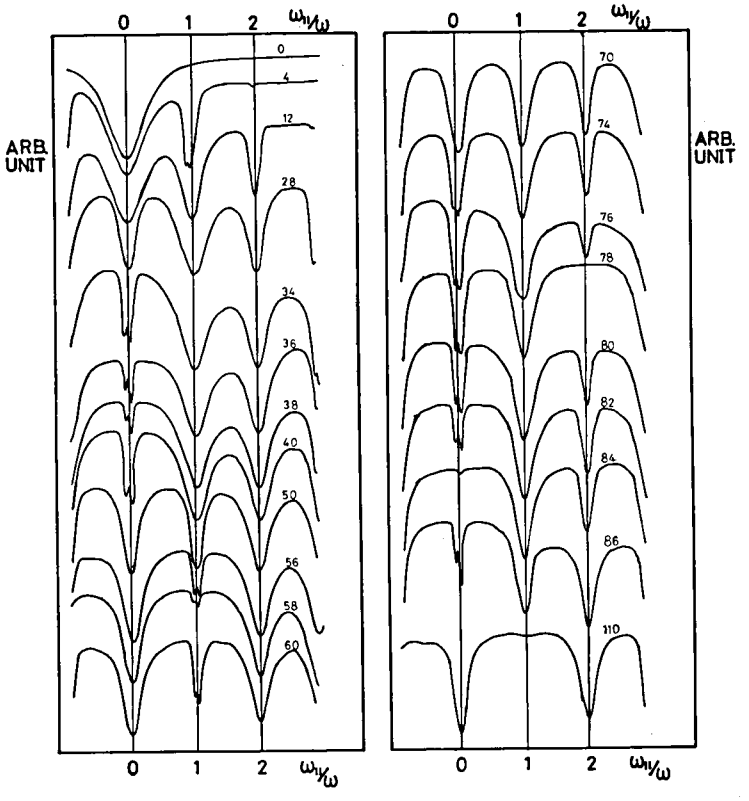

Fig. 4.9. Experimental recordings for the mixture of the longitudinal resonance and the transverse resonance. Experimental condition: $\omega/2\pi$ = 5 KHz. The value written by each trace gives the relative intensity of H_1.

This equation expresses that the resonances occur at $\omega_0 = (p + 1)\omega$. These resonances correspond to the ordinary or the multiple quantum resonances, caused by the misalignment of the oscillating rf field. Usual multiple quantum resonances induced by an oscillating rf field, perpendicularly to the static magnetic field, occur only at $\omega_0 = (2p + 1)\omega$. On the other hand, if we set $M_{0z} = 0$ and $M_{0x}^2 + M_{0y}^2 = M_0$, i.e., for the transverse pumping, equation (4.42) becomes

$$M_n^p(0) = \frac{1}{4} \sum_{m=-\infty}^{\infty} J_{m-p-1}^2(a) \left\{ \frac{(\cos\beta + 1)^2}{1 + (m\omega + X)^2 \tau^2} + \frac{(\cos\beta - 1)^2}{1 + (m\omega - X)^2 \tau^2} + \frac{2 \sin^2\beta}{1 + (m\omega\tau)^2} \right\} \cdot M_0 \quad . \tag{4.45}$$

This expresses that the resonances occur at $m\omega \pm X = 0$, i.e., $\omega_0 = \{ m \pm (p + 1) \} \omega = n\omega$, where m and n are any integer, positive negative or zero. We call this type of resonances "transverse".

4.3.2. Discussion

As we can see from the resultant equation (4.42), under the influence of the effects of both the longitudinal pumping and the transverse pumping, the main effect of misalignment of the oscillating rf field is appearance of the different two types of the magnetic resonances at $\omega_0 = \cdots\cdots, -2\omega - \omega, 0, \omega, 2\omega, \cdots\cdots$, simultaneously. One of them belongs to the longitudinal resonance, which includes ordinary resonance and the multiple quantum resonance, and the other is the transverse resonance, which includes the parametric resonance and the Haroche resonance. The simultaneous existence of the longitudinal resonance and the transverse resonance has been observed as shown in Fig.4.9.

For the case $\theta = 90^\circ$ and $M_{0x} = M_0$, eq.(4.42) becomes as follows;

$$M_n^p(0) = \sum_{m=-\infty}^{\infty} J_{m-p-1}^2 \left(\frac{2\omega_1}{\omega} \right) \frac{M_0}{1 + \{\omega_0 + (m-p-1)\omega\}^2 \tau^2} \quad . \tag{4.46}$$

This expression agrees with the result obtained for the parameteic resonance (for example Aleksandrov et al. 1963, Favre et al. 1964, Polonsky et al. 1965a,b,c). While for the case that $\theta = 0^o$, $M_{0x} = M_0$, m=1 and p=0, eq. (4.42) becomes as follows;

$$M_n^0(0) = \frac{1}{4} \frac{(\cos\beta + 1)^2}{1 + (\omega + \omega_e)^2 \tau^2} + \frac{(\cos\beta - 1)^2}{1 + (\omega - \omega_e)^2 \tau^2} + \frac{2 \sin^2\beta}{1 + (\omega\tau)^2} M_0 \, , \tag{4.47}$$

where

$$\omega_e = \{ (\omega_0 - \omega)^2 + \omega_1^2 \}^{1/2} \, . \tag{4.48}$$

This expression agrees with the result of the Haroche resonance or off-diagonal resonance obtained for the case of the rotating rf field (Aleksandrov et al. 1972, Tsukada et al. 1972). Therefore, we can understand that the "transverse resonance" given in eq.(4.45) expresses both the parametric resonance and the Haroche resonance inclusively. The parametric resonance and tne Haroche resonance correspond to the special cases of the "transverse resonance" given in eq.(4.45). Finally we can say that there is no essential difference between the parametric resonance and the Haroche resonance. For small misalignment angle, the nature of the Haroche resonance appears strongly, and for large misalignment angle the nature of the parametric resonance appears strongly.

We show the experimental recordings for the mixture of the longitudinal resonance and the transverse resonance in Fig.4.9. In the Fig.4.9, the longitudinal resonances appear as decrease of the intensity in the transmitted light, while the transverse resonances appear as increase of the transmitted

light intensity. The transverse resonances can be seen for $V_1 = 34 \sim 40$ and $V_1 = 76 \sim 86$ at $\omega_{//}/\omega = 0$, and for $V_1 = 4$ and $V_1 = 56 \sim 60$ at $\omega_{//}/\omega = 1$.

4.4. Conclusion

In section 4.2, we have shown by classical and quantum mechanical treatments the fact that the atomic g-factor is modified by the oscillating rf field when the Hanle effect and the parametric resonance take place. Theory has been verified by the experiment with optically pumped cesium vapor, where we have considered in the rotating coordinate system.

It should be noted that the expression for the secular component of the magnetization $\mathbf{M}$ derived in the classical theory is quite general and coincides with the theoretical results derived previously for the particular cases. In the case that the rf field $\mathbf{H}_1(t)$ is absent, eq.(4.5) agrees with the expression derived by Bell and Bloom (1957), who have analyzed for the ordinary magnetic resonance in optically pumped atoms, and in the case that both the fields $\mathbf{H}_1(t)$ and $\mathbf{H}_{//}$ are absent, eq.(4.7) gives the expression for the Hanle effect. Moreover, eq.(4.5) agrees approximately with the theory by Novikov et al. (1968), which is valid for the case that $\omega_1 \sin\theta \ / \omega < 1$. The expression for the g-factor obtained here agrees with the previous theory by Cohen-Tannoudji and Haroche (1969b), for the particular case that $\omega_{//} = 0$, in which the relaxation process is neglected. If we take account of the relaxation process, the condition should be revised as given by the inequality (4.6). The existence of the term $1/\tau$ in this condition is important, particularly when we try to detect the modification of the g-factor of the excited state with a short life time. In addition, we have obtained the concept of the anisotropic g-factor (Landré et al. 1970, Yabuzaki et al. 1972b) which may be observed as the response to additional small, static field in

arbitrary direction with respect to the oscillating rf field. This effect has been verified by using the optically pumped cesium vapor magnetometer.

We then consider the case that the static magnetic field and the pumping light beam make arbitrary angle with respect to the oscillating rf field in section 4.3. As a result, we have shown that two types of magnetic resonances, i.e., the longitudinal and the transverse resonances, may be appeared at $\omega_0 = p\omega$, where p is an integer, simultaneously. The "transverse resonance" expresses both the parametric resonance and the Haroche resonance inclusively. Namely, the parametric resonance and the Haroche resonance correspond to the special cases of the "transverse resonance", respectively. We can say that there is no essential difference between the parametric resonance and the Haroche resonance. For small misalignment angle, i.e., the static field $\mathbf{H}_0$ is nearly perpendicular to the oscillating rf field $\mathbf{H}_1$, the nature of the Haroche resonance appears strongly, and for large misalignment angle, i.e., the fields, $\mathbf{H}_0$ and $\mathbf{H}_1$, are nearly parallel to each other, the nature of the parametric resonance appears strongly.

Some of the experimental results have been shown for verification of the theory.

CHAPTER 5

SATURATION EFFECTS IN RF SPECTROSCOPY

5.1. Introduction

Several theoretical approaches have recently been developed for determining higher order terms in the expression for the Bloch-Siegert shift. This renewal of interest has been stimulated by an article of Chang and Stehle (1971), who derive the shift from a quantum electrodynamics calculation.

Chang and Stehle find, in particular, that for a two-level system interacting with a strong field both the power broadening and the Bloch-Siegert shift become oscillatory functions of the rf intensity. This is partly disagreement with the results of several other treatments: Shirley's theory (1965) using Floquet states, Pegg and Series' treatment (1970,1973a, see also Pegg 1973b) based on appropriate changes of reference frames, Stenholm's calculations (1972a,b) leading to continued fractions.

The experimental works by the group of Cohen-Tannoudji (for example see Haroche 1971b page 336) support qualitatively a monotonic behavior. The quantitative measurements by Morand and Theobald (1969) agree well with the semiclassical calculations. A detailed comparison of their work with the theory has been published by Stenholm (1973d).

However, the experimental test of the higher order terms of the Bloch-Siegert shift in the multiple quantum resonances is not easy: when the rf field H_1 increases, the resonance is not only shifted, but also broadened and distorted, so that a precise determination of its center becomes difficult. Fortunately, other kinds of magnetic resonance, namely the Haroche resonance, exist which are easier to study experimentally (Cohen-Tannoudji et al. 1973b, Tsukada and Ogawa 1973a, Tsukada, Murakani and Ogawa 1973a).

In this Chapter, we will investigate these kinds of magnetic resonance theoretically and experimentally.

In section 5.2, the continued fraction representation which has been recently adapted to the longitudinal optical pumping by Stenholm (1972a,b) is used to solve the Bloch equation for the case of the transverse pumping and the results of the calculations of the positions and the shapes of the Haroche resonances, caused by the large intensity rf field, are given. The computational convenience of the continued fraction makes the possible to combine the concept of the modification of the atomic g-factor with the Haroche resonances. We want to show that the behaviors , position, width and magnitude etc., of the various Haroche resonances obtained by the experiments for large intensity of the rf field are entirely described by the continued fraction representation. As a result, the broadening of the Hanle curve by the oscillating rf field, i.e., the modification of the atomic g-factor, is due to the position and the width of the Haroche resonances. It seems we had better say that the modification of the atomic g-factor is due to the "resonant" effect rather than "nonresonant" effect. In addition, we study the saturation effects of the longitudinal resonances. We observe the time-dependent components contained in tne transmitted light and report the first observation of the modulation in absorption for the longitudinal pumping experiment.

In section 5.3, we show the theoretical analysis based on numerical integration of Bloch equation for the strong rf field and for the general configuration of the magnetic fields. The new type resonances are expected and the resonances appear at $H_{//} = n\omega/\gamma$. Behaviors of these type of resonances are similar to those of the Haroche resonance. It is shown that the agreement between the numerical and the experimental results is excellent. For the very low frequency and for large intensity of the rf field, the anti-crossing curve near zero magnetic field is deformed and is then sharpened by the new type resonances.

5.2. Saturation Effects of the Transverse Resonance

The continued fraction representation which has been recently adapted to the longitudinal optical pumping by Stenholm (1972a) is used in the Bloch equation to study the saturation effects of the Haroche resonance, caused by the transverse pumping. This section gives calculations of the position and shape of the Haroche resonance for large intensity of the rf field, which differ from the earlier work for weak rf field by Cohen-Tannoudji and Haroche (1967). It is shown that the variation of the width of the Hanle curve by the oscillating rf field, i.e., the modification of the atomic g-factor, is due to the Haroche resonance. The position of the Haroche resonance observed for the large intensity of the rf field agrees well with those of our continued fraction solutions rather than those of the perturbation theory (Cohen-Tannoudji and Haroche 1967). The saturation effects of the resonance intensity of the Haroche resonance, which is due to the large intensity of the rf field, is also verified theoretically and experimentally.

5.2.1. Bloch Equation and Continued Fraction

The external magnetic field $\mathbf{H}$ is the rf field $\mathbf{H}_1(t) = \mathbf{H}_1 \cos \omega t$ in the x direction and the static magnetic field $\mathbf{H}_0$ in the z direction; we obtain

$$\mathbf{H} = (H_1 \cos \omega t, \quad 0 \quad , \quad H_0) . \tag{5.1}$$

Consider that the pumping light creates the magnetization in an arbitrary direction and we introduce the quantities M_{0x}, M_{0y} and M_{0z} for the component of the magnetization in the x, y and z direction. Then we have

$$\mathbf{M}_0' = \frac{\tau}{T_p} (M_{0x}, M_{0y}, M_{0z}) , \tag{5.2}$$

with

$$M_0^2 = M_{0x}^2 + M_{0y}^2 + M_{0z}^2 \ .$$

Inserting eqs.(5.1) and (5.2) into eq.(2.16), we have

$$\frac{d M_x}{dt} = \omega_0 M_y - \frac{M_x}{\tau} + \frac{M_{0x}}{T_p} \ , \tag{5.3a}$$

$$\frac{d M_y}{dt} = - \omega_0 M_x + \omega_1 \cos \omega t \, M_z - \frac{M_y}{\tau} + \frac{M_{0y}}{T_p} \ , \tag{5.3b}$$

$$\frac{d M_z}{dt} = - \omega_1 \cos \omega t \, M_y - \frac{M_z}{\tau} + \frac{M_{0z}}{T_p} \ . \tag{5.3c}$$

Using the well-known relations between density matrix and the components of the magnetization; $\rho_{++} - \rho_{--} = M_z$, $\rho_{+-} - \rho_{-+} = i M_x$ and $\rho_{+-} + \rho_{-+} = M_x$, and putting $M_{0x} = M_{0y} = 0$, eqs.(5.3) becomes to the same one given by Stenholm (1972a).

We use a Fourier expansion technique and write

$$M_x = \sum_{n=-\infty}^{\infty} c_n \, e^{in\omega t} \ , \tag{5.4a}$$

$$M_y = \sum_{n=-\infty}^{\infty} s_n \, e^{in\omega t} \ , \tag{5.4b}$$

$$M_z = \sum_{n=-\infty}^{\infty} d_n \, e^{in\omega t} \ , \tag{5.4c}$$

and find from equations (5.3) by equating the coefficients of equal powers of $\exp(i\omega t)$ the recurrence relations

$$n\omega c_n = - i \omega_0 s_n + i \Gamma c_n - i \lambda_x \delta_{n0} \ , \tag{5.5a}$$

$$n\omega s_n = - i \frac{1}{2} \omega_1 (d_{n+1} + d_{n-1}) + i \omega_0 c_n + i\Gamma s_n - i\lambda_y \delta_{n0} \ , \tag{5.5b}$$

$$n\omega d_n = i \frac{1}{2} \omega_1 (s_{n+1} + s_{n-1}) + i\Gamma d_n - i\lambda_z \delta_{n0} \ , \tag{5.5c}$$

with

$$\Gamma = \tau^{-1}, \quad \lambda_x = M_{0x}/T_p, \quad \lambda_y = M_{0y}/T_p \text{ and } \quad \lambda_z = M_{0z}/T_p \, .$$

From eq.(5.5a) we get

$$c_n = \frac{\omega_0}{\Gamma + i\, n\omega}\, s_n + \frac{\lambda_x}{\Gamma}\, \delta_{n0} \, . \tag{5.6}$$

Inserting this into eqs.(5.5b) and (5.5c) we find

$$s_n = \frac{\omega_1}{4} \left[\frac{1}{\Gamma + i\,(n\omega - \omega_0)} + \frac{1}{\Gamma + i\,(n\omega + \omega_0)} \right] (d_{n+1} + d_{n-1}) - \frac{\omega_0}{\Gamma^2 + \omega_0^2}\, \lambda_x \delta_{n0} + \frac{\Gamma}{\Gamma^2 + \omega_0^2}\, \lambda_y \delta_{n0}, \tag{5.7}$$

and

$$d_n = -\frac{1}{\Gamma + i\, n\omega} \left(\frac{\omega_1}{2}\right)(s_{n+1} + s_{n-1}) + \frac{1}{\Gamma}\, \lambda_z \delta_{n0}. \tag{5.8}$$

In our case, the transverse optical pumping, eqs.(5.7) and (5.8) can be combined with one equation by writing

$$X_n = \begin{cases} \dfrac{\Gamma^2 + \omega_0^2}{-\omega_0 \lambda_x + \Gamma \lambda_y}\, s_n & n \text{ even}, \\[2ex] \dfrac{\Gamma^2 + \omega_0^2}{-\omega_0 \lambda_x + \Gamma \lambda_y}\, d_n & n \text{ odd}, \end{cases} \tag{5.9}$$

$$D(n) = \begin{cases} \dfrac{1}{2} \left[\dfrac{1}{\Gamma + i\,(n\omega - \omega_0)} + \dfrac{1}{\Gamma + i\,(n\omega + \omega_0)} \right] & n \text{ even}, \\[2ex] \dfrac{1}{\Gamma + i\, n\omega} & n \text{ odd}, \end{cases} \tag{5.10}$$

and the difference equation to be solved is

$$x_n = (-1)^n \frac{\omega_1}{2} D(n) (x_{n+1} + x_{n-1}) + \delta_{n0} . \qquad (5.11)$$

This equation is just the same one obtained by Stenholm (1972a) and the solution is given in the form

$$\frac{x_1}{x_0} = \frac{d_1}{s_0} = \cfrac{-\frac{1}{2}\omega_1 D(1)}{1 + \cfrac{\frac{1}{4}\omega_1^2 D(1)D(2)}{1 + \cfrac{\frac{1}{4}\omega_1^2 D(2)D(3)}{(1 + \cdots\cdots)}}} , \qquad (5.12)$$

$$\frac{x_{-1}}{x_0} = \cfrac{-\frac{1}{2}\omega_1 D(-1)}{1 + \cfrac{\frac{1}{4}\omega_1^2 D(-1)D(-1)}{(1 + \cdots\cdots)}} = \frac{d_1^*}{s_0} . \qquad (5.13)$$

Inserting these into eq.(5.7) with n=0 we get

$$s_0 = (-\omega_0 \lambda_x + \Gamma \lambda_y)/[\Gamma^2 + \omega_0^2 + (\omega_1^2/2)\Sigma], \qquad (5.14)$$

where

$$\Sigma = \mathrm{Re} \cfrac{\Gamma D(1)}{1 + \cfrac{\frac{1}{4}\omega_1^2 D(1)D(2)}{(1 + \cdots\cdots)}} . \qquad (5.15)$$

Moreover inserting eqs.(5.14) and (5.15) into eq.(5.6) we obtain

$$c_0 = \frac{1}{\Gamma} \left(1 - \frac{\omega_0^2}{\Gamma^2 + \omega_0^2 + (\omega_1^2/2)\Sigma} \right) \lambda_x + \frac{\omega_0}{\Gamma^2 + \omega_0^2 + (\omega_1^2/2)\Sigma} \lambda_y . \qquad (5.16)$$

The amount of the absorption of the pumping light beam by atoms is given by eq.(2.23). We are interested in the component of the transmitted light intensity which are taken time average. If the pumping light beam directs to the x direction, i.e., $\lambda_y = \lambda_z = 0$, c_0 in eq.(5.16) gives the time averaged component, or unmodulated component, of M_x. On the other hand, if the pumping light beam directs to the y direction, i.e., $\lambda_x = \lambda_z = 0$, s_0 in eq.(5.14) gives the time averaged component of M_y.

It has been known that the resonances for the transverse pumping are at $\omega_0 \approx 2n\omega$ for weak rf field (Cohen-Tannoudji and Haroche 1967, 1969a). From the continued fraction of (5.15), we can see why these occur. All the even D functions have a resonance whereas the odd ones are nonresonant. As a result, we see that the resonance is at the position

$$\omega_0 = 2n\omega \left\{ 1 - \frac{\omega_1^2}{4\,(4n^2 - 1)\,\omega^2} \right\} , \qquad (5.17)$$

for weak rf field. This coincides with the result derived from resolvant formalism by Cohen-Tannoudji and Haroche (1969a).

5.2.2. Computed Results

In this section we intend to discuss the saturation effects of the Haroche resonances and the Hanle effect using the solutions of the continued fraction. We consider the case with one decay rate Γ only and choose

$$\Gamma = 0.02\,\omega \quad . \qquad (5.18)$$

The main results of computations for the case that the pumping light beam directs to x direction, i.e., $\lambda_x = M_0/T_p$, $\lambda_y = \lambda_z = 0$, are given in Fig.5.1. The comparison of the positions of the Haroche resonances between the results of the exact calculation of equation (5.16) and the approximate expression (5.17) are shown in Fig.5.2. This is done for ω_1 up to 700Γ and for resonances up to 12ω. All of the Haroche resonances

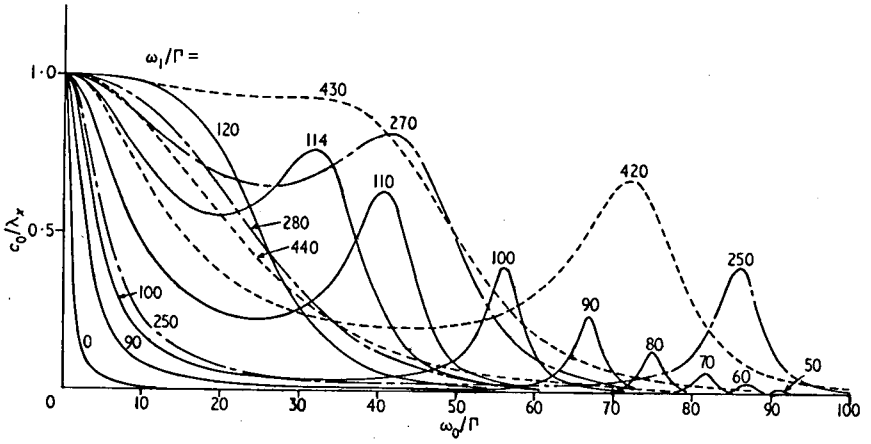

Fig. 5.1. The appearance of the Haroche resonances in an optical detection experiment; the solid lines are the resonance at $\omega_0 = 2\omega$, the dotted broken lines are the resonance at $\omega_0 = 4\omega$ and the broken lines are the resonance at $\omega_0 = 6\omega$. This shows how the resonance is shifted and broadened as the rf field ω_1 is increased. The Hanle curves for ω_1/Γ = 50, 60, 70 and 80 are not shown. These Hanle curves are shown in Fig. 5.3(a).

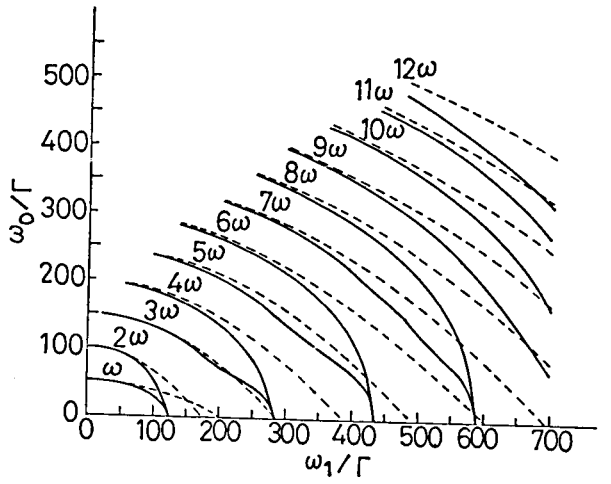

Fig. 5.2. Positions of the various Haroche resonance peaks as a function of the rf amplitude ω_1. The peaks are seen to appear, shift and disappear. The solid lines for even resonances are the result of this paper, the dashed lines for even resonances are the approximate expression (5.17). Positions of the multiple quantum resonance peaks given in the paper of Stenholm (1972b) are also shown.

are seen to move down in frequency more rapidly than eq.(5.18). The deviations from the approximate expression increase with the order of resonance. We can observe the appearance of higher order Haroche resonance as ω_1 is increased. Positions of the multiple quantum resonances for up to 11ω are also shown in Fig.5.2. Two lines, for the multiple quantum resonance at $\omega_0 = (2n - 1)\omega$ and the Haroche resonance at $\omega_0 = 2n\omega$, overlap each other before they enter the zero field. It should be noticed that the values of ω_1, at which two lines enter the zero field, coincides with the values at the zeros of zeroth order Bessel function $J_0(\omega_1/\omega)$. This fact can be expected from the modification of the atomic g-factor introduced in the paper of Cohen-Tannoudji and Haroche (1969b). The variation of the width of the Hanle curve calculated from eq.(5.16) is shown in Fig.5.3(a). The width of the Hanle curve is represented as $\Gamma/J_0(\omega_1/\omega)$ at the region $\omega_0 \ll \omega$. This fact has been analyzed, for the condition $\omega_0 \ll \omega$, quantum mechanically by Cohen-Tannoudji and Haroche (1966), semiclassically by Pegg and Series (1970), and classically by Yabuzaki et al. (1972a). However, eq.(5.16) can be used for the arbitrary value of ω_0/ω and even for arbitrary intensity of the rf field.

The behavior of the Hanle curve for the case that the pumping light beam directs to y direction, i.e., $\lambda_y = M_0/T_p$ and $\lambda_x = \lambda_z = 0$, is obtained from eq.(5.14) and is shown in Fig.5.3(b). For this case, the peaks of the Hanle curves remarkably decrease as the intensity ω_1 increases. The variation of the peaks of the Hanle curves for the case is well represented by $J_0^2(\omega_1/\omega)$. This fact agrees well with the result recently obtained by Tsukada et al.(Tsukada, Yabuzaki and Ogawa 1973) and that expected from the parametric resonance at zero magnetic field (for example Polonsky and Cohen-Tannoudji 1965).

5.2.3. Experiments

For the purpose to confirm the theoretical conclusions, experiments are

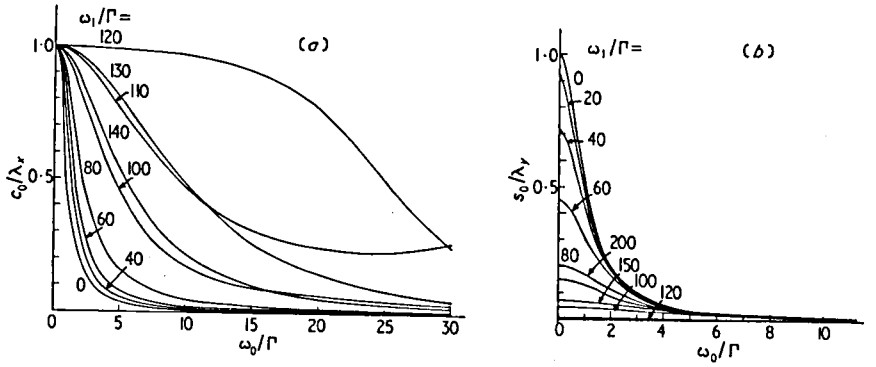

Fig. 5.3. The variation of the width of the Hanle curve as a function of ω_1/Γ. The width is given by the expression $\Gamma'/J_0(\omega_1/\omega)$, for the region $\omega_0 \ll \omega$. The Hanle curves for the case that the pumping light beam directs to x direction are shown in (a) and for the pumping light beam directs to y direction in (b).

made with optically pumped cesium atoms. An absorption cell with wall coated with paraffin, containing saturated vapor of cesium at temperature about 25°C, is situated at the center of a set of Helmholtz coils. The static field H_0 is provided by a Helmholtz pair of diameter 80 cm. It is arranged to vary the static field H_0 continuously from -100 to 100 mG. Stray fields are reduced to less than 2 mG by two pairs of Helmholtz coils of diameters 90 cm and 100 cm at right angle. We can estimate the magnitude of the stray field from the width of the anticrossing curve in the absence of the rf field. The width is given as $[(\gamma H_s/2\pi)^2 + \Gamma^2]^{1/2}$, where H_s is the magnitude of the stray field which exists on the perpendicular plane with respect to the static field H_0. The oscillating rf field $H_1 \cos \omega t$ is applied perpendicular to the static field H_0 by a Helmholtz pair of diameter about 20 cm. The source of cesium pumping light is electrodeless rf discharge lamp. Both the D_1 and D_2 lines are used for optical pumping of the cesium atoms in the cell. After passing through a circularly polarizer, the light incidents parallel to the oscillating rf field on absorption cell. An change in the intensity of the light transmitted through the cell detected with a photocell. The magnitude of absorption in the unmodulated component and the depth of modulation at frequency 2ω or 4ω as function of the static field H_0 are recorded. The experimental disposition of apparatus is shown in Fig.5.4.

The recorder traces of the resonance for $\omega_0 = 2\omega$ appearing in the unmodulated component are shown in Fig.5.5(a), where each resonance corresponds to a different value of the input voltage V_1 of the rf coils, and $\omega/2\pi = 10$ KHz. A peak at zero field is due to the anticrossing curve rather than the Hanle curve. There are stray transverse static fields and these can stimulate a resonance at zero frequency, so-called anti-crossing curve for zero frequency. From Fig.5.5(a) we can find that the

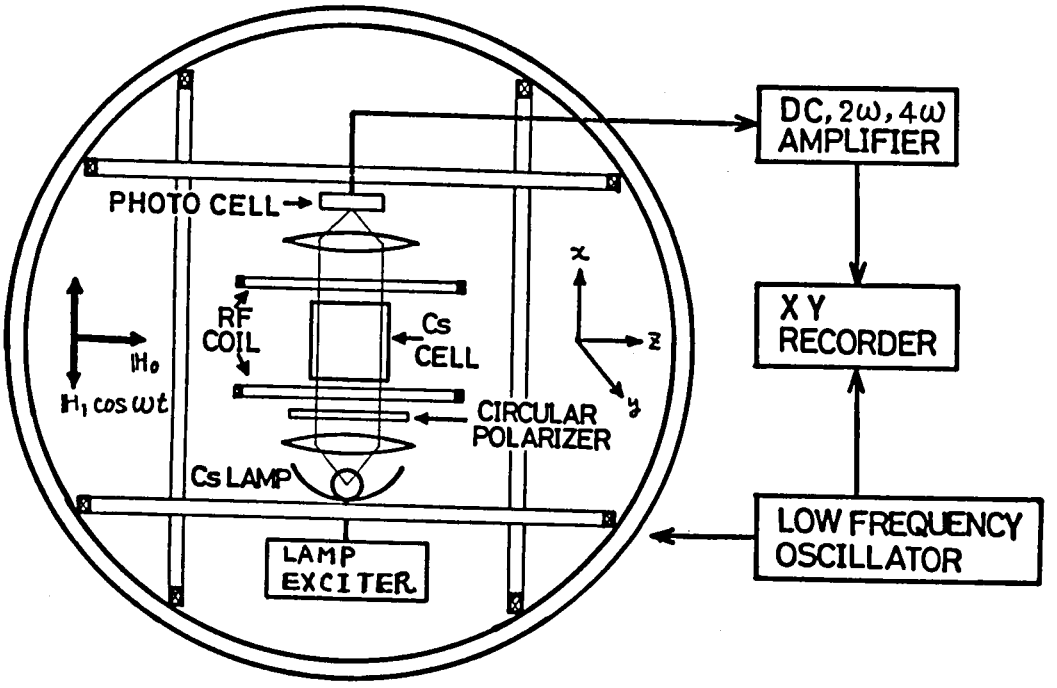

Fig. 5.4. Disposition of apparatus. The static magnetic field H_0 is in the direction of z axis. The rf field H_1 is in the direction of the pumping light beam (x axis).

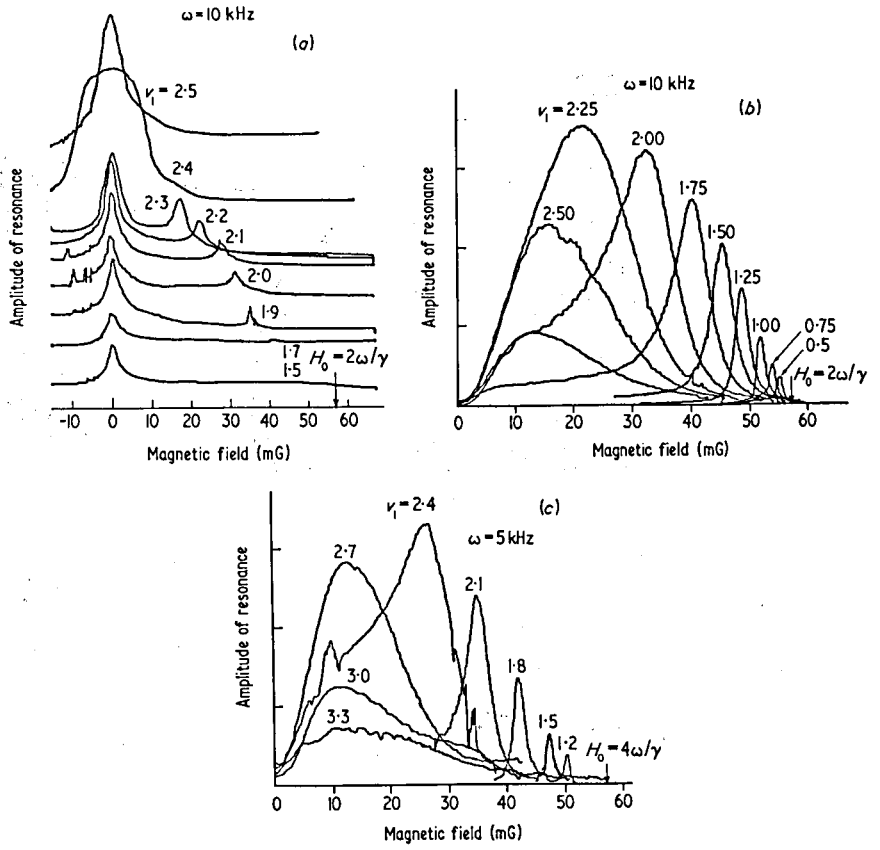

Fig. 5.5. Experimental curves as a function of H_0: the resonance curves for (a) $\omega_0 = 2\omega$ in the unmodulated component, (b) $\omega_0 = 2\omega$ in the component modulated at 2ω, (c) $\omega_0 = 4\omega$ in the component modulated at 4ω. The number written by each curve is the input voltage V_1 of the rf coils (in millivolt), which is proportional to H_1.

resonance curves for $\omega_0 = 2\omega$ move towards the low field region and are broadened as the intensity of H_1 is increased. It should be noticed that when the Haroche resonance shifts towards low field region the Hanle curve is broadened gradually. When the Haroche resonance overlaps the Hanle curve, in this case anticrossing curve at zero frequency, the width of the Hanle curve or the anticrossing curve is maximized and it is then narrowed again. We showed in our previous paper (Tsukada and Ogawa 1973a) that the value of H_1, at which one of the Haroche resonances overlaps on the Hanle curve, coincides with one of the values of the zeros of zeroth order Bessel function $J_0(\gamma H_1/\omega)$.

The recorder traces of the resonance for $\omega_0 = 2\omega$ appearing in the componont modulated at 2ω are shown in Fig.5.5(b), where each resonance corresponds to a different value of V_1, and $\omega/2\pi = 10$ KHz. The recorder traces of the resonance for $\omega_0 = 4\omega$ appearing in the component modulated at 4ω are shown in Fig.5.5(c). In this case the frequency of the rf field is 5 KHz.

5.2.4. Discussion

In this section, we want to compare the experimental results with the theoretical results obtained previous section. The amount of the variation in the unmodulated component of the pumping light transmitted through the vapor cell is given in the form as eq.(5.16). We can also obtain the analytical expressions for the components modulated at 2ω and 4ω from eqs. (5.5) and (5.6). The amplitude of these components, $|c_2|$ and $|c_4|$, can be expressed as follows;

$$|c_2| = \frac{\omega_0}{[\Gamma^2 + (2\omega)^2]^{1/2}} |s_2| , \tag{5.19}$$

$$|c_4| = \frac{\omega_0}{[\Gamma^2 + (4\omega)^2]^{1/2}} |s_4| , \tag{5.20}$$

where

$$s_2 = \left(\frac{\omega_1}{2}\right)^2 \left(\frac{D(2)}{1 + \frac{1}{4}\omega_1^2 D(2)D(3)/(1 + \cdots)}\right) \times \left(\frac{D(1)}{1 + \frac{1}{4}\omega_1^2 D(1)D(2)/(1 + \cdots)}\right) s_0, \qquad (5.21)$$

$$s_4 = \left(\frac{\omega_1}{2}\right)^2 \left(\frac{D(4)}{1 + \frac{1}{4}\omega_1^2 D(4)D(5)/(1 + \cdots)}\right) \times \left(\frac{D(3)}{1 + \frac{1}{4}\omega_1^2 D(3)D(4)/(1 + \cdots)}\right) s_2, \qquad (5.22)$$

and s_0 is given by eq.(5.14). The main results of the computational calculation of eqs.(5.16), (5.19) and (5.20) are given in Figs.5.6(a)~(c). Figure 5.6(a) shows the behavior of the unmodulated component for the resonance for $\omega_0 = 2\omega$. Figures 5.6(b) and (c) show the behaviors of the resonance for $\omega_0 = 2\omega$ in the component modulated at 2ω and the resonance for $\omega_0 = 4\omega$ in the component modulated at 4ω. The parameter chosen is

$$\omega_0 = 50\Gamma. \qquad (5.23)$$

The behaviors of the theoretical curves in Figs.5.6(a)~(c) agree well with those of the experimental curves in Figs.5.5(a)~(c) in shape and magnitude. The experimental results obtained by Cohen-Tannoudji and Haroche (1965) show that the saturation effects of the resonance intensities in the components modulated at 2ω and 4ω become noticeable for large intensity of rf field H_1. This saturation effect may be explained with eqs.(5.19) and (5.20), indeed Figs.5.6(b) and (c) show the saturation effect for large intensity of the rf field.

Figure 5.7 shows the positions of the peaks of various resonances as a function of V_1/ω. The points, the crosses and the triangles are experi-

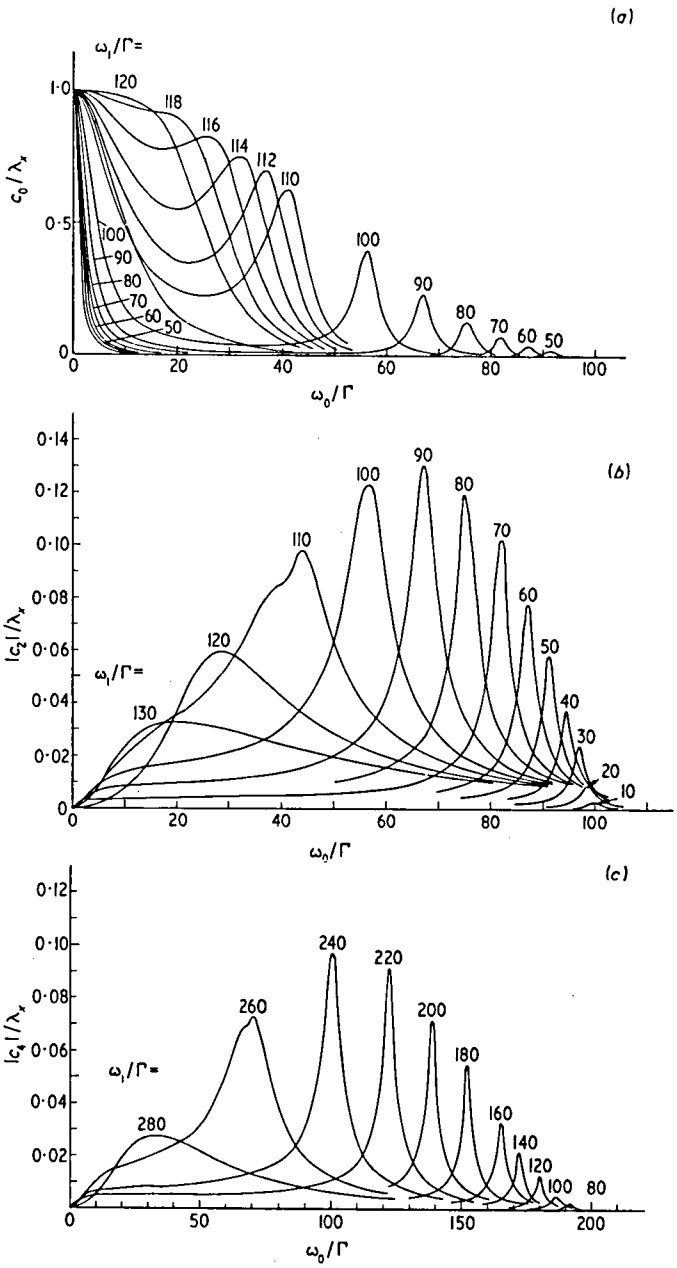

Fig. 5.6. Theoretical curves as a function of H_0 (ω_0): the resonance curves for (a) $\omega_0 = 2\omega$ in the unmodulated component calculated from eq.(5.16) for various values of rf amplitude H_1 (ω_1), (b) $\omega_0 = 2\omega$ in the component modulated at 2ω calculated from eq.(5.19), (c) $\omega_0 = 4\omega$ in the component modulated at 4ω calculated from eq.(5.20).

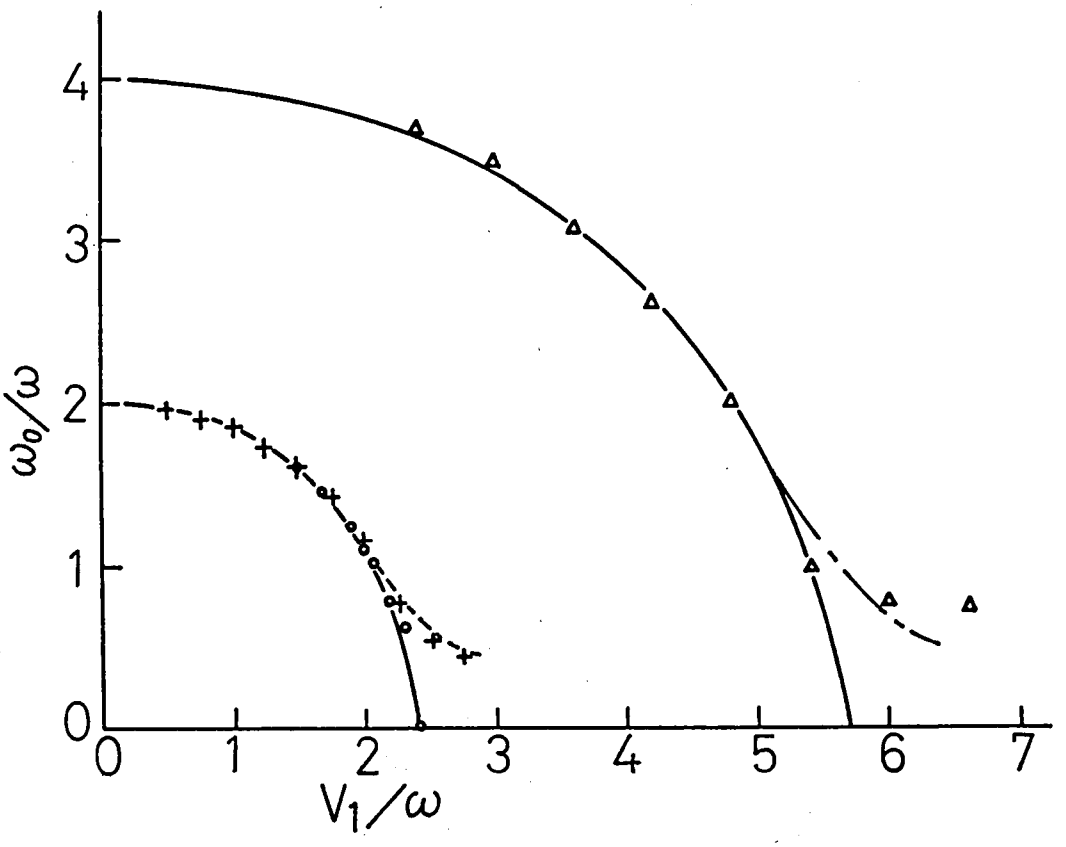

Fig. 5.7. Positions of various resonance peaks as a function of the rf amplitude V_1/ω or ω_1/ω. The circles, the crosses and the triangles are experimental points. The circles show the resonance for $\omega_0 = 2\omega$ in the unmodulated component, the crosses for $\omega_0 = 2\omega$ in the component modulated at 2ω and the triangles for $\omega_0 = 4\omega$ in the component modulated at 4ω. The solid lines are obtained from eq.(5.16), and the broken line and the dotted broken line are obtained from eqs.(5.19) and (5.20), respectively.

mental points. The circles show the resonance for $\omega_0 = 2\omega$ in the unmodulated component and the crosses and the triangles show the resonances for $\omega_0 = 2\omega$ in the component modulated at 2ω and for $\omega_0 = 4\omega$ in the component modulated at 4ω, respectively. The solid lines show the theoretical curves obtained by eq.(5.16). They show the positions of the resonances for $\omega_0 = 2\omega$ and 4ω in the unmodulated component. The broken line is the theoretical curve of the resonance for $\omega_0 = 2\omega$ in the component modulated at 2ω. Then the dotted broken line is the theoretical curve of the resonance for $\omega_0 = 4\omega$ in the component modulated at 4ω. The agreement between the experiment and the theory is quite satisfactory.

For the case that $\omega_0 \approx 2\omega$ and $\omega \gg \Gamma$, eq.(5.19) becomes

$$|c_2| = \frac{\omega_1^2}{\left[\Gamma^2 + \{2\omega - \omega_0 - \frac{1}{6}(\omega_1^2/\omega)\}^2\right]^{1/2}} M_0' . \qquad (5.24)$$

For the case that $\omega_0 \approx 4\omega$ and $\omega \gg \Gamma$, eq.(5.20) becomes

$$|c_4| = \frac{\omega_1^4}{\left[\Gamma^2 + \{4\omega - \omega_0 - \frac{1}{15}(\omega_1^2/\omega)\}^2\right]^{1/2}} M_0' . \qquad (5.25)$$

From eqs.(5.24) and (5.25), we see that for small intensity rf field the shift and the intensity of the resonance for $\omega_0 = 2\omega$ in the component modulated at 2ω are proportional to ω_1^2 and the shift of the resonance for $\omega_0 = 4\omega$ in the component modulated at 4ω is proportional to ω_1^2 and the intensity to ω_1^4. This coincides with the results obtained by Cohen-Tannoudji (1965).

Figure 5.8 shows the level crossing signal with an oscillating rf field to be compared with the experimental results shown in Fig.4.7. Agreement between the calculated results and the experimental results is excellent.

The introduction of several different decay rate into our equations

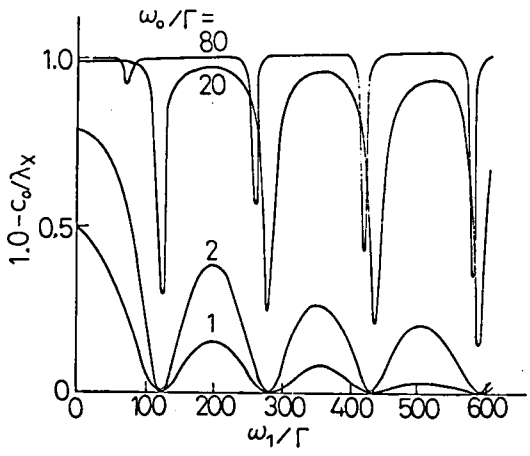

Fig. 5.8. Level crossing signal as a function of the intensity of rf field for various values of ω_0. This figure corresponds to the experimental results in Fig. 4.7.

would change the quantitative behavior only but not affect the qualitative behavior. Evaluation of the continued fraction is done with the recent work by Feldman and Feld (1972).

5.2.5. Modulation in Absorption for the Longitudinal Pumping

Recently, we have investigated the saturation effects of the transverse resonances, including the Hanle effect and the Haroche resonance, theoretically (Tsukada and Ogawa 1973a) and experimentally (Tsukada, Murakami and Ogawa 1973a). On the other hand, the saturation effects of the longitudinal resonance, including the ordinary resonance and the multiple quantum resonance, have theoretically been investigated by Stenholm (1972a,b). Experimental studies of the saturation effects of the time-independent component, i.e., multiple quantum transitions in the time-independent component, have been reported by Margerie and Brossel (1955), Cohen-Tannoudji (1968) and Haroche (1971b). However, the experimental study on the time-dependent components of the longitudinal resonance has not been reported yet. In the longitudinal pumping experiment, the oscillating rf field $\mathbf{H}_1 \cos \omega t$ is perpendicular to the static magnetic field $\mathbf{H}_0$ and the circularly polarized light is parallel to $\mathbf{H}_0$. We have observed the time-dependent components contained in the transmitted light passing through a vapor cell (Tsukada, Murakami and Ogawa 1973b). Resonance curves expected for this case can be obtained from the papers of Stenholm (1972a) and Tsukada (1973a). The quantities to be detected in the experiments correspond to the Fourier coefficients d_n's in the paper of Stenholm (1972a). The resonances at $\omega_0 = \gamma H_0 = (2p + 1)\omega$ in the various odd harmonics $2n\omega$, where p and n are integers, are expected for the longitudinal optical pumping.

The basic apparatus used is the standard one used in the experiment in which the pumping radiation is circularly polarized light and the transmitted light is monitored. An absorption cell with wall coated with paraffin,

containing saturated vapor of cesium at temperature about 25°C, was situated at the center of a set of Helmholtz coils which compensates geomagnetic field and produces a constant magnetic field H_0. The stray field was reduced to about 2 milligauss. The frequency of the oscillating rf field was set at 10 KHz. The transmitted light was monitored by a solar cell

We have observed the components modulated at 2ω and 4ω, which corresponds to the Fourier coefficients d_2 and d_4 in the paper of Stenholm (1972a). The behaviors of the resonances at $\omega_0 = \omega$ and $\omega_0 = 3\omega$ in the component modulated at 2ω and at $\omega_0 = 3\omega$ and $\omega_0 = 5\omega$ in the component modulated at 4ω were observed for various values of the rf field. Figs.5.9(a) and (b) show the resonance curves in the component modulated at 2ω and 4ω for various values of the input voltage V_1 of the rf coil. Figs.5.10(a) and (b) show the theoretical curves for the component modulated at 2ω and 4ω which are calculated for $\omega = 50$, $\Gamma = 2$, where ω and Γ correspond to ν and γ of Stenholm's notations, respectively. The resonance curves are not simple Lorentzians but the more complicated functions, especially the resonance at $\omega_0 = 3\omega$ in the component modulated at 2ω is complicated function. As the rf amplitude ω_1 is small, the resonance curve at $\omega_0 = 3\omega$ becomes more like a conventional dispersion curve, and as the rf amplitude ω_1 is large, it becomes similar to B function of Dodd et al. (1959). The resonance curves are shifted and broadened as the rf amplitude ω_1 is increased. Very sharp resonances comparing the time-independent component, which corresponds to the Fourier coefficient d_0 in Stenholm's paper (1972a), can be seen, because power broadening affects those resonances less than the time-independent component. Figure 5.11 shows the positions of the resonance peaks and dips for the component modulated at 2ω as a function of the rf amplitude ω_1. Black circles are experimental points for the resonance at $\omega_0 = \omega$ and the encircles, crosses, triangles are experimental points for the resonance at $\omega_0 = 3\omega$. The

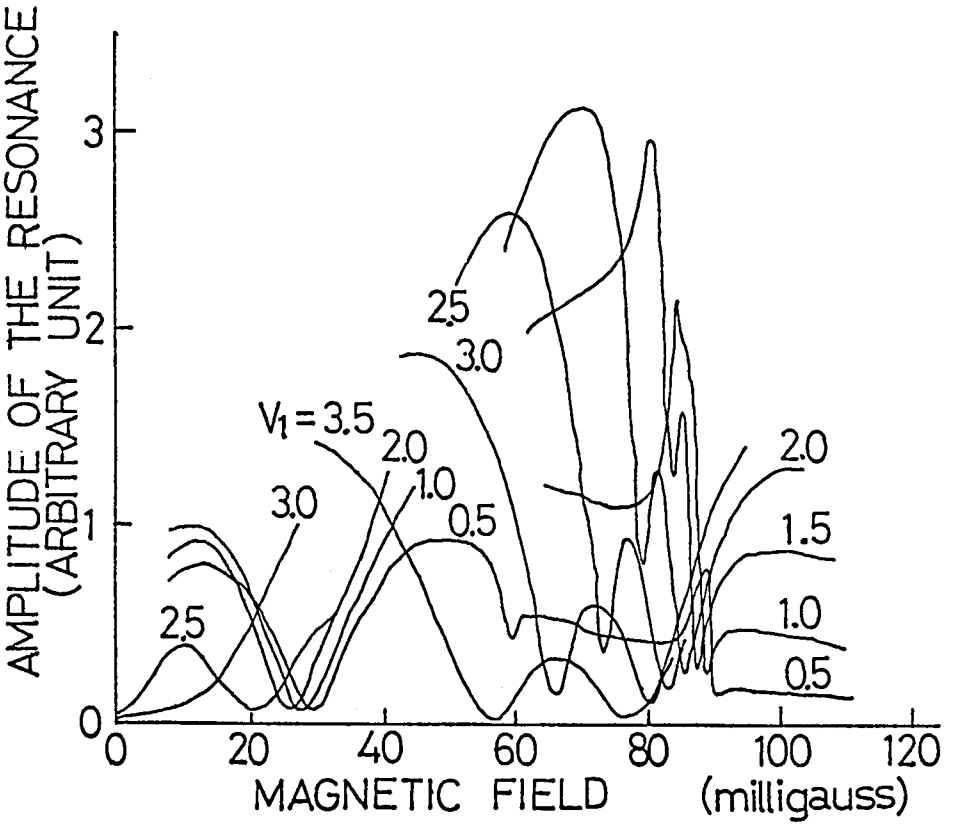

Fig. 5.9. (a). Experimental recordings for the resonances at $\omega_0 = \omega$ and $\omega_0 = 3\omega$ in the component modulated at 2ω.
Experimental condition: $\omega / 2\pi$ = 10 KHz.

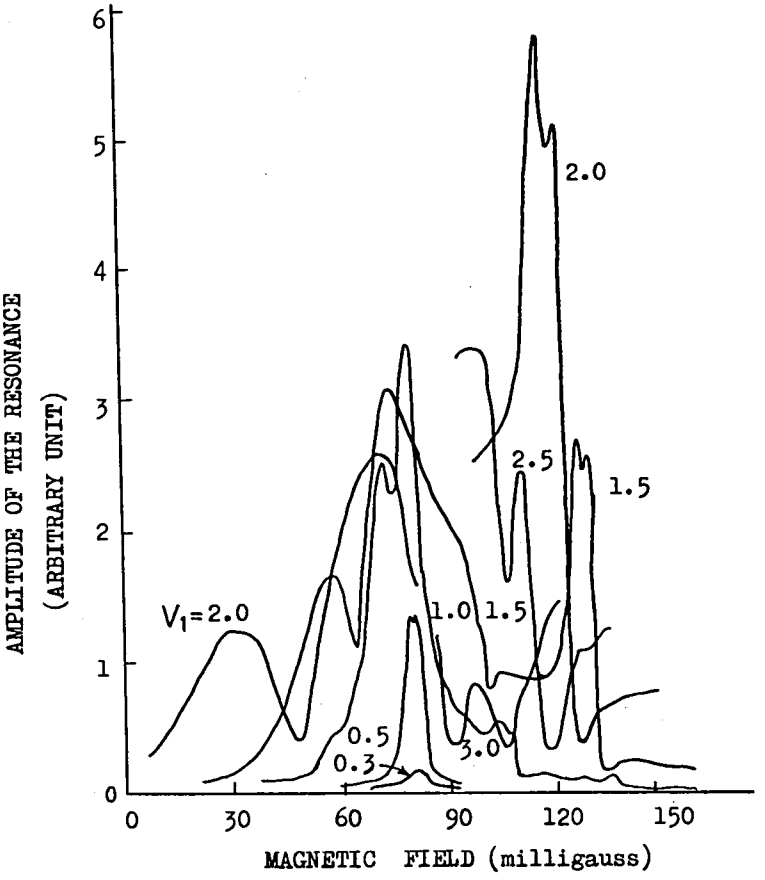

Fig. 5.9. (b). Experimental recordings for the resonances at $\omega_0 = 3\omega$ and $\omega_0 = 5\omega$ in the component modulated at 4ω. Experimental condition: $\omega / 2\pi = 5$ KHz.

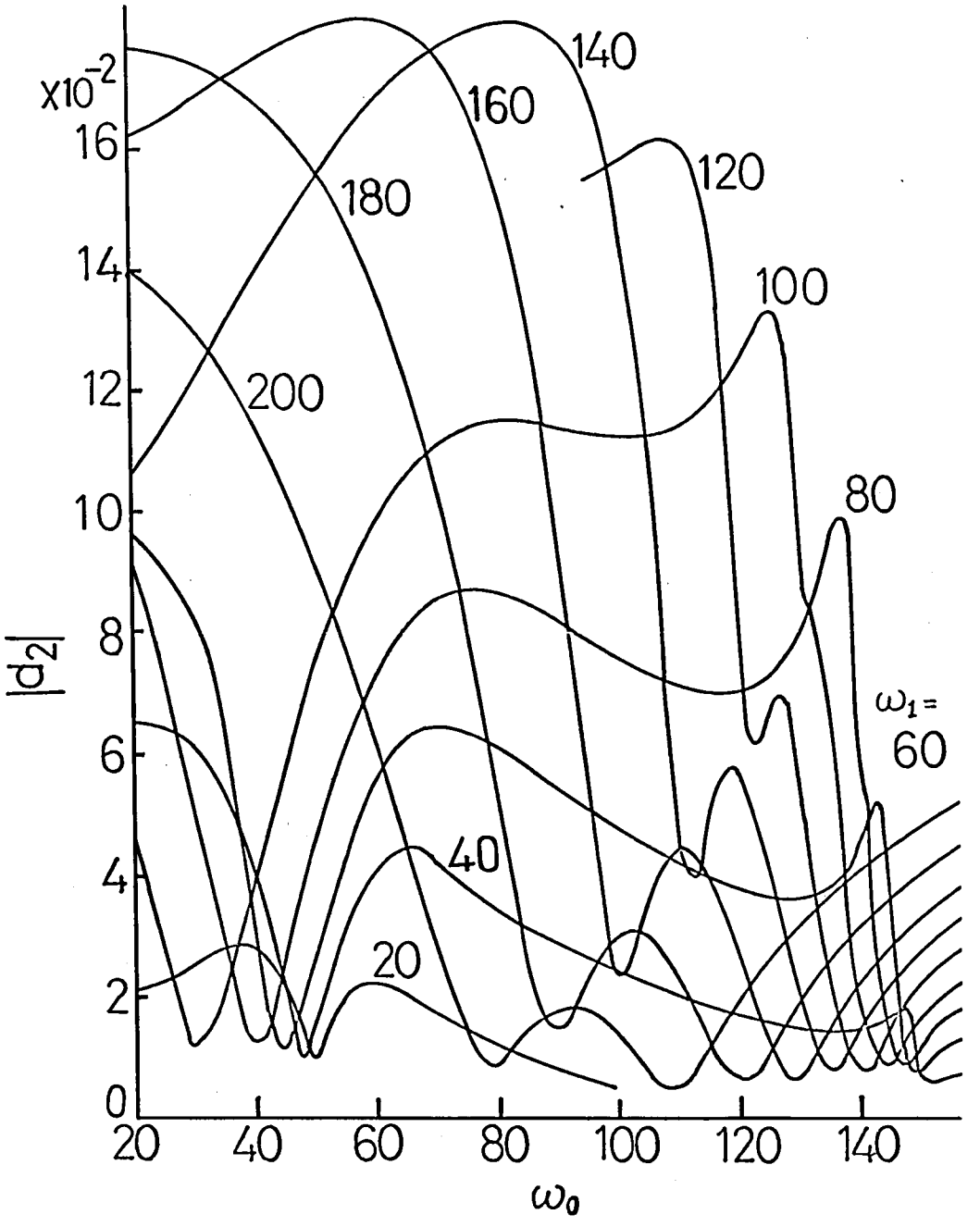

Fig. 5.10. (a). Theoretical curves for the component modulated at 2ω.

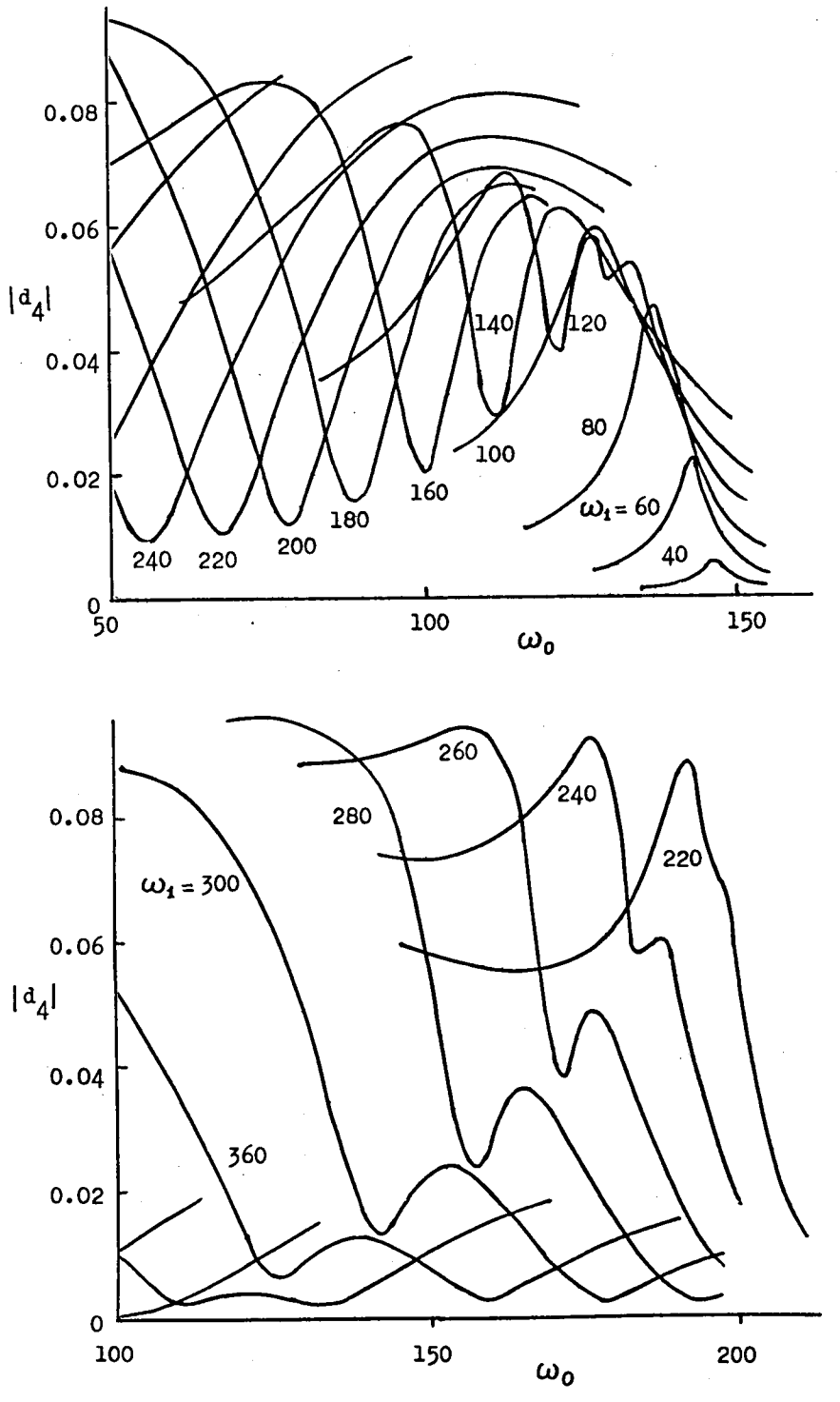

Fig. 5.10. (b). Theoretical curves for the component modulated at 4ω.

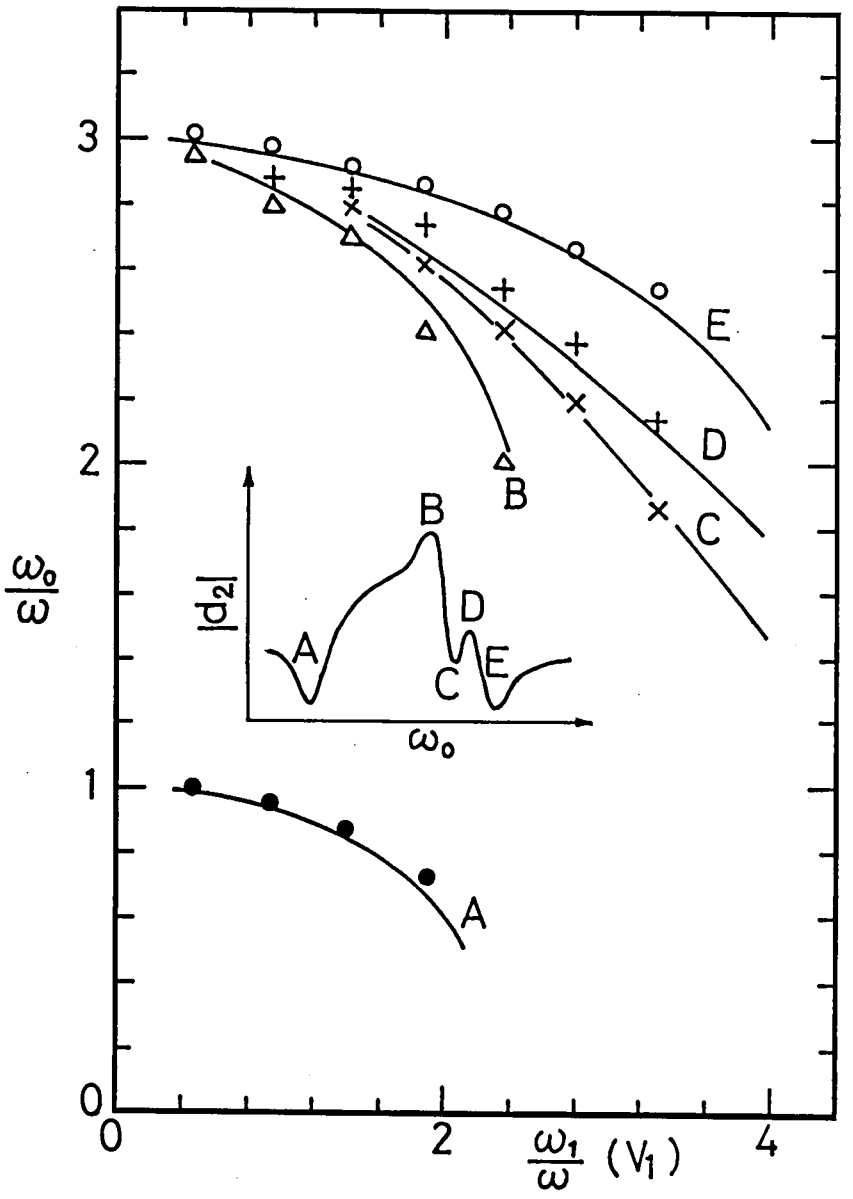

Fig. 5.11. Positions of the resonance peaks and dips as a function of the rf amplitude ω_1. Various marks are experimental points and solid lines are theoretical curves.

solid lines are theoretical curves obtained from Fig.5.10(a).

We can see that the behavior of the resonances obtained experimentally agree with that obtained theoretically. The discrepancy between the theory and the experimental results for the small values of ω_0 or H_0 is due to the influence of the stray field existing in the plane perpendicular to the static field H_0. The resonances in the modulation of the transmitted light for the case of the transverse pumping experiment, in which the circularly polarized light is parallel to the oscillating rf field, are well known as the Haroche resonance. However, the resonance of the modulation in absorption for the longitudinal pumping experiment was not reported. In this section, we reported the first observation of the modulation in absorption for the longitudinal pumping experiment.

5.3. Saturation Effects in Magnetic Resonances for General Magnetic Fields Configuration

Various magnetic resonances appearing in optical pumping experiments have been analyzed theoretically and experimentally. However, there are not so many works with regard to the saturation effects caused by the strong rf field. Recently, the saturation effects of the multiple quantum resonances and of the Haroche resonance have been investigated by Stenholm (1972a,b) and Tsukada and Ogawa (1973a), respectively. In this section, we treat the saturation effects for more general case that the static magnetic field with arbitrary magnitude directs to an arbitrary direction with respect to the oscillating rf field with arbitrary intensity. The experimental results are compared with the exact solutions computed by numerical integration of the Bloch equation. It is shown experimentally and theoretically that the resonances similar to the Haroche resonance appear at $\omega_{//} = n\omega$, where $\omega_{//} = \gamma H_{//}$, n is an integer and $H_{//}$ is the parallel component of the

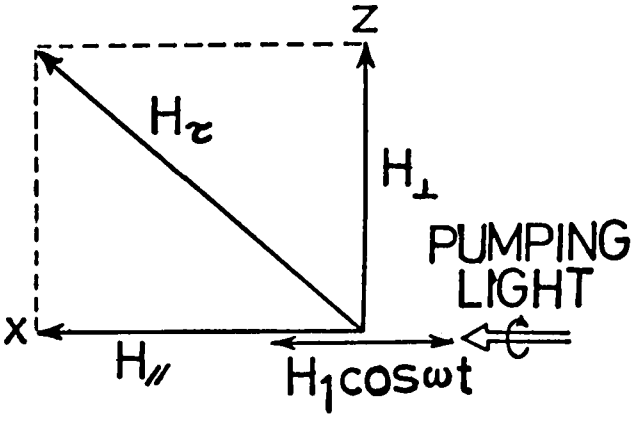

Fig. 5.12. This figure shows the directions of the magnetic fields and the pumping light beam to be considered in this section.

static magnetic field with respect to the oscillating rf field and γ is the gyromagnetic ratio.

5.3.1. Experimental Results

The experimental arrangement resembled the arrangement described in the preceding section 5.2.5. The sample cell in this experiment contained saturated vapor of cesium at temperature about 25°C. The sample cell was placed in a weak static field $\mathbf{H}_z$. It is necessary to compensate for stray fields only to a small fraction of the width of the ground state. The sweeping field $\mathbf{H}_\perp$ was provided by Helmholtz coil and additional Helmholtz coils were used to compensate stray fields. The stray field reduced within 1 milligauss. Experiments were made for the case that the pumping light was parallel to the oscillating rf field. The frequency ω of the oscillating rf field was set at 5 KHz. The transmitted light was monitored by a solar cell. Arrangement of the experiment is that the static field $\mathbf{H}_{//}$ and the oscillating rf field $\mathbf{H}_1 \cos \omega t$ are transverse to the sweeping field $\mathbf{H}_\perp$. The directions of the magnetic fields and the pumping light beam are shown in Fig.5.12.

Figure 5.13 shows the experimental result for $\omega_{//} = 0$, i.e., the real transverse pumping experiment. This is the similar experimental results which has beem reported in our previous paper (Tsukada, Murakami and Ogawa 1973a) and shows the behavior of the Haroche resonance and the Hanle curve as the rf field is increased. Variation of the peak of the Hanle curve is due to the stray field which exists on the perpendicular plane with respect to $\mathbf{H}_\perp$ and $\mathbf{H}_{//}$. Therefore, the curve existing on $H_\perp = 0$ is the anti-crossing curve rather than the crossing curve (Hanle curve). In our previous paper (Tsukada et al. 1972), the real Hanle curve together with the Haroche resonance was obtained in the rotating frame.

Figure 5.14 shows the deformation of the anti-crossing curve by the oscillating rf field and the appearance of the Haroche like resonance for

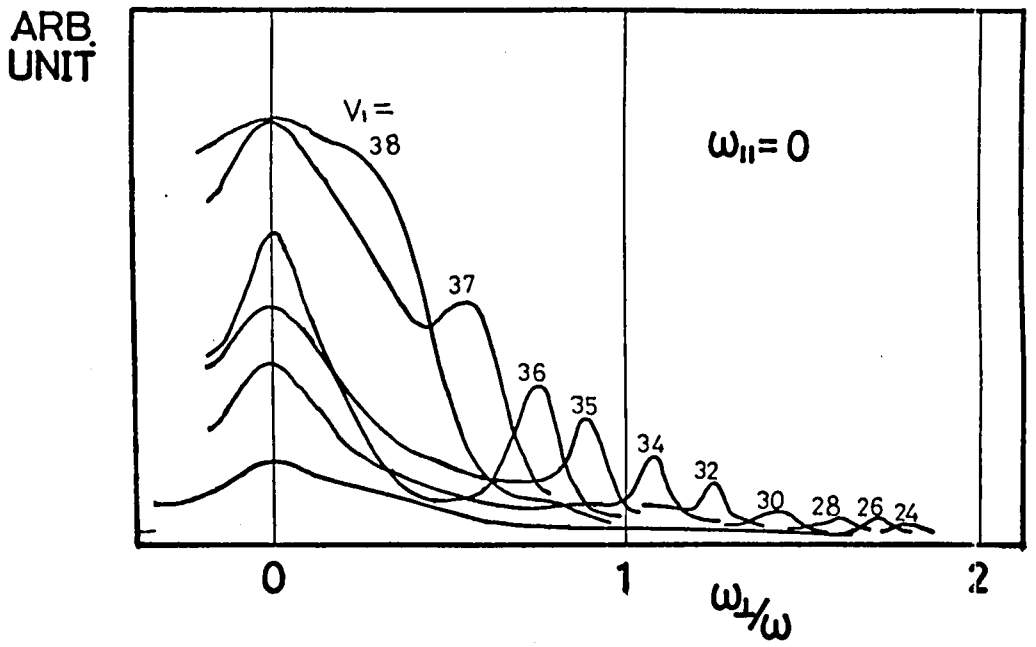

Fig. 5.13. Experimental result for $\omega_{//} = 0$. As the intensity of the rf field is increased, a Haroche resonance is seen to appear and shift towards low field region. The value $\omega/2\pi$ = 5 KHz was used in this experiment.

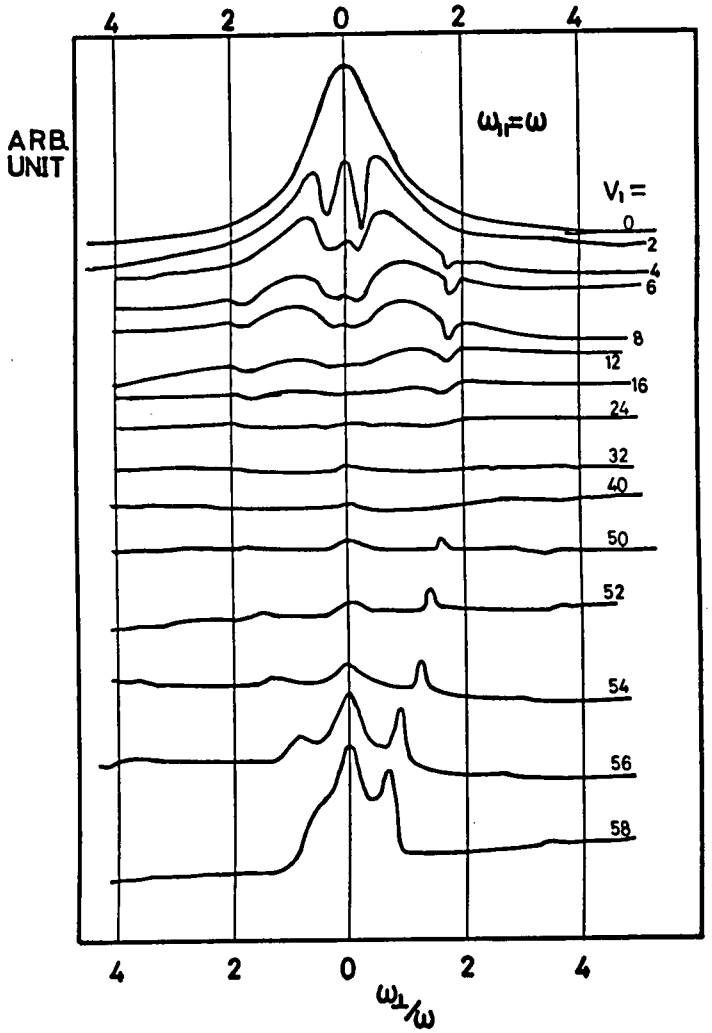

Fig. 5.14. Deformation of the anticrossing curve by the oscillating rf field. A number written in each trace is the input voltage V_1 of the rf coils (in millivolt), which is proportional to H_1. For small intensity of the rf field, $V_1 = 2 \sim 8$, the multiple quantum resonances appear on the slope of the anticrossing curve. As the intensity of the rf field is increased, the multiple quantum resonances saturate at $V_1 \sim 24$ and the Haroche like resonances appear at $V_1 \sim 50$.

$\omega_{//} = \omega$. If the oscillating rf field is absent, i.e., $H_1 = 0$, this situation corresponds to the anticrossing experiment (for example Series 1963) and the width of the curve is given as $\sqrt{(1/\tau)^2 + (\gamma H_{//})^2}$. As the intensity of the rf field is increased, the dips appear on the slope of the anticrossing curve. The dips grow up and completely erase the anticrossing curve. After that, the new resonances appear near $H_\perp = 2\omega/\gamma$, grow up and shift towards low field region. A number written in each trace gives the input voltage V_1 ofthe rf coils in millivolt, which is proportional to the intensity of the rf field H_1. The resonance peak appearing for above $V_1 = 50$ at $H_\perp = 0$ is the anticrossing curve appeared again. At $V_1 = 58$, the first new resonances exist on the slope of the anticrossing curve and the second new resonances appear near $\omega_\perp = 3.5$. Hereafter, we call the new resonances "Haroche like resonance". More detailed behavior of the Haroche like resonance is shown in Fig.5.15; (a) and (b) show the first and the second Haroche like resonances for $\omega_{//} = \omega$, respectively. Figures 5.16(a) and (b) show the Haroche like resonances for $\omega_{//} = 2\omega$. Furthermore, the Haroche like resonance for $\omega_{//} = 3\omega$ is shown in Fig.5.17. It is seen from Figs.5.15, 5.16 and 5.17 that the Haroche like resonances grow up, shift towards low field region as the intensity of the rf field is increased and then disturb the anticrossing curve.

We then investigate the behaviors of the Haroche like resonances near $\omega_{//} = 0, \omega$. Figure 5.18 shows the Haroche like resonance near $\omega_{//} = 0$; (a), (b) and (c) are for $\omega_{//} = 0$, 0.1ω and 0.2ω , respectively. Figure 5.19 shows the Haroche like resonances near $\omega_{//} = \omega$; (a), (b) and (c) are for $\omega_{//} = \omega$, 1.05ω and 1.10ω , respectively. As the deviation from $\omega_{//} = 0$ or ω is increased, the width of the Haroche like resonances become larger and the peaks become smaller than those for just $\omega_{//} = 0, \omega$. The theoretical analysis for the Haroche like resonance is given in the next section.

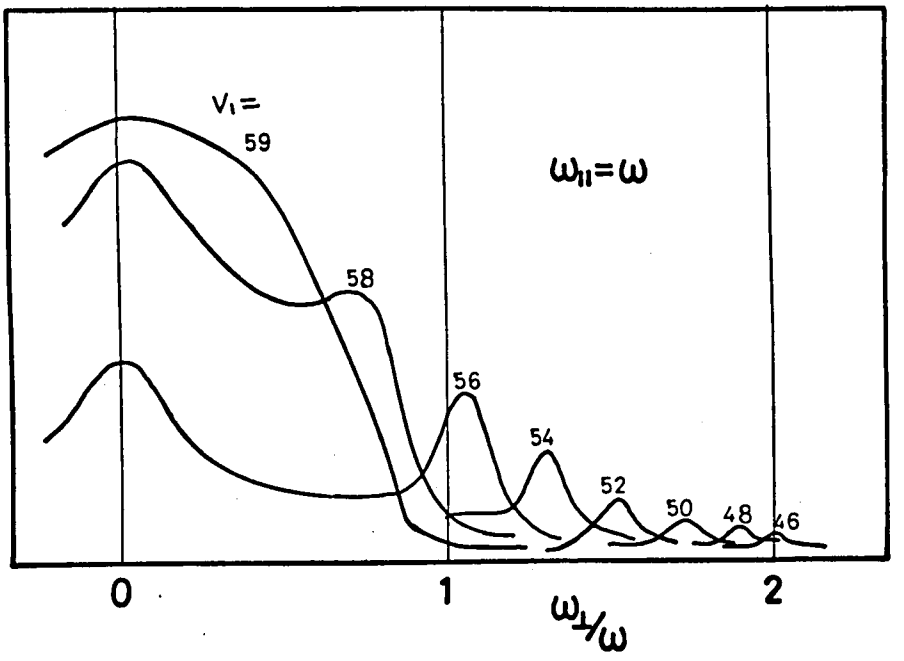

(a)

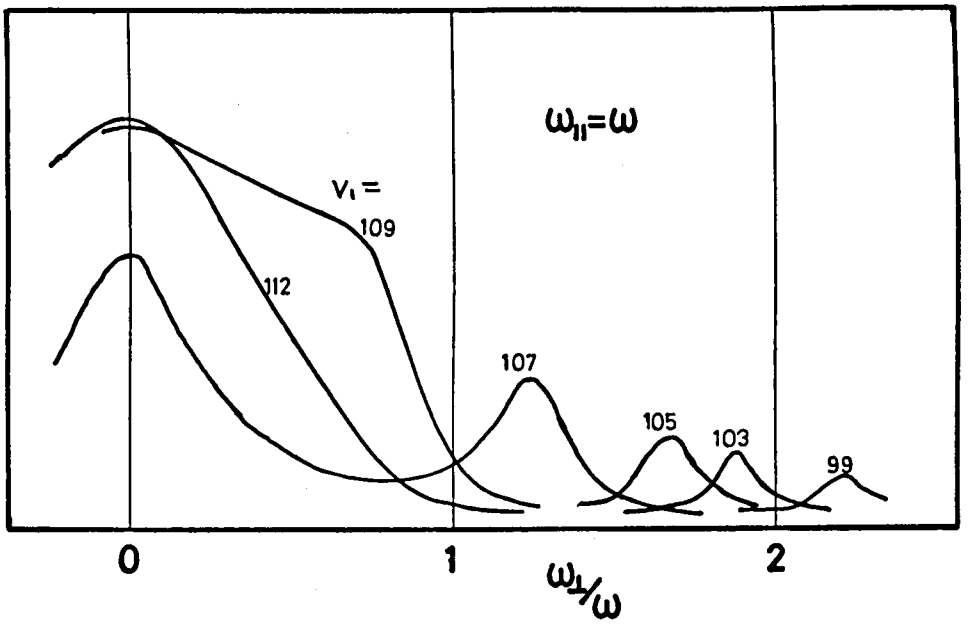

(b)

Fig. 5.15. The Haroche like resonances observed for $\omega_{//} = \omega$; (a) and (b) show the first and the second Haroche like resonances, respectively.

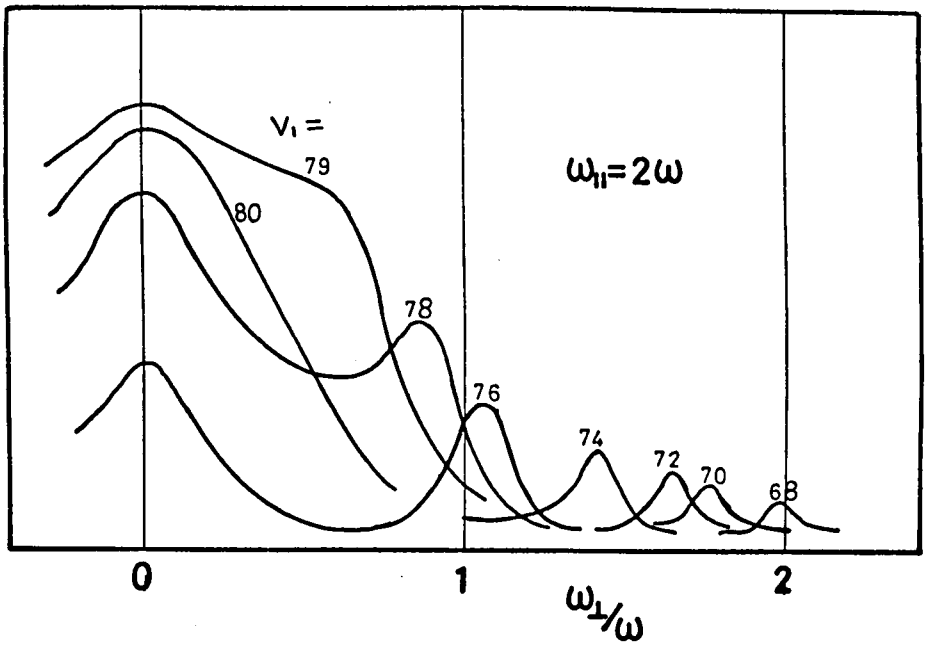

(a)

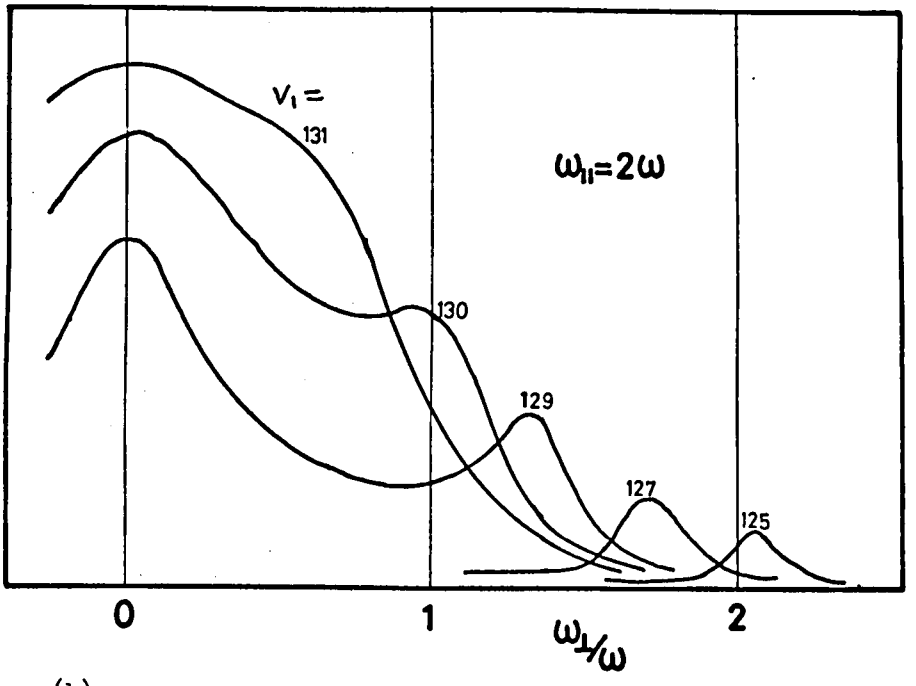

(b)

Fig. 5.16. Same as for Fig. 5.15 but for $\omega_{//} = 2\omega$; (a) and (b) show the first and the second Haroche like resonances, respectively.

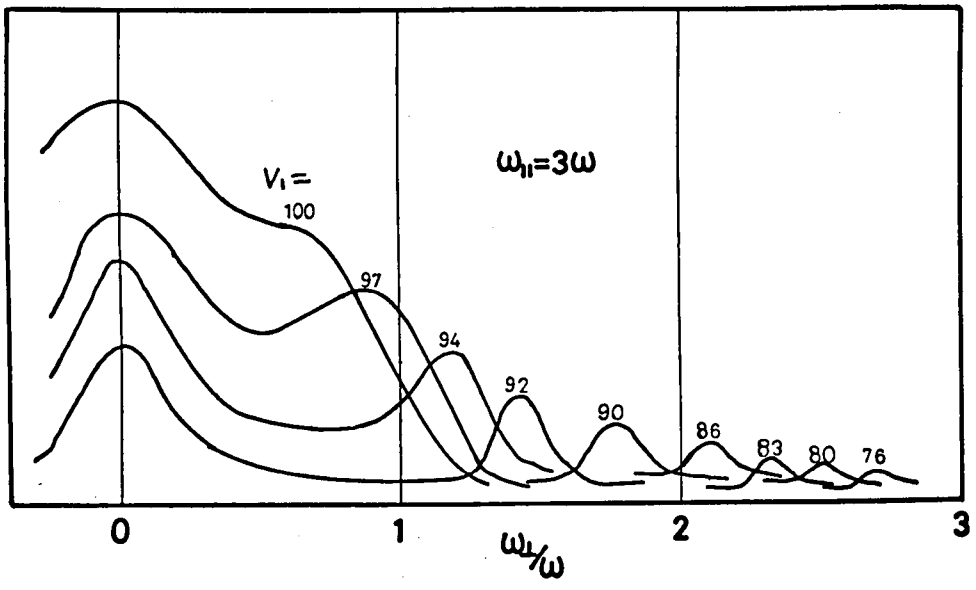

Fig. 5.17. Same as for Fig.5.15 but for $\omega_{//} = 3\omega$.

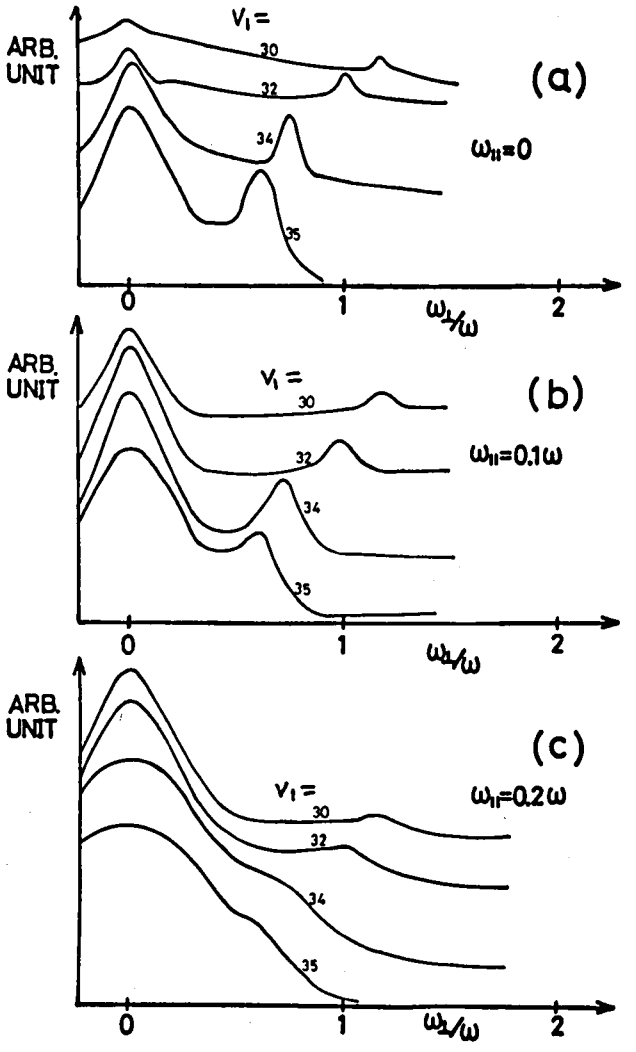

Fig. 5.18. Behavior of the Haroche like resonance near $\omega_{//} = 0$; (a), (b) and (c) are same as for Fig.5.15 but for $\omega_{//} = 0$, 0.1ω and 0.2ω, respectively.

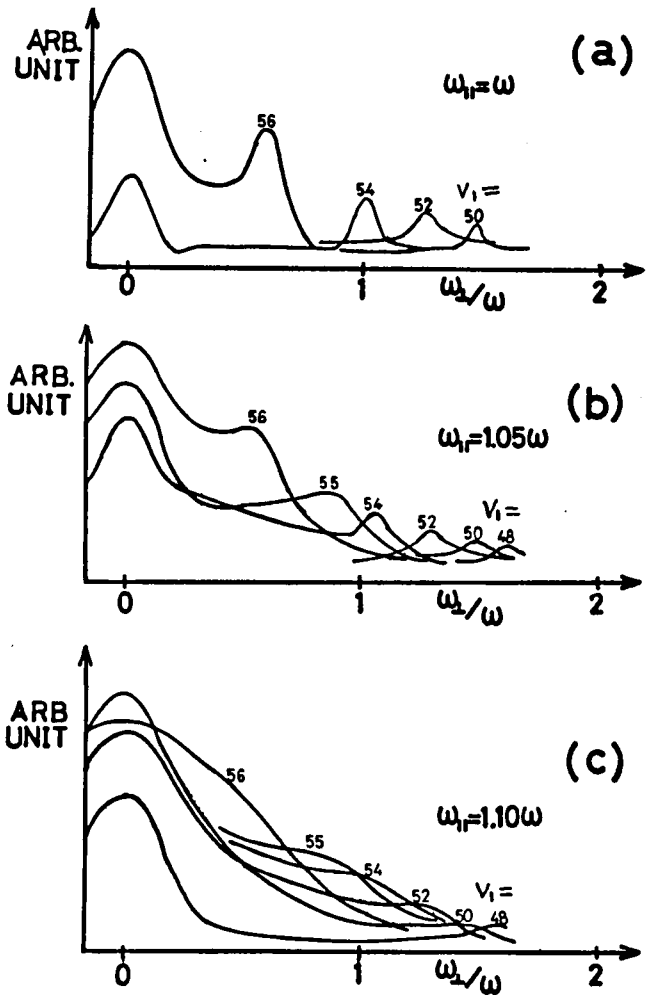

Fig. 5.19. Same as for Fig.5.18 but for $\omega_{//} = \omega$; (a), (b) and (c) are for $\omega_{//} = \omega$, 1.05ω and $1.10\,\omega$, respectively.

5.3.2. Theoretical Discussion

(a) Equation of Motion

We can obtain the equations governing the motion of the three components of the magnetization **M** for the situation of the magnetic fields and the pumping light beam given in Fig.5.12 as follows;

$$\frac{d M_x}{dt} = \omega_\perp M_y + \frac{1}{\tau} (M_0' - M_x) , \tag{5.26a}$$

$$\frac{d M_y}{dt} = - \omega_\perp M_x + (\omega_{//} + \omega_1 \cos \omega t) M_z - \frac{M_y}{\tau} , \tag{5.26b}$$

$$\frac{d M_z}{dt} = - (\omega_{//} + \omega_1 \cos \omega t) M_y - \frac{M_z}{\tau} . \tag{5.26c}$$

The system of eqs.(5.26) under the condition that $H_\perp$ must be small enough to allow the approximation, $\gamma H_\perp \ll \omega$, has been investigated independently by Pegg and Series (1970) and Yabuzaki et al. (1972a) as mentioned in section 4.2. The system of eqs.(5.26) for $\omega_{//} = 0$ has been investigated theoretically and experimentally by Tsukada and Ogawa (1973a, see also Tsukada, Murakami and Ogawa 1973a) as shown in section 5.2.

(b) Numerical Results

Here, we want to show the some results of the numerical calculations of the system of eqs.(5.26) and will compare those with the experimental results in the next section. We are interested in the time-independent component of the steady state solution. For preliminary test, the solutions of the numerical integration for $\omega_{//} = 0$ were compared with the continued fraction solutions obtained in the section 5.2. The deviation between the numerical integration results and the continued fraction results is smaller than 1% allover the resonance curves which are presented in Fig.5.20. All of the numerical calculations are made for the parameters

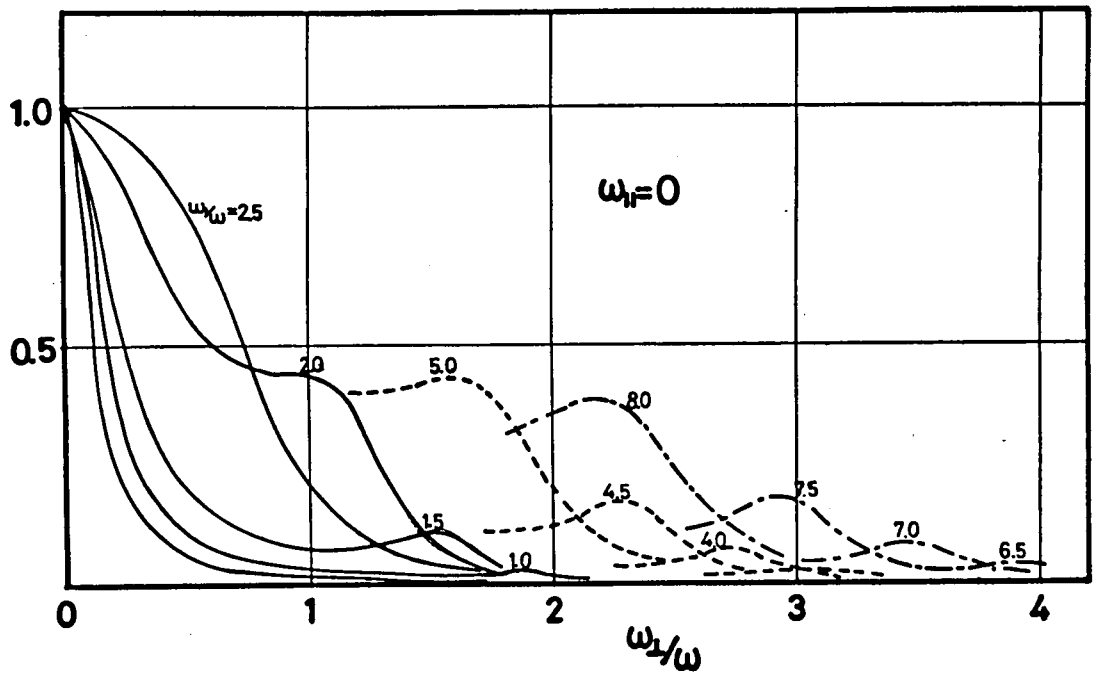

Fig. 5.20. Numerical result tobe compared with Fig.5.13, in which the Haroche resonance for $\omega_{\parallel} = 0$ obtained in experiment is shown. The solid lines show the first Haroche resonance and the Hanle curve as a function of $\omega_{\perp}/\omega$. The dashed lines and the dotted broken lines show the second and the third Haroche resonances, respectively.

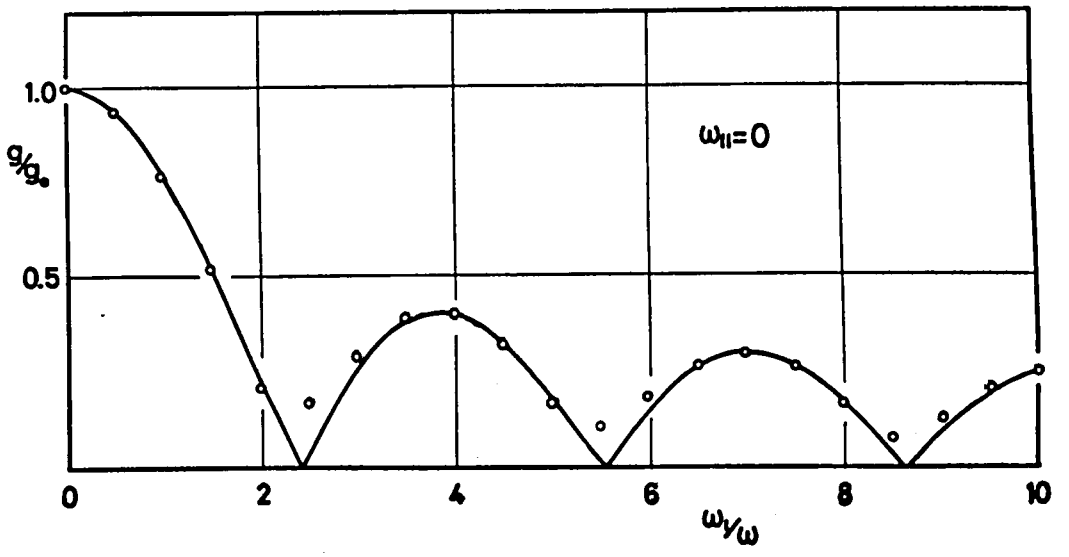

Fig. 5.21. Effective g-factor derived from the width of the Hanle curves in Fig.5.20. The computational results derived from Fig.5.20 are represented by the encircled points and the zeroth-order Bessel function as a function of ω_1/ω is represented by the solid line for comparison.

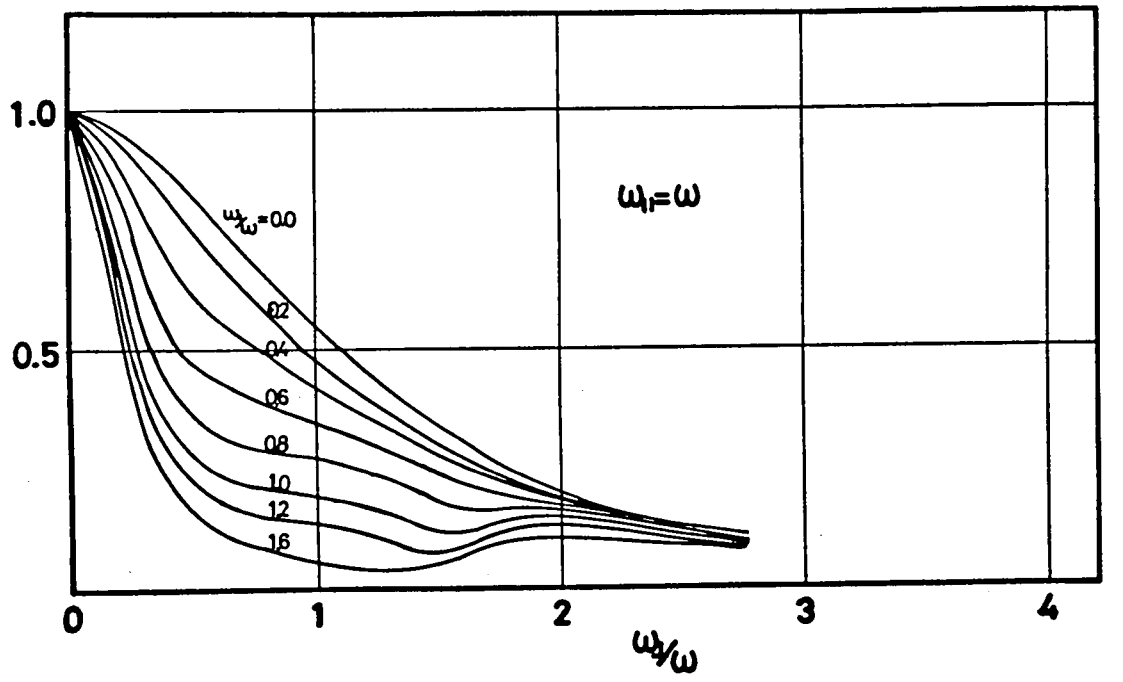

(a)

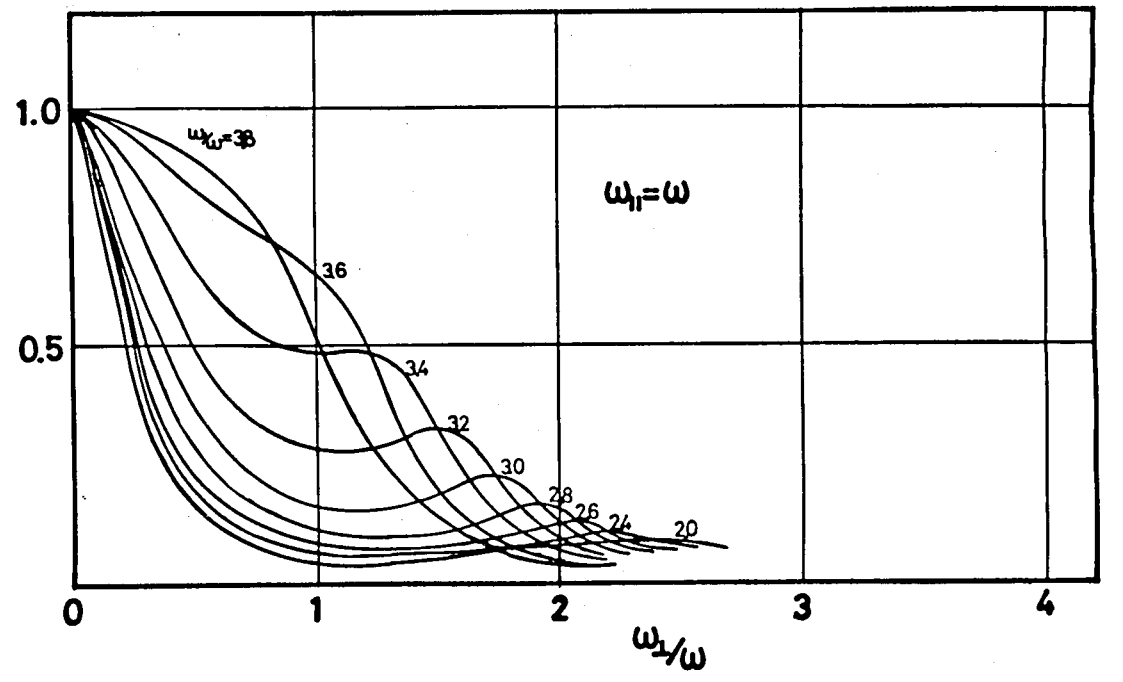

(b)

Fig. 5.22. (a) and (b), For legend see P.159.

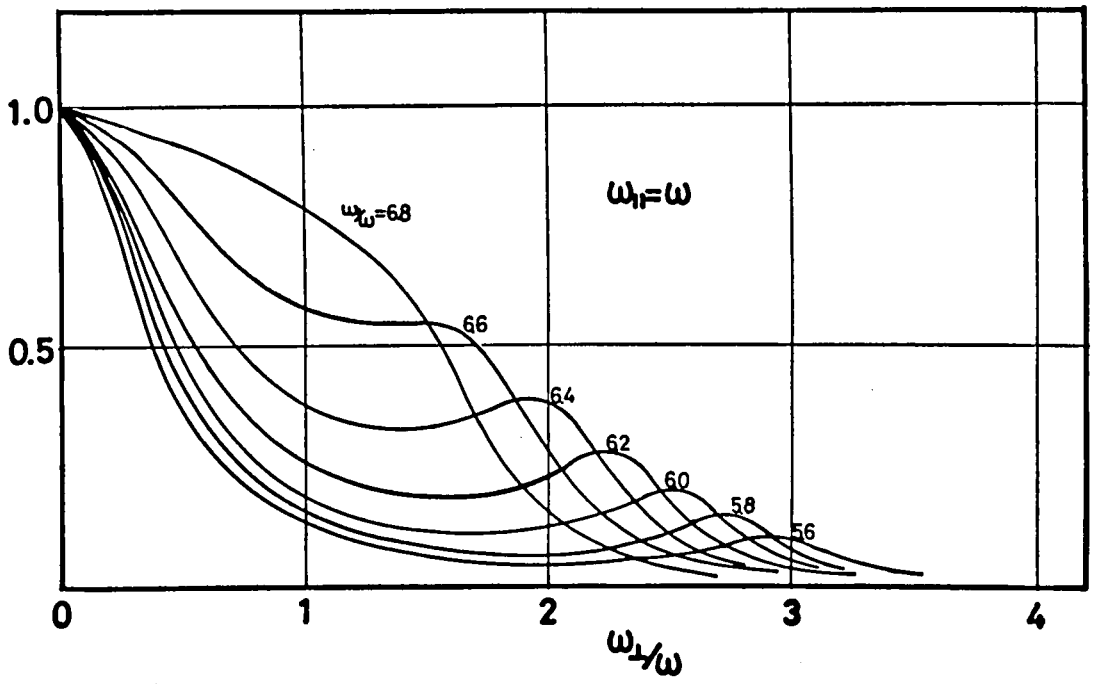

(c)

Fig. 5.22. This figure is to be compared with Fig.5.14. In Fig.5.14, the peak of the anticrossing curve decreases at $V_1 = 0 \sim 18$ as the intensity of the rf field is increased. There is however no variation of the peak of the anticrossing curve in (a). This discrepancy between theory and experiment is due to the stray field existing in the experiment. (b) and (c) show the behavior of the first and the second Haroche like resonances for $\omega_{//} = \omega$, respectively.

$$\omega/2\pi = 500 \text{ Hz}, \quad \Gamma = \tau^{-1} = 400 \text{ Hz}. \tag{5.27}$$

Figure 5.20 shows the graphs of numerical integration for $\omega_{//} = 0$, and as mentioned above this case has been investigated in detail in section 5.2. Figure 5.21 shows the variation of the effective g-factor reduced from the width of the Hanle curves in Fig.5.20. The deviation between the computational results, which are represented by the encircled points, and the zeroth order Bessel function, which is represented by the solid line, becomes larger as the value of the Bessel function approaches to zeros. The deviation, however, decreases as the intensity of the rf field is increased.

Figure 5.22 shows the same graphs as for Fig.5.20. but for $\omega_{//} = \omega$. In Fig.5.22(a), the curve in the absence of the rf field, i.e., $\omega_1 = 0$ is an anticrossing curve, As the intensity ω_1 is increased, the curve is deformed strongly. This deformation is due to the longitudinal resonances, i.e., ordinary resonances and multiple quantum resonances. The longitudinal resonances appear as decrease or absorption of the transmitted light. As the intensity ω_1 is increased more and more, the longitudinal resonances saturate and the transverse resonances or Haroche like resonances appear and grow up. The transverse resonances appear as increase or emission of the transmitted light. Figures 5.22(b) and (c) show, the behavior of the first and the second Haroche like resonances for $\omega_{//} = \omega$, respectively. Figure 5.23 shows the variation of the effective g-factor reduced from the width of the anticrossing curves in Fig.5.22(a), (b) and (c). The encircled points are computational results given in Figs.5.22 and the solid line is the first order Bessel function. We can see from Fig.5.23 that the effective g-factor for $\omega_{//} = \omega$ is approximately given as $J_1(\omega_1/\omega)g_0$, where g_0 is the unperturbed g-factor in the absence of the rf field. This fact is consistent with the results obtained by Pegg and Series (1970) and Yabuzaki et al. (1972a), in which the width of the Hanle curve or anticrossing curve

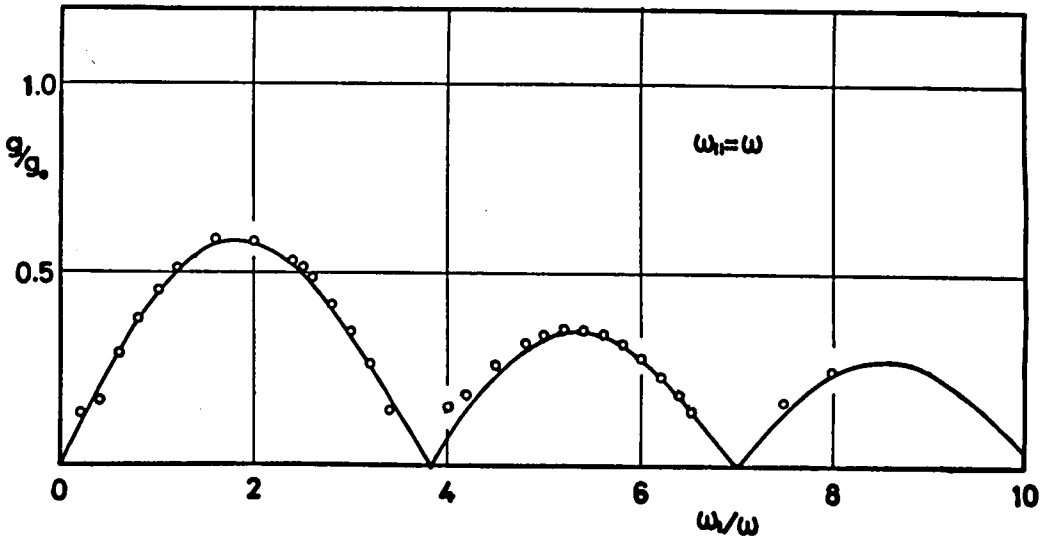

Fig.5.23. Effective g-factor derived from the width of the anticrossing curves in Fig.5.22. The computational results derived from Fig.5.22 are represented by the encircled points and the first order Bessel function is shown with the solid line.

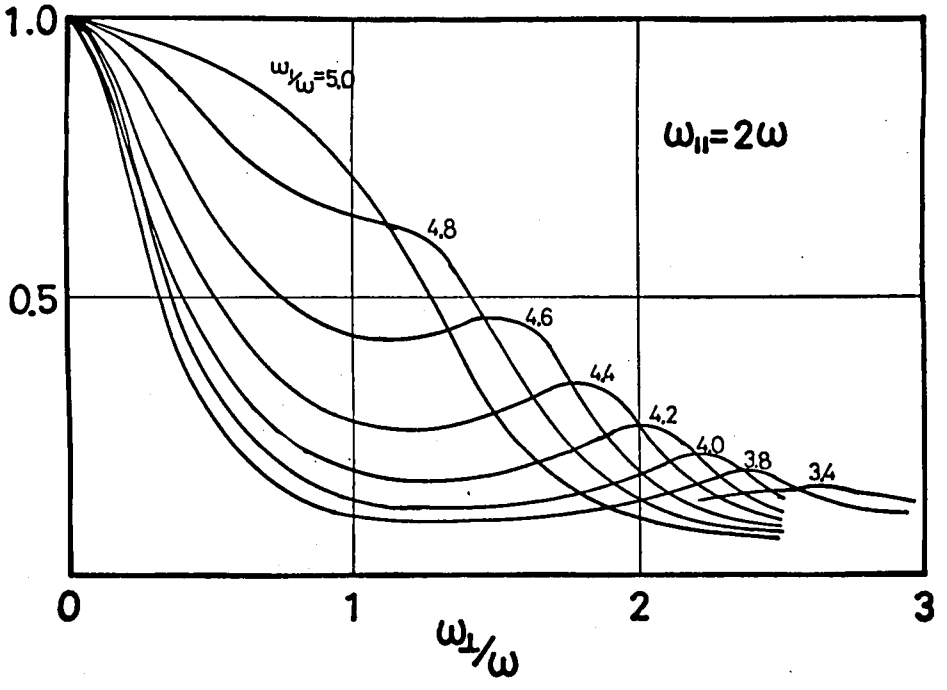

Fig. 5.24. Same as for Fig.5.20 but for $\omega_{\parallel} = 2\omega$.

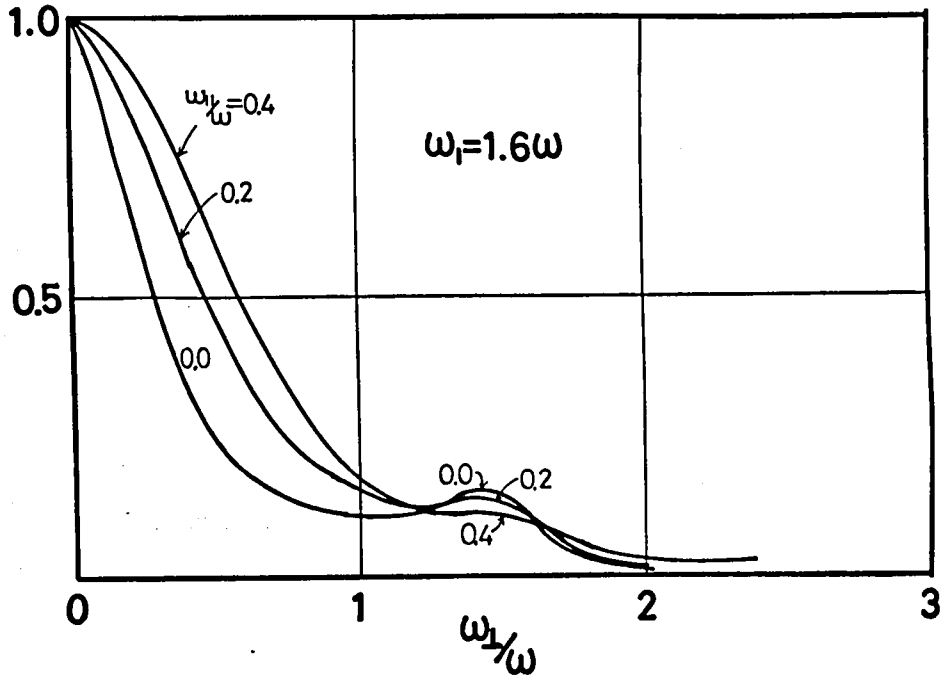

Fig. 5.25. Behavior of the Haroche like resonance near $\omega_{//} = 0$. The numerical results for $\omega_{//} = 0,\ 0.2\omega\ ,\ 0.4\omega$ at $\omega_1 = 1.6\omega$ are shown in this figure. This figure is to be compared with the experimental results in Fig.5.18.

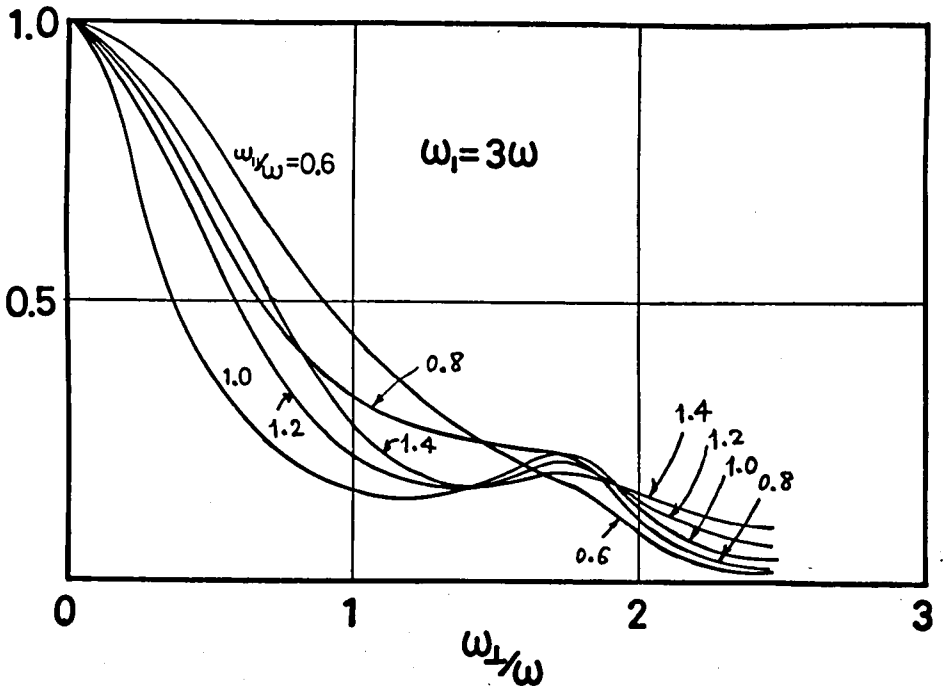

Fig. 5.26. Same as for Fig.5.25 but for $\omega_{//} = 0.6\omega$, 0.8ω , ω , 1.2ω and 1.4ω at $\omega_1 = 3\omega$. This figure is to be compared with the experimental results in Fig.5.19.

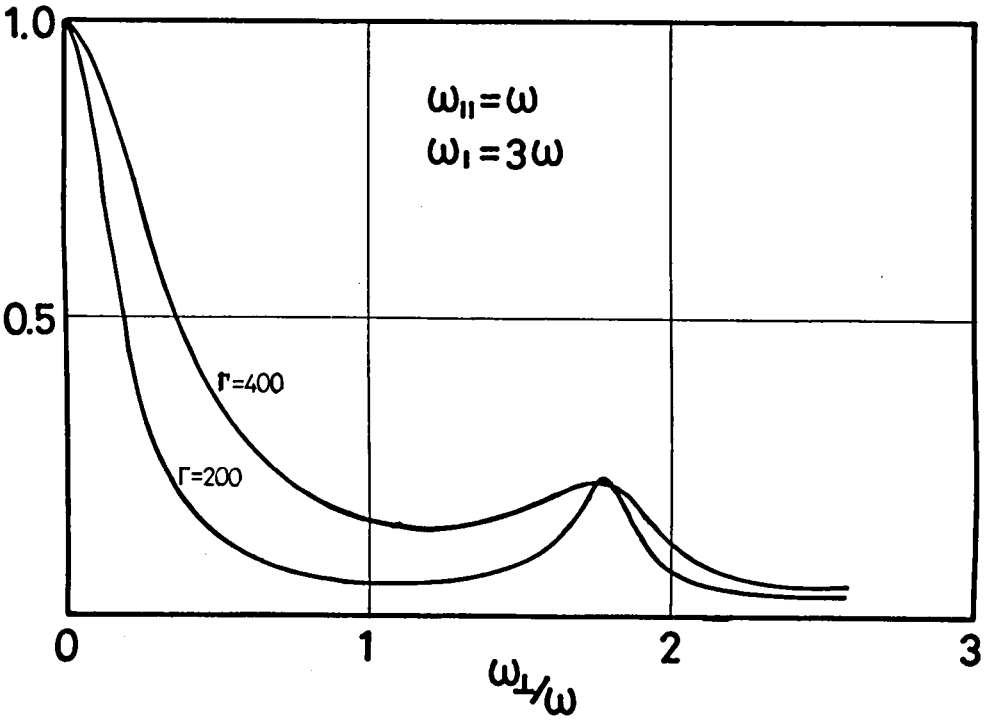

Fig. 5.27. Influence of the decay rates on the Haroche like resonances. The widths of the Haroche like resonances are strongly influenced with the decay rates. The small decay rates lead the sharp resonance curves. The positions of the Haroche like resonances are however hardly influenced with the decay rates.

should vary as $\Gamma|J_q(\omega_1/\omega)|^{-1}$ in the presence of an additional static field $H_{//}$ parallel to the oscillating rf field and of magnitude $q\omega/\gamma$, where q is an integer. It should be noticed that for $\omega_{//} = 0$, only the transverse resonance occurs, but for $\omega_{//} = n\omega$ $(n \neq 0)$ both the longitudinal resonance and the transverse resonance occur. Figure 5.24 shows the numerical result for $\omega_{//} = 2\omega$.

Figure 5.25 shows the behavior of the Haroche like resonances near $\omega_{//} = 0$; calculations were made for $\omega_{//} = 0,\ 0.2\omega,\ 0.4\omega$ at $\omega_1 = 1.6\omega$. Figures 5.26(a) and (b) show same graphs as for Fig.5.25 but for $\omega_{//} = \omega$; calculations were made for $\omega_{//} = 0.6\omega,\ 0.8\omega,\ \omega,\ 1.2\omega$ and 1.4ω at $\omega_1 = 3\omega$. As the deviation from $\omega_{//} = 0$, or ω is increased, the width of the Haroche like resonances become larger and the peaks become smaller. Figures 5.25 and 5.26 correspond to the experimental results given in Figs. 5.18 and 5.19 and show a qualitatively good agreement.

It appears from the comparisons between the experimental and the theoretical results that the experimental lines have got a smaller width than the theoretical one. The widths of the Haroche like resonances of the numerical results can easily be made small by choosing of the small values of Γ as shown in Fig.5.27. However, the influence of the decay rates Γ on the positions of the Haroche like resonance is very small.

5.3.3. Comparisons between the Experimental Results and the Numerical Results

We have studied the behaviors of the Haroche like resonances similar to the Haroche resonance experimentally and theoretically. The Haroche like resonances can be obsreved near $\omega_{//} = n\omega$ for strong rf field and shift towards $\omega_{\perp} = 0$. The peaks of the Haroche like resonances which appear at $\omega_{//} = n\omega$ are seen to appear, shift and disappear. Figure 5.2 shows the positions of the various Haroche like resonances as a function of the rf amplitude ω_1. The encircled points are experimental results and the

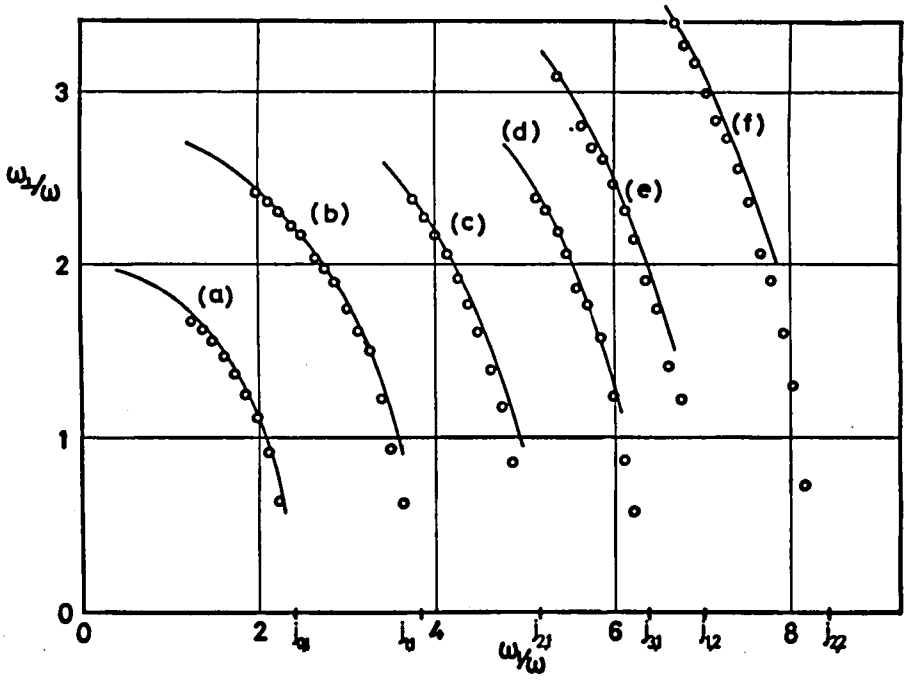

Fig. 5.28. Positions of the various Haroche like resonances as a function of ω_1; (a) is the first Haroche resonance, (b), (c) and (d) are the first Haroche like resonances for $\omega_{//} = \omega$, 2ω, 3ω, respectively. (e) and (f) are the second Haroche like resonances for $\omega_{//} = \omega$, 2ω, respectively. The encircled points are the experimental results and the solid lines show the numerical results. It should be noticed that the values of ω_1/ω, at which the Haroche like resonances for $\omega_{//} = q\omega$ enter the zero field of $H_\perp$, corresponding to the values at the zeros of the q-th order Bessel function $J_q(\omega_1/\omega)$. The values of $J_{n,m}$'s represent the m-th zero of the n-th order Bessel function $J_n(\omega_1/\omega)$.

solid lines are numerical solutions; (a) is the first Haroche resonance for $\omega_{//} = 0$, (b), (c) and (d) are the first Haroche like resonances for $\omega_{//} = \omega$, 2ω and 3ω, respectively, and (e) and (f) are the second Haroche like resonances for $\omega_{//} = \omega$ and 2ω. Agreement between the observed results and the numerical results is extremely excellent. It should be noticed that the values of ω_1/ω, at which the Haroche like resonances for $\omega_{//} = n\omega$ shift and enter the zero field, i.e., $H_\perp = 0$, correspond to the values at the zeros of n-th order Bessel function $J_n(\omega_1/\omega)$. This fact is consistent with that the modification of the atomic g-factor by the linearly oscillating rf field at $\omega_{//} = n\omega$ is given as $J_n(\omega_1/\omega)g_0$. For $\omega_{//} = 0$, only the transverse resonances or Haroche like resonances occur, but for $\omega_{//} = n\omega$ ($n \neq 0$), both the longitudinal or multiple quantum resonances and the transverse resonances play important roles simultaneously. The longitudinal resonances appear as the absorption of the pumping light and the transverse resonances appear as increase of the transmitted light. As the intensity of the rf field is small, only the longitudinal resonances appear. For middle intensity of the rf field, both the longitudinal resonances and the transverse resonances appear simultaneously, and for large intensity of the rf field, the longitudinal resonances saturate and hence only the transverse resonances can be observed. It seems from the experimental results of Figs.5.18 and 5.19, and from the theoretical results of Figs.5.24 and 5.25 that the Haroche like resonances do not shift towards $\omega_\tau = (\omega_{//}^2 + \omega_\perp^2)^{1/2} = 0$ but $\omega_\perp = 0$. Therefore, it seems convenient to consider for strong rf field that the total magnetic field $\mathbf{H}_\tau$ is separated into the parallel and the perpendicular components, $\mathbf{H}_{//}$ and $\mathbf{H}_\perp$, with respect to the oscillating rf field.

Further investigations for various directions of the pumping light beam and the transient solutions for the system of eqs.(5.26) may introduce some interesting phenomena. This type of the numerical approach may be imporant to describe the experiments performed in more general situations.

5.3.4. Competition of the Longitudinal Resonance and the Transverse Resonance

Saturation effects of the longitudinal and the transverse resonances for the case that an oscillating rf field $H_1 \cos \omega t$ is perpendicular to the static magnetic field H_0 have been investigated theoretically by Stenholm (1972a,b) and Tsukada and Ogawa (1973a), respectively. This section descrives an experimental investigation of the competition of the longitudinal and the transverse resonances. The geometric configuration of the experiment is shown in Fig.5.29. The circularly polarized light beam is parallel to the

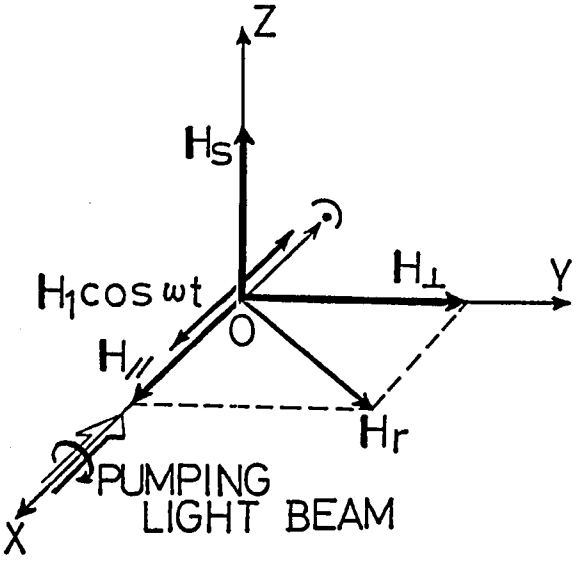

Fig. 5.29. Geometric disposition to be considered.

oscillating rf field H_1 and it is taken to be in the X direction. The component of the magnetic field in the XY-plane is denoted by H_r, and $H_{//}$ and $H_\perp$ are the components of H_r along the X and Y directions, respectively. We have observed the variation of the light intensity after passing through the absorption cell, as the magnetic field H_s taken to be in the Z direction is varied negative to positive through zero. If the oscillating rf field is absent, this situation corresponds to the anticrossing experiment. When the two levels become degenerate, they can be coupled by a static interaction,

and hence the anticrossing experiment can be regarded as a double resonance experiment at zero frequency.

We want to observe the deformation of the anticrossing curve as the intensity of the rf field is increased. Experiments were made for various values of ω_r/ω with optically pumped cesium atoms. We show the experimental results for the two special cases, i.e. $\omega_r \ll \omega$ and $\omega_r \gg \omega$, where ω_r denotes γH_r. For the case $\omega_r \ll \omega$, the recoredr traces are shown in Fig.5.30(a). On the other hand, for the case $\omega_r \gg \omega$, the recorder traces are shown in Fig.5.30(b). Comparing Fig.5.30(a) with (b), we see that the behavior of the variation of the transmitted light intensity for the special two cases are quite different from each other. When the condition $\omega_r \ll \omega$ is satisfied, we can expect the variation of the light intensity by using the notion of "dressed atom" introduced by Cohen-Tannoudji and Haroche (1969a,b). The variation of the transmitted light ΔI_T for this case is given as follows;

$$\Delta I_T = \frac{1 + (\bar{\omega}_{//} \tau)^2}{1 + (\bar{\omega}_{//}^2 + \bar{\omega}_{\perp}^2 + \bar{\omega}_s^2) \tau^2} \tag{5.28}$$

where

$$\bar{\omega}_{//} = \bar{\gamma}_{//} H_{//} , \quad \bar{\omega}_{\perp} = \bar{\gamma}_{\perp} H_{\perp} , \quad \bar{\omega}_s = \bar{\gamma}_s H_s ,$$

$$\bar{\gamma}_{//} = \gamma \quad , \quad \bar{\gamma}_{\perp} = J_0(\gamma H_1/\omega) \gamma \ , \ \bar{\gamma}_s = J_0(\gamma H_1/\omega) \gamma . \tag{5.29}$$

The experimental results obtained for the case $\omega_r \ll \omega$ agree well with eq.(5.28).

However, there has been no theory which could explain the behavior of the variation of the transmitted light intensity for the case $\omega_r \gg \omega$. Fortunately, this behavior is able to be explained quantitatively by using the theory of the saturation effects of the longitudinal and the transverse resonances (Stenholm 1972a,b, Tsukada and Ogawa 1973a). From their results,

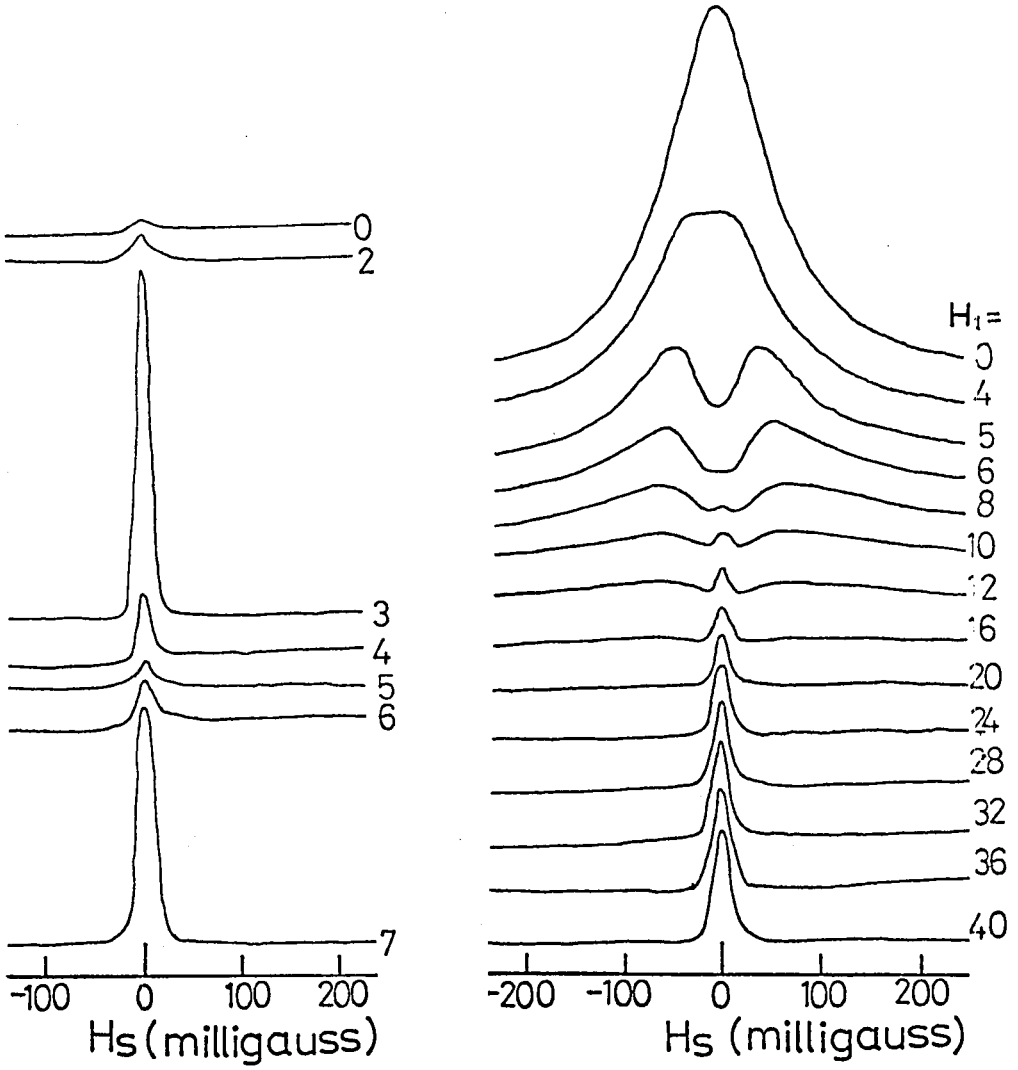

(a) (b)

Fig. 5.30. Recorder traces showing the variation of anticrossing curve. A number written in each traces gives the value H_1; H_1 = number x 7 milligauss. Experimental conditions: (a) $\omega/2\pi$ = 3 KHz, $\omega_r/2\pi$ = 1 KHz, (b) $\omega/2\pi$ = 300 Hz, $\omega_r/2\pi$ = 35 KHz.

we can see that at the same value of H_1, the width of the longitudinal resonance is much larger than that of the transverse resonance, and the transverse resonance appears at large value of H_1. Therefore the deformation of the anticrossing curve is explained as follows; (1) as H_1=0, the curve coincides with the anticrossing experiment, so-called anticrossing curve, (2) the dip of the center of the anticrossing curve at H_1= 4 or 5 is due to the longitudinal resonance, (3) the longitudinal resonance is nearly saturated by the rf field over all the anticrossing curve at H_1 = 8 or 10, (4) the peak appearing at the center of the dip as H_1 is increased is due to the transverse resonance corresponding to "crossing" of the energy levels. At the values above H_1= 16, the longitudinal resonance is completely saturated. Therefore, the variation of the transmitted light intensity is due to only the transverse resonance. As is expected from the results of the saturation effects, the magnitude of the transverse resonance increases with the order of resonance at the same value of H_1 as the H_1 is increased. The width of the curve of the transverse resonance is of the order of the decay rate $\Gamma = 1/\tau$ of the atom for small value of rf intensity and become larger as H_1 is increased.

If we use the crossing curve due to the transverse resonance instead of the anticrossing curve, the components of the external magnetic field could be measured with better accuracy than the measurement by using the anticrossing curve (Aleksandrov et al. 1968).

5.4. Conclusion

In section 5.2, we have shown that the Haroche resonances can be described entirely by the continued fraction representations. These resonances occur at $\omega_0 = 2n\omega$ as the intensity of the rf field H_1 is small. Cohen-Tannoudji and Haroche (1965, 1969a) have shown that the width of the Haroche resonances is determined only by the decay rate. Namely, they have concluded that the

resonances are shifted but not broadened as the intensity H_1 is increased. But their results are applicable only to weak rf field. We have shown that the resonances are shifted and broadened as the intensity H_1 is increased, and the broadening is remarkably for large H_1.

It has been also shown that the variation of the width of the Hanle curve by the oscillating rf field, i.e. the modification of the atomic g-factor, is due to the Haroche resonances, especially for large intensity of the rf field. If the pumping light beam directs to the y-direction, i.e. perpendicularly to the oscillating rf field, the Haroche resonances are very small and it is difficult to observe them.

The experimental results obtained are in fairly good agreement with the continued fraction solutions. In the past, the variation of the width of the Hanle curve by the oscillating rf field, i.e. the modification of the atomic g-factor, has not been related to the Haroche resonance. It should be noticed that the Haroche resonance plays an important role on the variation of the width of the Hanle curve. We also showed from the continued fraction solutions that the positions of the Haroche resonances for large intensity of H_1 deviate from those obtained with perturbation theory. These facts have been verified in optical pumping experiments with cesium vapor. Moreover, the saturation effects of the resonance intensity for the large intensity of the rf field have been investigated in the modulated components in the transmitted light beam not only for the transverse pumping but also the for the longitudinal pumping.

In section 5.3, we have treated the saturation effects for more general cases that the static magnetic field with arbitrary magnitude directs an arbitrary direction with respect to the oscillating rf field with arbitrary intensity. The experimental results have been compared with the exact solutions based on the numerical integration of the Bloch equation. It has been

shown experimentally and theoretically that there exist the resonances similar to the Haroche resonance at $\omega_{//} = n\omega$, where n is an integer or zero. As is expected from section 4.3, both the longitudinal resonance and the transverse resonance appear simultaneously. The longitudinal resonances appear as the absorption of the pumping light beam and the transverse resonances appear as the increase of the transmitted light. As the intensity of the rf field is small, only the longitudinal resonances appear, and for middle intensity of the rf field both the longitudinal and the transverse resonances can be observed. for extremely large intensity of the rf field, the longitudinal resonances saturate and only the transverse resonances can be observed.

CHAPTER 6

SUMMARY AND CONCLUSION

We have discussed the effects of the transverse optical pumping for various configurations of the static magnetic field and the rf field(s), by use of the Bloch equation.

In Chapter 2, we have briefly reviewed that for spin-1/2 system the equation of motion of the density matrix is equivalent to the phenomenological Bloch equation, and have evaluated the monitoring operator and the excitation matrix. By using these results, we have analyzed two simple cases, i.e., the level crossing (or the Hanle effect) and the anticrossing experiment. Various resonances treated in the later chapters can be essentially separated into these two kinds of resonances.

In Chapter 3, the effects of the transverse pumping in the presence of the rotating rf field(s) are discussed. For a rotating rf field which exists in a perpendicular plane with respect to the static magnetic field, the transverse pumping leads the new type resonance at twice the rotating rf frequency in the unmodulated component and the component modulated at 2ω in the transmitted light beam. Then we have demonstrated that the Hanle curve is broadened and is shifted towards high field region as the intensity of the rotating rf field is increased.

On the other hand, the theory on the transverse pumping in the presence of the two rotating rf fields with different frequencies and with different magnitudes predicts the resonances corresponding to the process of even number of rf photons, i.e., zero photon process (the Hanle effect), two photon process, four photon process etc., and the modulation of the beat frequencies between the two rotating frequencies. The effects of the misalignment of the rotating rf field in the magnetic resonance have been investigated.

Three main effects arise: a shift in the resonance frequency, a reduction in power broadening, and the appearance of the multiple quantum resonances at integral multiples of the rotating field frequency. In addition it has been shown that for weak static field the rotating rf field is regarded as a static fictitious magnetic field along the rotating axis of the rf field.

In Chapter 4, the effects of the transverse optical pumping with the linear oscillating rf field have been investigated. In the first instance, the interaction between the atoms and the strong rf field has been studied by analyzing classically and quantum mechanically the behavior of the optically pumped atoms. The theory shows that the medium irradiated by a strong linear oscillating rf field becomes anisotropic and the atomic g-factor becomes a tensorial quantity, and predicts that the component of the g-factor perpendicular to the rf field is drastically modified by the rf field when the Hanle effect or the parametric resonance takes place. The theoretical predictions have been verified by the experiments with cesium vapor. The atomic g-factor has so far been considered to be determined only by atomic constants, so that the fact obtained here that the g-factor is controllable by applying a strong rf field might become important for the atomic physics, especially for the rf spectroscopy and for studies on atomic spin exchange between different species. In addition we can expect the enhancement of the Overhauser effect by applying this effect to the nuclear level.

Secondary, the misalignment effects of the linearly oscillating rf field lead two types of magnetic resonances, the longitudinal and the transverse resonances. It has been shown that the parametric resonance and the Haroche resonance correspond to the special cases of the transverse resonance. There is no essential difference between the parametric resonance and the Haroche resonance. For small misalignment angle, i.e., the static field is nearly perpendicular to the oscillating rf field, the nature of the Haroche resonance appears

strongly, and for large misalignment angle, i.e., the static field and the rf field are nearly parallel to each other, the nature of the parametric resonance appears strongly. In the experiment, simultaneous existence of the longitudinal resonance and the transverse resonance has been observed.

In Chapter 5, semiclassical theory leading to the continued fraction solution has been adapted to study saturation effects of the Haroche resonance. We have shown that the resonances are shifted and broadened as the intensity of the oscillating rf field is increased, and the broadening is remarkable for large intensity of the rf field. Fortunately, however, the Haroche resonances are shifted without being broadened appreciably when the rf power is increased over a large range. So the Haroche resonances are the most interesting for precise check of the higher order terms of the Bloch-Siegert shift. It has been cleared that the experimental results for the shifts of the Haroche resonances support the semiclassical approaches by Shirley, Pegg and Stenholm rather than the quantum electrodynamics approach by Chang and Stehle.

It has been also shown that the variation of the width of the Hanle curve by the linearly oscillating rf field, namely the modification of the atomic g-factor, is due to the Haroche resonances. For the transverse pumping perpendicular to the rf field axis, the Hanle curve is not only broadened but also diminished in its peak as the intensity of the rf field is increased.

The experimental results obtained are in fairly good agreement with the continued fraction solutions. In the past, the variation of the width of the Hanle curve by the linearly oscillating rf field has not been related to the Haroche resonances. We have cleared that the Haroche resonances play an important role on the variation of the width of the Hanle curve. We also showed from the continued fraction solutions that the positions of the Haroche resonances for the large intensity of the rf field deviate from those obtained

with the perturbation theory.

In addition, we have observed the oscillating terms at twice and four times the rf field frequency for one and three, and three and five quantum transitions, respectively. Their behaviors are in very good agreement with those expected from Stenholm's theory.

We have, last of all, studied the new type resonances when the static magnetic field with an arbitrary intensity is oriented in an arbitrary direction with respect to the strong oscillating field. The resonances of this type appear at $H_{//} = n\omega/\gamma$. The behavior of the resonances is similar to those of the Haroche resonance. As the intensity of the rf field is increased, the resonances are seen to appear, shift and disappear. It has been cleared that the modification of the atomic g-factor at $\omega_{//} = n\omega$ is related to these Haroche like resonances. Namely, the values of ω_1/ω, at which the Haroche like resonances for $\omega_{//} = n\omega$ shift and enter $H_\perp = 0$, correspond to the values at the zeros of n-th order Bessel function $J_n(\omega_1/\omega)$. For $\omega_{//} = 0$, only the transverse resonances or the Haroche resonances occur, but for $\omega_{//} = n\omega$ ($n \neq 0$), both the longitudinal or the multiple quantum resonances and the transverse resonances or the Haroche like resonances play important roles, simultaneously. The longitudinal resonances appear as the absorption of the pumping light and the transverse resonances appear as the increase of the transmitted light intensity. As the intensity of the rf field is small, only the longitudinal resonances appear. For the middle intensity of the rf field, both the longitudinal and the transverse resonances appear simultaneously, and for large intensity of the rf field, the longitudinal resonances nearly saturate and hence only the transverse resonances can be observed. It seems from the experimental results and from the theoretical results that the Haroche like resonances do not shift towards $H_0 = (H_{//}^2 + H_\perp^2)^{1/2} = 0$ but $H_\perp = 0$.

For low frequency of the rf field, i.e., $\omega \leq \Gamma$, the anticrossing curve

which is described in Chapter 2 is defirmed strongly as the intensity of the rf field is increased, and ultimately the sharp transverse resonance (Haroche like resonance) appears.

Further investigations for various directions of the pumping light beam and the transient solutions of the Bloch equation may introduce some interesting phenomena.

APPENDIX A Density Matrix Treatment for the Rotating RF Field

The equation of motion of the density matrix $\rho(t)$, for ensemble of spin **J** particles subjected to a constant magnetic field, a steady rotating rf field, relaxation or damping process, and regeneration process which maintain a population difference between the Zeeman sublevels, is given as follows;

$$\dot{\rho} = \frac{i}{\hbar}[\rho, \mathcal{H}] + \Gamma[\rho - \mathbf{I}] + W\rho^0 \quad , \tag{A.1}$$

where

$$\mathcal{H} = J_z \omega_0 + \omega_1 (J_x \cos\omega t + J_y \sin\omega t) \quad , \tag{A.2}$$

I is the unit or identity matrix, $\Gamma = \tau^{-1}$, W represents the rate at which particles are steadily supplied to the states of an ensemble in a constant configuration ρ^0 by means of optical pumping process. The solution of the equation has been given by Carver et al. (1966) as follows;

$$\rho_{m,m'}(t) = \sum_{\substack{n,n' \\ m_0,m_0'}} e^{-i(m-m'-m_0+m_0')\omega t} W\rho^0_{m_0,m_0'} \cdot \frac{R_{m,n} R_{n,m_0} R_{m',n'} R_{n',m_0'}}{\Gamma + i[(m_0 - m_0')\omega + (n-n')\omega_e]} \quad , \tag{A.3}$$

where $(m,m',m_0$ and $m_0')\hbar\omega$ are eigenvalues of $J_z\omega$, $(n,$ and $n_0)\hbar\omega_e$ are eigenvalues of $J_z\omega_e$ and $R_{m,n}$'s are the individual matrix elements of the rotation operator. They have applied this result to the considerably simplified cases that the $m_0 - m_0'$ termes can be neglected, i.e., ρ^0 does not contain off diagonal elements. They have introduced a monitoring operator **Q**, and shown that the signals in various resonant experiments can be easily obtained by the expectation value of **Q**,

$$\langle Q \rangle = \text{Trace}\,(\rho Q) = \sum_{m,m'} \rho_{m,m'}(t)\, Q_{m',m} \,. \tag{A.4}$$

For the transverse pumping, the off-diagonal elements of ρ^0 are important and cannot be neglected, since they give rise to the effects of the transverse pumping.

For the case that the system is spin 1/2 and for single beam, matrices ρ^0, $\mathbf{Q}$ and $\mathbf{R}$ are given by

$$\mathbf{Q} = \begin{vmatrix} 1+\cos\theta & \sin\theta \\ \sin\theta & 1-\cos\theta \end{vmatrix} , \tag{A.5}$$

$$\rho^0 = \begin{vmatrix} 1+\cos\theta & \sin\theta \\ \sin\theta & 1-\cos\theta \end{vmatrix} M_0' , \tag{A.6}$$

$$\mathbf{R} = \begin{vmatrix} \cos(\beta/2) & -\sin(\beta/2) \\ \sin(\beta/2) & \cos(\beta/2) \end{vmatrix} . \tag{A.7}$$

From eq.(A.2), the elements of the density matrix for spin 1/2 can be obtained as follows;

$$\rho_{\frac{1}{2}\frac{1}{2}} = \frac{W}{\Gamma}\,{}_{\frac{1}{2},\frac{1}{2}}\left(1-\frac{1}{2}P\right) + \frac{W}{2\Gamma}\rho^0_{-\frac{1}{2},-\frac{1}{2}}P$$

$$+\frac{W}{4}\rho^0_{\frac{1}{2},-\frac{1}{2}}\left\{\frac{2(\Gamma-i\omega)}{\Gamma^2+\omega^2}\sin\beta\cos\beta - \frac{\Gamma-i(\omega+\omega_e)}{\Gamma^2+(\omega+\omega_e)^2}\sin\beta(1+\cos\beta)\right.$$

$$\left.+\frac{\Gamma-i(\omega-\omega_e)}{\Gamma^2+(\omega-\omega_e)^2}\sin\beta(1-\cos\beta)\right\}e^{i\omega t} + \frac{W}{4}\rho^0_{-\frac{1}{2},\frac{1}{2}}\left\{\frac{2(\Gamma+i\omega)}{\Gamma^2+\omega^2}\right.$$

$$\times(-\sin\beta\cos\beta) - \frac{\Gamma+i(\omega-\omega_e)}{\Gamma^2+(\omega-\omega_e)^2}\sin\beta(1-\cos\beta)$$

$$\left.-\frac{\Gamma+i(\omega+\omega_e)}{\Gamma^2+(\omega+\omega_e)^2}\sin\beta(1+\cos\beta)\right\}e^{-i\omega t} , \tag{A.8}$$

$$\rho_{\frac{1}{2},-\frac{1}{2}} = \rho^*_{-\frac{1}{2},\frac{1}{2}} = \frac{W}{2\Gamma}\rho^0_{\frac{1}{2},\frac{1}{2}}(\chi' + i\chi'')e^{-i\omega t} + \frac{W}{2\Gamma}\rho^0_{-\frac{1}{2},-\frac{1}{2}}(\chi'-i\chi'')e^{i\omega t}$$

$$+\frac{W}{4}\rho^{0}_{\frac{1}{2},-\frac{1}{2}}\left\{\frac{2(\Gamma-i\omega)}{\Gamma^2+\omega^2}(-\sin^2\beta)+\frac{\Gamma-i(\omega+\omega_e)}{\Gamma^2+(\omega+\omega_e)^2}(1+\cos\beta)^2\right.$$

$$\left.+\frac{\Gamma-i(\omega-\omega_e)}{\Gamma^2+(\omega-\omega_e)^2}(1-\cos\beta)^2\right\}e^{i2\omega t}+\frac{W}{4}\rho^{0}_{-\frac{1}{2},\frac{1}{2}}\left\{\frac{2(\Gamma+i\omega)}{\Gamma^2+\omega^2}\right.$$

$$\left.+\frac{\Gamma+i(\omega+\omega_e)}{\Gamma^2+(\omega+\omega_e)^2}+\frac{\Gamma+i(\omega-\omega_e)}{\Gamma^2+(\omega-\omega_e)^2}\right\}(-\sin^2\beta)\,e^{-i2\omega t}, \tag{A.9}$$

$$\rho_{-\frac{1}{2},-\frac{1}{2}}=\frac{W}{2\Gamma}\rho^{0}_{\frac{1}{2},\frac{1}{2}}+\frac{W}{\Gamma}\rho^{0}_{-\frac{1}{2},-\frac{1}{2}}\left(1-\frac{1}{2}P\right)+\frac{W}{4}\rho^{0}_{\frac{1}{2},-\frac{1}{2}}\left\{\frac{2(\Gamma-i\omega)}{\Gamma^2+\omega^2}\right.$$

$$\times\sin\beta\cos\beta+\frac{\Gamma-i(\omega+\omega_e)}{\Gamma^2+(\omega+\omega_e)^2}\sin\beta\,(1+\cos\beta)-\frac{\Gamma-i(\omega-\omega_e)}{\Gamma^2+(\omega-\omega_e)^2}$$

$$\left.\times\sin\beta\,(1-\cos\beta)\right\}e^{i\omega t}+\frac{W}{4}\rho^{0}_{-\frac{1}{2},\frac{1}{2}}\left\{\frac{2(\Gamma+i\omega)}{\Gamma^2+\omega^2}\sin\beta\cos\beta\right.$$

$$\left.+\frac{\Gamma+i(\omega+\omega_e)}{\Gamma^2+(\omega+\omega_e)^2}\sin\beta(1+\cos\beta)-\frac{\Gamma+i(\omega-\omega_e)}{\Gamma^2+(\omega-\omega_e)^2}\sin\beta(1-\cos\beta)\right\}$$

$$\times e^{-i\omega t}, \tag{A.10}$$

where

$$P=\frac{\omega_1^2}{\Gamma^2+\omega_e^2},\qquad \chi'=\frac{\Delta\omega\,\omega_1}{\Gamma^2+\omega_e^2},\qquad \chi''=\frac{\omega_1\Gamma}{\Gamma^2+\omega_e^2}. \tag{A.11}$$

By substituting eqs.(A.5) (A.10) into eq.(A.4), we can obtain the same result as eq.(3.8).

APPENDIX B Parametric Resonance

The pumping light beam is perpendicular to the static field H_0, and $H_1\cos\omega t$ is parallel to H_0 (see Fig.1.2(d)). As mentioned previously, the transverse pumping creates a magnetization in the vapor only for small fields. This is the Hanle effect, or the zero field level crossing.

If the rf field is presented, the situation is changed, and the transverse pumping creates a magnetization not only for small fields but also strong fields. In the parametric resonance case, the Bloch equation becomes as follows;

$$\frac{d M_+}{dt} = - i(\omega_0 + \omega_1 \cos \omega t) M_+ - \frac{1}{\tau} M_+ + \frac{M_0'}{\tau} , \qquad (A.12a)$$

$$\frac{d M_z}{dt} = - \frac{M_z}{\tau} , \qquad (A.12b)$$

$$M_+ = M_x + i M_y . \qquad (A.12c)$$

The solution of eq.(A.12b) is $M_z = 0$. We can rewrite eq.(A.12a) as follows;

$$[\frac{d}{dt} + \frac{1}{\tau} + i (\omega_0 + \omega_1 \cos \omega t)] M_+ = \frac{M_0'}{\tau} . \qquad (A.13)$$

The solution of eq.(A.13) without the right handed term is given

$$M_+(t) = \lambda \; e^{-t/\tau} \, e^{-i(\omega_0 t + \frac{\omega_1}{\omega} \sin\omega t)} . \qquad (A.14)$$

Substituting eq.(A.14) into eq.(A.13), λ becomes a function of t (method of the variation of constant). Therefore, we obtain the following equation for λ ;

$$\frac{d\lambda}{dt} = \frac{M_0'}{\tau} e^{-t/\tau} \, e^{i \omega_0 t} \, e^{i \frac{\omega_1}{\omega} \sin\omega t} . \qquad (A.15)$$

For integration of eq.(A.15), we use the well-known relation as follows;

$$e^{\pm i \frac{\omega_1}{\omega} \sin\omega t} = \sum_{n=-\infty}^{\infty} J_n(\frac{\omega_1}{\omega}) \, e^{\pm in\omega t} , \qquad (A.16)$$

where J_n is the Bessel function of n-th order, and n is an integer or zero. When n is an integer of negative, we have

$$J_n = (-1)^n J_{-n} . \qquad (A.17)$$

Using the relation (A.16) into eq.(A.15), it becomes

$$\frac{d\lambda}{dt} = \frac{M_0'}{\tau} \sum_{n=-\infty}^{\infty} J_n\left(\frac{\omega_1}{\omega}\right) e^{\left[\frac{1}{\tau} + i\,(\omega_0 + n\omega)\right] t} . \qquad (A.18)$$

This equation can be immediately integrated and λ is given as

$$\lambda = \frac{M_0'}{\tau} \sum_{n=-\infty}^{\infty} \frac{J_n(\omega_1/\omega)\, e^{[(1/\tau) + i(\omega_0 + n\omega)]t}}{(1/\tau) + i(\omega_0 + n\omega)} . \qquad (A.19)$$

In eq.(A.19), we have zero as the constant of integration, because the constant may disappear after the relaxation time τ . By use of eq.(A.16), we can

$$M_+(t) = \lambda \sum_{q=-\infty}^{\infty} J_q\left(\frac{\omega_1}{\omega}\right) e^{-\left[\frac{1}{\tau} + i(\omega_0 + q\omega)\right] t} . \qquad (A.20)$$

Substituting eq.(A.19) into eq.(A.20) and replacing $n-q = p$, M_+ becomes as follows;

$$M_+(t) = \frac{M_0'}{\tau} \sum_{n=-\infty}^{\infty} \sum_{p=-\infty}^{\infty} \frac{J_n\left(\frac{\omega_1}{\omega}\right) J_{n-p}\left(\frac{\omega_1}{\omega}\right)}{(1/\tau) + i(\omega_0 + n\omega)} e^{ip\omega t} . \qquad (A.21)$$

Rewriting this again,

$$\frac{M_+(t)}{M_0'} = A_0 + \sum_{p=-1}^{\infty} \left(A_p e^{ip\omega t} + A_{-p} e^{-ip\omega t} \right) , \qquad (A.22)$$

with

$$A_0 = \sum_{n=-\infty}^{\infty} \frac{J_n^{\,2}\left(\frac{\omega_1}{\omega}\right)}{1 + i(\omega_0 + n\omega)\tau} , \qquad (A.23a)$$

$$A_{\pm p} = \sum_{n=-\infty}^{\infty} \frac{J_n\left(\frac{\omega_1}{\omega}\right) J_{n+p}\left(\frac{\omega_1}{\omega}\right)}{1 + i(\omega_0 + n\omega)\tau} . \qquad (A.23b)$$

By using the relation (A.12c), M_x and M_y are given as $M_x = \mathrm{Re}\, M_+$, $M_y = \mathrm{Im}\, M_+$. We know from eq.(A.22) that the resonances occur for $\omega_0 = n\omega$. As the intensity of the rf field is increased, we observe no shift and no broadening of the resonance curves. These resonances may be detected at the various harmonics $p\omega$ of the transmitted light beam. Their intensities as a function of ω_1/ω have been theoretically predicted and experimentally measured (Polonsky and Cohen-Tannoudji 1965, Favrè and Geneux 1964, Aleksandrov, Constantinov and Perel`1963).

APPENDIX C Transient Phenomena in the Presence of the Oscillating RF Field

We consider the behavior of the free induction decay of the magnetization undergoing the affection of a linearly oscillating rf field. For this case the Bloch equation is given in the form

$$\frac{dM_x}{dt} = \omega_0 M_y - \frac{M_x}{\tau} \quad , \tag{A.24a}$$

$$\frac{dM_y}{dt} = -\omega_0 M_x + \omega_1 \cos\omega t\, M_z - \frac{M_y}{\tau} \quad , \tag{A.24b}$$

$$\frac{dM_z}{dt} = -\omega_1 \cos\omega t\, M_y - \frac{M_z}{\tau} \quad . \tag{A.24c}$$

Consider now the transformation of the coordinate system, that is a transformation to a frame Ox'y'z' rotating about the x axis with a frequency-modulated angular velocity $\Theta(t) = \frac{\omega_1}{\omega} \sin\omega t$. Under this transformation, the Bloch equation is written as follows;

$$\frac{dM_{x'}}{dt} = \omega_0 \cos\Theta(t)\, M_{y'} + \omega_0 \sin\Theta(t)\, M_{z'} - \frac{M_{x'}}{\tau} \quad , \tag{A.25a}$$

$$\frac{dM_{y'}}{dt} = -\omega_0 \cos\Theta(t)\, M_{x'} - \frac{M_{y'}}{\tau} \quad , \tag{A.25b}$$

$$\frac{d M_{z'}}{dt} = - \omega_0 \sin \Theta(t)\, M_{x'} - \frac{M_{z'}}{\tau} \quad . \tag{A.25c}$$

Using the relation (A.16) and assuming that ω_0 must be small enough to allow the approximation $\omega_0 \ll \omega$, eqs.(A.25) become

$$\frac{d M_{x'}}{dt} = \omega_0 J_0(\frac{\omega_1}{\omega})\, M_{y'} - \frac{M_{x'}}{\tau} \quad , \tag{A.26a}$$

$$\frac{d M_{y'}}{dt} = - \omega_0\, J_0(\frac{\omega_1}{\omega})\, M_{x'} - \frac{M_{y'}}{\tau} \quad , \tag{A.26b}$$

$$\frac{d M_{z'}}{dt} = - \frac{M_{z'}}{\tau} \quad . \tag{A.26c}$$

The solutions of eqs.(A.26) can be obtained as

$$M_{x'} = C_1\, e^{-t/\tau} \cos\ \omega_0\, J_0(\frac{\omega_1}{\omega})t \quad , \tag{A.27a}$$

$$M_{y'} = C_1\, e^{-t/\tau} \sin\ \omega_0\, J_0(\frac{\omega_1}{\omega})t \quad , \tag{A.27b}$$

$$M_{z'} = C_2 \quad , \tag{A.27c}$$

where C_1 and C_2 are the integral constants, which are decided by the initial conditions. Suppose a 90° pulse is applied and M_0' lies along the x axis. The initial conditions for this case is that at $t = 0$, $M_{x'} = M_0'$, and hence $C_1 = M_0'$, $C_2 = 0$. Returning to the laboratory coordinate, the components of magnetization are

$$M_x = M_0'\, e^{-t/\tau} \cos\{\, \omega_0\, J_0(\frac{\omega_1}{\omega})t\} \quad , \tag{A.28a}$$

$$M_y = M_0'\, e^{-t/\tau} \sin\{\, \omega_0\, J_0(\frac{\omega_1}{\omega})t\}\{J_0(\frac{\omega_1}{\omega}) + \sum_{\substack{\text{even} \\ \text{harmonics}}} 2J_p(\frac{\omega_1}{\omega})\cos p\omega t\}. \tag{A.28b}$$

$$M_z = - M_0'\, e^{-t/\tau} \sin\{\, \omega_0\, J_0(\frac{\omega_1}{\omega})t\}\{ \sum_{\substack{\text{odd} \\ \text{harmonics}}} 2J_p(\frac{\omega_1}{\omega})\sin p\omega t\}. \tag{A.28c}$$

These expressions are the same one as derived by Series and Pegg (Series 1970, Pegg and Series 1970). Neglecting the harmonics of rf, one find that the magnetization becomes

$$M_x = M_0' \, e^{-t/\tau} \cos\{\omega_0 J_0(\frac{\omega_1}{\omega})t\}, \tag{A.29a}$$

$$M_y = M_0' \, e^{-t/\tau} J_0(\frac{\omega_1}{\omega}) \sin\{\omega_0 J_0(\frac{\omega_1}{\omega})t\}, \tag{A.29b}$$

$$M_z = 0 . \tag{A.29c}$$

Transverse component $\mathbf{M}_\perp$ with respect to $\mathbf{H}_0$ is

$$\mathbf{M}_\perp = M_0' \, e^{-t/\tau}[\mathbf{i} \cos\{\omega_0 J_0(\frac{\omega_1}{\omega})t\} + \mathbf{j} J_0(\frac{\omega_1}{\omega})\sin\{\omega_0 J_0(\frac{\omega_1}{\omega})\}], \tag{A.30}$$

which shows that the Larmor precession around $\mathbf{H}_0$ is no more circular but elliptical. This equation can be rewritten as follows;

$$\begin{aligned} \mathbf{M} = & \frac{1 + J_0(\frac{\omega_1}{\omega})}{2} M_0' \, e^{-t/\tau}[\mathbf{i} \cos\{\omega_0 J_0(\frac{\omega_1}{\omega})t\} + \mathbf{j} \sin\{\omega_0 J_0(\frac{\omega_1}{\omega})t\}] \\ & + \frac{1 - J_0(\frac{\omega_1}{\omega})}{2} M_0' \, e^{-t/\tau}[\mathbf{i} \cos\{\omega_0 J_0(\frac{\omega_1}{\omega})t\} - \mathbf{j} \sin\{\omega_0 J_0(\frac{\omega_1}{\omega})t\}]. \end{aligned} \tag{A.31}$$

This expression shows that the magnetization $\mathbf{M}_\perp$ consists of the two rotating components with the angular frequencies $\pm \omega_0 J_0(\omega_1/\omega)$, and their magnitudes are $2^{-1}(1 + J_0(\omega_1/\omega))$ and $2^{-1}(1 - J_0(\omega_1/\omega))$, respectively. This result was obtained by Cohen-Tannoudji and Haroche (1969b) and Landrè et al. (1971). They have shown theoretically and experimentally that the "dressing" by a nonresonant linearly oscillating rf field $H_1 \cos \omega t$ introduces an anisotropy in the magnetic properties of an atomic system: the Lande g-factor depends on the angle between the static field $\mathbf{H}_0$ and $\mathbf{H}_1$; the Larmor precession is no more circular but elliptical.

REFERENCES

Abragam,A., 1961 The Principles of Nuclear Magnetism(Clarendon Press,Oxford)P.24.

Aleksandrov,E.B., Bonch-Bruevich,A.M. and Khodvoi,V.A., 1967 Opt. Spect. 22 151.

Aleksandrov,E.B., Konstantinov,O.V., Perel',V.I. and Khodvoi,V.A. 1963 Soviet Physics-JETP 18 346.

Aleksandrov,E.B.and Perel',V.I., 1966 Soviet Physics-JETP 22 70.

Aleksandrov,E.B. and Sokorov,A.P., 1972 Soviet Physics-JETP 34 48.

Allegrini,N. and Arimond,E., 1971 J. Phys. B: Atom. molec. Phys. 4 1008.

Arimond,E., 1968 Ann. Phys., Paris 3 425.

Autler,S.H. and Townes,C.H., 1955 Phys. Rev. 100 703.

Barrat,J.P. and Cohen-Tannoudji,C., 1961a J. Phys. Radium 22 329.

Barrat,J.P. and Cohen-Tannoudji,C., 1961b J. Phys. Radium 22 443.

Bell,W.E. and Bloom,A.L., 1957 Phys. Rev. 107. 1557.

Bell,W.E. and Bloom,A.L., 1961 Phys. Rev. Letters, 6 280.

Bloch,F., 1946 Phys. Rev. 70 460.

Bloch,F. and Siegert,A., 1940 Phys. Rev. 57 522.

Brossel,J., 1965 Pompage Optique in Quantum Optics and Electronics (ed. C. Dewitt et al. Gordon and Breach, New York) P.226

Brossel,J. and Bitter,F., 1952 Phys. Rev. 86 308.

Brossel,J., Kastler,A. and Winter,J., 1952 J. Phys. Radium 13 668.

Carver,T.R., 1963 Science 141 599.

Carver,T.R. and Partridge,R.B., 1966 Amer. J. Phys. 34 339.

Chang,C.S. and Stehle,P., 1971 Phys. Rev. A 4 641.

Chapman,G.D., 1970 J. Phys. B: Atom. molec. Phys. 3 L36.

Cohen-Tannoudji,C., 1962a Ann. Phys. (Paris) 7 423.

Cohen-Tannoudji,C., 1962b Ann. Phys. (Paris) 7 469.

Cohen-Tannoudji,C., 1968 Cargesé Lectures in Physics Vol.2 ed. M. Levy

(New York), PP.347-93.

Cohen-Tannoudji,C. and Dupont-Roc,J., 1972 Phys. Rev. A 5 968.

Cohen-Tannoudji,C., Dupont-Roc,J. and Fabré,C., 1973a J. Phys. B: Atom. molec. Phys. 6 L214.

Cohen-Tannoudji,C., Dupont-Roc,J. and Fabré,C., 1973b J. Phys. B: Atom. molec. Phys. 6 L218.

Cohen-Tannoudji,C., Dupont-Roc,J., Haroche,S. and Laloé,F., 1969 Phys. Rev. Letters, 22 758.

Cohen-Tannoudji,C. and Kastler,A., 1966 in Progress in Optics, Vol.V, ed. E. Wolf (North-Holland), P.3.

Cohen-Tannoudji,C. and Haroche,S., 1965 Compt. Rend. Acad. Sci. 261 5400.

Cohen-Tannoudji,C. and Haroche,S., 1966 Compt. Rend. Acad. Sci. 262 268.

Cohen-Tannoudji,C. and Haroche,S., 1967 Compt. Rend. Acad. Sci. 264 626.

Cohen-Tannoudji,C. and Haroche,S., 1969a J. Phys. Radium 30 125.

Cohen-Tannoudji,C. and Haroche,S., 1969b J. Phys. Radium 30 153.

Colegrove,F.D., Franken,P.A., Lewis,P.R. and Sands,R.H., 1959 Phys. Rev. Letters 3 420.

Condon,E.U. and Shortly,G.H., 1951 The Theory of Atomic Spectra (Cambridge University Press, London), P.61.

Crisp,M.D. and Jaynes,E.T., 1969 Phys. Rev. 50 4071.

Dehmelt,H.G., 1957 Phys. Rev. 105 1924.

Dodd,J.N., Fox,W.N., Series,G.W. and Taylor,M.J., 1959 Proc. Phys. Soc. (London) 74 789.

Dodd,J.N. and Series,G.W., 1961 Proc. Roy. Soc. (London) A263 353.

Dupont-Roc,J., Polonsky,N., Cohen-Tannoudji,C. and Kastler,A., 1967 Phys. Letters, 25A 87.

Eck,T.G., Foldy,L.L. and Wider,H., 1963 Phys. Rev. Letters, 10 239.

Favre,C.J. and Geneux,E., 1964 Phys. Letters, 8 190.

Feldman,B.J. and Feld,M.S., 1972 Phys. Rev. A 5 899.

Feynman,R.P., Vernon,F.L. and Hellwarth,R.W., 1957 J. Appl. Phys. 28 49.

Fontana,P.R. and Lynch,D.L., 1970 Phys. Rev. A 2 347.

Franken,P.A., 1961 Phys. Rev. 121 508.

Gallagher,A. and Lurio,A., 1963 Phys. Rev. Letters, 10 25.

Glauber,R.J., 1963 Phys. Rev. 131 2766.

Goldberger,M.L. and Watson,K.M.W., 1964 Collision Theory (J. Wiley and Sons, New York).

Gush,R. and Gush,H.P., 1972 Phys. Rev. A 6 129.

Hahn,E.L., 1950 Phys. Rev. 80 580.

Hanle,W., 1924 Z. Physik 30 93.

Happer,W., 1970 in Progress in Quantum Electronics, Vol. 1, Part 2, eds. J.H. Sanders and K.W.H.Stevens (Pergamon Press, Oxford).

Happer,W., 1972 Rev. Mod. Phys. 44 169.

Hannaford,P., Pegg,D.T. and Series,G.W., 1973 J. Phys. B: Atom. molec. Phys. 6 L222.

Haroche,S., 1971a Ann. Phys. (Paris) 6 189.

Haroche,S., 1971b Ann. Phys. (Paris) 6 327.

Haroche,S. and Cohen-Tannoudji,C., 1970 Phys. Rev. Letters, 24 974.

Haroche,S., Cohen-Tannoudji,C., Audoin,C. and Shermann,J.P., 1970 Phys. Rev. Letters, 24 861.

ter Harr,D., 1966 J. Appl. Phys. 37 1164.

Hawkins,W.B. and Dike,R.H., 1953 Phys. Rev. 91 1008.

Ito,T., Kondo,K. and Hashi,T., 1968 Japan. J. Appl. Phys. 7 565.

Kastler,A., 1950 J. Phys. Radium 11 255.

Kastler,A., 1957 J. Opt. Soc. Am. 47 460.

Kastler,A., 1963 J. Opt. Soc. Am. 53 902.

Khodovoi,V.A., 1964 Soviet Physics-JETP 19 227.

Kush,P., 1956 Phys. Rev. 101 627.

Landré,C., Cohen-Tannoudji,C., Dupont-Roc,J. and Haroche,S., 1970 J. Phys. Radium 31 971.

Lehman,J.C. and Cohen-Tannoudji,C., 1964 Compt. Rend. Acad. Sci. 258 4463.

Lewis,P.R. and Sands,R.H., 1959 Phys. Rev. 115 1850.

Mandel,L. and Wolf,E., 1965 Rev. Mod. Phys. 37 231.

Mandel,L. and Wolf,E., 1966 Phys. Rev. 149 1033.

Margerie,J. and Brossel,J., 1955 Compt. Rend. Acad. Sci. 241 373.

Mitchell,A.C.G. and Zemansky,M., 1934 Resonance Radiation and Excited Atoms (Cambridge Univ. Press, London) Chap. 5.

Morand,S. and Theobald,G., 1969 Compt. Rend. Acad. Sci. 269 503.

Muriel,A., 1972 Phys. Letters, 40A 261.

Novikov,L.N., Pokazan'ev,V.L. and Yakub,L.I., 1968 Soviet Physics-JETP 26 752.

Pegg,D.T., 1971 J. Phys. B: Atom. molec. Phys. 5 L4.

Pegg,D.T., 1973a J. Phys. B: Atom. molec. Phys. 6 241.

Pegg,D.T., 1973b J. Phys. B: Atom. molec. Phys. 6 246.

Pegg,D.T. and Series,G.W., 1970 J. Phys. B: Atom. molec. Phys. 3 L33.

Pegg,D.T. and Series,G.W., 1973a Proc. Roy. Soc. London 332 281.

Pegg,D.T. and Series,G.W., 1973b Phys. Rev. A 7 371.

Pokazan'ev,V.G. and Novikov,L.N., 1968 Soviet Physics-JETP 54 1297.

Polonsky,N. and Cohen-Tannoudji,C., 1965a Compt. Rend. Acad. Sci. 260 5231.

Polonsky,N. and Cohen-Tannoudji,C., 1965b Compt. Rend. Acad. Sci. 261 369.

Polonsky,N. and Cohen-Tannoudji,C., 1965c J. Phys. Radium 26 409.

Rabi,I.I., 1937 Phys. Rev. 51 652.

Rabi,I.I., Ramsey,N.F. and Schwinger,J., 1954 Rev. Mod. Phys. 26 167.

Ramsey,N.F., 1955 Phys. Rev. 100 1191.

Rewis,R.R.Jr., 1969 Phys. Rev. 186 352.

Rose,M.E. and Carovillano,R.L., 1961 Phys. Rev. 122 1185.

Saltzman,W.R., 1971 Phys. Rev. Letters, 26 220.